1997

Selective spectroscopic methods for water analysis

Bikas Vaidya
Iowa State University

INFORMATION TO USERS

This manuscript has been reproduced from the microfilm master. UMI films the text directly from the original or copy submitted. Thus, some thesis and dissertation copies are in typewriter face, while others may be from any type of computer printer.

The quality of this reproduction is dependent upon the quality of the copy submitted. Broken or indistinct print, colored or poor quality illustrations and photographs, print bleedthrough, substandard margins, and improper alignment can adversely affect reproduction.

In the unlikely event that the author did not send UMI a complete manuscript and there are missing pages, these will be noted. Also, if unauthorized copyright material had to be removed, a note will indicate the deletion.

Oversize materials (e.g., maps, drawings, charts) are reproduced by sectioning the original, beginning at the upper left-hand corner and continuing from left to right in equal sections with small overlaps. Each original is also photographed in one exposure and is included in reduced form at the back of the book.

Photographs included in the original manuscript have been reproduced xerographically in this copy. Higher quality 6" x 9" black and white photographic prints are available for any photographs or illustrations appearing in this copy for an additional charge. Contact UMI directly to order.

UMI

A Bell & Howell Information Company
300 North Zeeb Road, Ann Arbor MI 48106-1346 USA
313/761-4700 800/521-0600

Selective spectroscopic methods for water analysis

by

Bikas Vaidya

A dissertation submitted to the graduate faculty

in partial fulfillment of the requirements for the degree of

DOCTOR OF PHILOSOPHY

Major: Analytical Chemistry

Major Professor: Marc D. Porter

Iowa State University

Ames, Iowa

1997

Graduate College

Iowa State University

This is to certify that the Doctoral dissertation of

Bikas Vaidya

has met the dissertation requirements of Iowa State University

Signature was redacted for privacy.

Major Professor

Signature was redacted for privacy.

For the Major Program

Signature was redacted for privacy.

For the Graduate College

TABLE OF CONTENTS

ACKNOWLEDGMENTS

The author gratefully acknowledges his major Professor Marc D. Porter for his guidance, encouragement, and patience during the past six years of study. Discussions with the other members of the Porter group have been invaluable throughout each of these research projects, and their contributions are greatly appreciated. Professor Richard Bartsch and his group from Texas Tech University are acknowledged for the synthesis of the chromogenic and fluorogenic crown ethers. Dr. Jerzy Zak for his help in solving the complex equilibria of the crown ethers and Dr. Monzir S. Abdel-Latif for his advice on the use of micelles with crown ethers are acknowledged. Dr. Shelley Coldiron, Dr. C. J. Zhong, Steve Watson and Jian-hong Wang from our group, and Joe Parrish, Roy Strausburg, Scott Brayman and Sharon Sloat from Hach Company are acknowledged for their contribution in the successful completion of the chloride removal project. Contributions of Dr. Shelley Coldiron, Jian-hong Wang and Steve Watson in the thin film pH sensor project are gratefully acknowledged. This research was funded by Hach Company, Microanalytical Instrumentation Center, Iowa State University, and Ames Laboratory. The Ames Laboratory is operated for the U. S. Department of Energy by Iowa State University under contract No. W-7405-eng-82.

ABSTRACT

This dissertation explores in large part the development of a few types of spectroscopic methods in analysis of water. Methods for the determination of some of the most important properties of water like pH, metal ion content, and chemical oxygen demand are investigated in detail. The first of the five papers included in this dissertation describes the synthesis, acid-base reactivity and metal ion binding selectivity of two novel crown ether compounds, N,N'-bis(2-hydroxy-5-nitrobenzyl)-4,13-diazadibenzo-18-crown-6 (CCE) and N,N'-bis(7-hydroxy-4-methylcoumarin-8-methylene)-4,13-diazadibenzo-18-crown-6 (FCE). Extraction constants for Ba(II), Ca(II), Cd(II), Cu(II), Hg(II), Pb(II), and Sr(II) have been determined for both reagents. Both CCE and FCE exhibit an unprecedented selectivity of $>10^6$ in the binding of Hg(II) over the other divalent metal cations.

The characterization of optical properties, acid-base equilibria, and metal binding capabilities of CCE in a mixed micellar solution are reported in the second paper. The formation constants for Hg(II), Cd(II), Ca(II) and Sr(II) have been determined. The potential application to a spectrophotometric chemical analysis based on the selectivity of CCE for Cd(II) is examined.

The third paper describes an efficient method for minimization of chloride interference for COD determinations in aqueous samples without using a mercury salt to mask chloride ion. Chloride is removed as HCl gas from an acidified sample solution at 150 °C in a closed vial by adsorption onto a bismuth-based adsorbent held in a specially designed Teflon-basket. The effects of adsorbent composition, basket design, acid

concentration, temperature, reflux time, and silver(I) in the removal of chloride ion and the COD determination are also discussed.

The formation of an ordered monolayer of 4-aminothiophenol (ATP) on gold, electrostatic attachment of anthraquinone mono- and disulfonates to the protonated ATP monolayer, and the determination of the orientation of each of the adsorbed anthraquinone sulfonates from their respective infrared spectra are described in the fourth paper. The orientation of the adsorbed anthraquinone mono- or disulfonate is largely directed by the anionic sulfonate group that binds to the surface bound ammonium group. Finally, the development of a thin-film optical sensor for measuring pH is described in the appendix.

CHAPTER 1. GENERAL INTRODUCTION

The importance of water to our civilization can not be over emphasized. No matter what the purpose, the suitability of water for human consumption and many other uses is strongly affected by dissolved and/or suspended substances.[1] Metals, pH, chemical oxygen demand(COD), biological oxygen demand (BOD), total organic carbon (TOC), dissolved oxygen, turbidity, and conductivity are just a few of the important parameters that define the critical characteristics of water.[2]

The presence of metal ions also affects the suitability of water. The effects of metals in water and waste water range from beneficial through troublesome to dangerously toxic. Some metals are essential nutrients, whereas others may adversely affect water consumers, waste water treatment systems, and receiving waters. Some metals may be beneficial or toxic depending on concentration.[2] Metals are commonly determined in water by various forms (flame, cold vapor, electrothermal and hydride generation) of atomic absorption spectrometry (AAS), inductively coupled plasma-atomic emission spectrometry (ICP-AES), anodic stripping voltammetry (ASV) and colorimetric methods.

In general, AAS and ICP-AES methods give superior results compared to the colorimetric methods. ASV can be a very sensitive method for the determination of some metals, but generally requires a much longer analysis time and can be used only for metals that form an amalgam.[2] Colorimetric methods, on the other hand, can be performed more

rapidly and are more cost effective; however, the suitability of the method greatly depends on the purpose of the determination, and the nature of the metal and the sample matrix.

Colorimetric methods for determination of metals include a wide variety of reagents and techniques.[3] Absorbance and fluorescence are the most common modes of determination. A chromogenic or fluorogenic indicator is used which directly or indirectly interacts with the metal ion, generally forming a metal complex and producing a change in either in intensity, color or both. Some methods require extraction of the metal complex into an organic phase[4] or micellar phase,[5] while others can be applied directly in the aqueous phase. However, few of the indicators used in such metal ion determinations are ideally selective. Most indicators require a masking agent to enhance selectivity.[2,3] To this end, crown ethers are being used by taking advantage of the size selectivity of their cavities.[4,6-41]

One of the most important and frequently used parameter in water analysis is pH, a term defined by Sorenson[42] as -log $[H^+]$. pH measurement is most commonly performed potentiometrically with a glass indicator electrode and a reference electrode.[2] However, a very large number of optical pH sensors have been developed.[43-73] The main advantage of optical pH sensors over the glass electrode is lack of necessity of reference electrode and electrical safety.[48] A theoretical comparison of the optical and electrochemical methods of pH measurements is found in the paper by Janata.[48] Most of the optical sensors developed for pH measurement are based on absorbance[43,44,46,51-53,55,58,59,61,68,71] or fluorescence[45,47,49,50,57,60,63,64,69] measurements in the UV-visible region via an indicator

immobilized on a support material. However, measurements based on changes in reflection[73], fluorescence lifetime[70], evanescent wave absorption[56,67,72] and infrared spectroscopy[54] have also appeared. A major portion of work done in this field in our laboratory has been based on the measurement of the absorbance of an indicator immobilized on a thin cellulosic membrane in the UV-visible[43,52,53,61] and infrared[54] regions.

Chemical oxygen demand (COD) determination is one of the most commonly used test in analysis for organic matter in water and wastewater. COD is an important delimiter for the effect of organic pollutants in water systems which can be empirically related to biological oxygen demand (BOD) or total organic carbon (TOC).[2] As organic pollutants are consumed by microorganisms, the oxygen content of water is depleted. This loss can have adverse effects on the balance of natural ecosystems if the oxygen content falls below the level necessary to support aquatic life. Acidic dichromate is commonly used for the oxidation of the organic material for a COD determination.[2,74-94] While not an organic pollutant, chloride ion can be oxidized by acidic dichromate which can result in a positive deviation in a COD determination. In addition, ammonia also gets oxidized in presence of chloride, which is otherwise not oxidized by the acidic dichromate.[95] Thus, the chloride interference in a sample containing ammonia is even more pronounced.

The present methods of COD determination mask the effect of chloride ion by addition of a mercury salt[2,74,75,79,81,82,88,92-94] which reacts with chloride ion to form an unreactive complex. Other attempted approaches to manage the problem of chloride ion interference include the addition of silver salts[84-87] to mask chloride ion, the addition of

chromium(III)[89] to reduce the oxidation potential, the determination of the amount of chloride oxidized by iodometric titration with a subsequent a correction for the oxidized chloride,[80] and the removal of chloride as hydrochloric acid from an acidified sample solution.[95,96] However, the effectiveness of these approaches for compensation vary depending on sample matrix. Furthermore, as environmental regulations are tightening, it has become increasingly important to develop a more environmentally friendly approaches for COD and other chemical analysis. Hence, an efficient and environmentally friendly method of chloride removal in COD determination is clearly needed.

Like many other sulfur containing organic compounds, 4-aminothiophenol (ATP) has drawn attention of many surface scientists, mainly because of its ability to form an ordered monolayer on metal surfaces like gold[97-103] and silver,[99] and have an amine which can be protonated or deprotonated by changing simply the pH of a solution in contact with the surface.[101] Anionic species like anthraquinone mono- and di-sulfonates can be electrostatically attached to the protonated ATP monolayer on gold. The anthraquinone moiety attached to the gold surface with the ATP is still electroactive and can be electrochemically reduced and oxidized.[101] In addition, the orientation of the anthraquinone moieties adsorbed on the surface can be manipulated by choosing an anthraquinone mono- or di-sulfonate isomer that adsorbs the desired way. The orientation of the anthraquinone moieties adsorbed on the surface can also be controlled by letting the anthraquinone derivative adsorb directly on the gold or over protonated ATP monolayer on gold. Such an electrochemically tunable surface has a great potential for use as a stationary phase in

electrochemically modulated liquid chromatography (EMLC)[104-106] for separation of organic or inorganic molecules and ions in future.

Dissertation Organization

This dissertation is divided into six chapters and an appendix. The general introduction is followed by four papers and a general conclusion and prospectus. Chapter 2 consists of a paper which describes synthesis, optical, acid-base and metal ion binding properties of two novel chromogenic and fluorogenic crown ethers, and their application in selective extraction and determination of Hg(II) and other divalent metal cations. Chapter 3 is another paper on the application of the chromogenic crown ether. The use of the chromogenic crown ether in a mixed micellar solution for selective spectroscopic determination of Cd(II) in water is described. Chapter 4 describes a method for minimization of chloride interference in COD determination without using mercury salts. The chloride is removed as hydrogen chloride gas from an acidified water sample, which is then trapped by a bismuth adsorbent. Chapter 5 consists of a paper dealing with surface functionality and orientation manipulation of adsorbed molecules on a gold electrode. Following these papers is a general summary and discussion which highlights the results of this work, and provides an overview of the future directions. Finally, the appendix is comprised of a paper on thin film optical sensor for measurement of pH.

References

1) Hunt, D. T. E.; Wilson, A. L. *The Chemical Analysis of Water: General Principles and Techniques*; 2nd ed.; The Royal Society of Chemistry: London, 1986.

2) APHA *Standard methods for the Examination of Water and Wastewater*; 19th ed.; American Public Health Association: Washington, DC, 1995.

3) Sandell, E. B. *Colorimetric Determination of Traces of Metals*; 3rd ed.; Interscience Publishers: New York, 1959.

4) Vaidya, B.; Zak, J.; Bastiaans, G. J.; Porter, M. D.; Hallman, J. L.; Nabulsi, N. A. R.; Utterback, M. D.; Strzelbicka, B.; Basrtsch, R. A. *Anal. Chem.* **1995**, *67*, 4101-4111.

5) Abdel-Latif, M. S. *Anal. Lett.* **1994**, *27*, 2341-2353.

6) Abrodo, P. A.; Gomis, D. B.; Sanz-Medel, A. *Microchem. J.* **1984**, *30*, 58-70.

7) Bartsch, R. A.; Czech, B. P.; Kang, S. I.; Stewart, L. E.; Walkowiak, W.; Charwicz, W. A.; Heo, G. S.; Son, B. *J. Am. Chem. Soc.* **1985**, *107*, 4997-4998.

8) Blair, T. L.; Desai, J.; Bachas, L. G. *Anal. Lett.* **1992**, *25*, 1823-1834.

9) Bradshaw, J. S. In *Synthetic Multidentate Macrocyclic Compounds*; Izatt, R. M. and Christensen, J. J., Eds.; Academic Press: New York, 1978; pp 53-109.

10) Brown, P. R.; Bartsch, R. A. In *Topics in Inclusion Science*; Osa, T. and Atwood, J. L., Eds.; Kluwer Academic Publishers: Dordrecht, 1991; Vol. 2, pp 1-57.

11) Czech, B. P.; Babb, D. A.; Czech, A.; Bartsch, R. A. *J. Heterocyclic Chem.* **1989**, *26*, 199-203.

12) Danesi, P. R.; Meider-Gorican, H.; Chiarizia, R.; Scibona, G. *J. Inorg. Nucl. Chem.* **1975**, *37*, 1479-1483.

13) Danesi, P. R.; Chiarizia, R.; Saltelli, A. *J. Inorg. Nucl. Chem.* **1978**, *40*, 1119-1123.

14) Frensdorff, H. K. *J. Am. Chem. Soc.* **1971**, *93*, 4684-4688.

15) Gokel, G. W.; Korzeniowski, S. H. *Reactivity and Structure Concepts in Organic Chemistry*; Springer-Verlag: New York, 1982; Vol. 13.

16) Hiroka, M. *Crown Compounds: Their Characteristics and Applications*; Elsevier: Amsterdam, 1982; Vol. 12.

17) Jawaid, M.; Ingman, F. *Talanta* **1978**, *25*, 91-95.

18) Katalnikov, S. G.; Mysheltsov, I. A. *Tr. Inst.-Mosk. Khim.-Tekhnol. Inst. im. D. I. Mendeleeva* **1989**, *156*, 3-24.

19) Katayama, Y.; Nita, K.; Ueda, M.; Nakamura, H.; Takagi, M. *Anal. Chim. Acta* **1985**, *173*, 193-209.

20) Katayama, Y.; Fukuda, R.; Takagi, M. *Anal. Chim. Acta* **1986**, *185*, 295-306.

21) Katayama, Y.; Fukuda, R.; Iwasaki, T.; Nita, K.; Takagi, M. *Anal. Chim. Acta* **1988**, *204*, 113-125.

22) Kimura, K.; Tanaka, M.; Kitazawa, S.; Shono, T. *Chem. Lett.* **1985**, 1239-1240.

23) Kimura, K.; Tanaka, M.; Shono, T. *Bull. Chem. Soc. Jpn.* **1987**, *60*, 3068-3070.

24) Nakamura, H.; Nishida, H.; Takagi, M.; Ueno, K. *Anal. Chim. Acta* **1982**, *139*, 219-227.

25) Nazarenko, A. Y.; Pyatnitskii, I. V.; Stolyarchuk, T. A. *Zhur. Anal. Khim.* **1981**, *36*, 1719-1721.

26) Nishida, H.; Tazaki, M.; Takagi, M.; Ueno, K. *Mikrochim. Acta* **1981**, *1*, 281-287.

27) Nishida, H.; Katayama, Y.; Katsuki, H.; Nakamura, H.; Takagi, M.; Ueno, K. *Chem. Lett.* **1982**, 1853-1854.

28) Pannell, K. H.; Hambrick, D. C.; Lewandos, G. S. *J. Organometal. Chem.* **1975**, *99*, C21-C23.

29) Pedersen, C. J. *J. Am. Chem. Soc.* **1967**, *89*, 7017-7036.

30) Pyatnitskii, I. V.; Nazarenko, A. Y. *Russian J. Inorg. Chem.* **1980**, *25*, 592-594.

31) Sadakane, A.; Iwachido, T.; Toei, K. *Bull. Chem. Soc. Jpn.* **1975**, *48*, 60-63.

32) Sakai, Y.; Kawano, N.; Nakamura, H.; Takagi, M. *Talanta* **1986**, *33*, 407-410.

33) Sanz-Medel, A.; Gomis, D. B.; Alvarez, J. R. G. *Talanta* **1981**, *28*, 425-430.

34) Sanz-Medel, A.; Gomis, D. B.; Fuente, E.; Jimeno, S. A. *Talanta* **1984**, *31*, 515-519.

35) Sasaki, K.; Pacey, G. *Anal. Chim. Acta* **1985**, *174*, 141-149.

36) Shiga, M.; Nishida, H.; Nakamura, H.; Takagi, M.; Ueno, K. *Bunseki Kagaku* **1983**, *32*, E293-E300.

37) Sumiyoshi, H.; Nakahara, K.; Ueno, K. *Talanta* **1977**, *24*, 763-765.

38) Takagi, M.; Ueno, K. *Top. Curr. Chem.* **1984**, *121*, 39-65.

39) Takagi, M.; Nakamura, H. *J. Coord. Chem.* **1986**, *15*, 53-82.

40) Takagi, M. In *Cation Binding by Macrocycles*; Inoue, Y. and Gokel, G. W., Ed.; Dekker: New York, 1990, pp 465-495.

41) Wilcox, K.; Pacey, G. E. *Talanta* **1991**, *38*, 1315-1324.

42) Sorenson, S. *Biochem. Z.* **1909**, *21*, 131.

43) Porter, M. D.; Coldiron, S. J.; Vaidya, B. *SAE Technical Paper Series* **1993**, *932207*, 1-5.

44) Harper, G. B. *Anal. Chem.* **1975**, *47*, 348-351.

45) Saari, L. A.; Seitz, W. R. *Anal. Chem.* **1982**, *54*, 821-823.

46) Kirkbright, G. F.; Narayanaswamy, R.; Welti, N. A. *Analyst* **1984**, *109*, 1025-1028.

47) Munkholm, C.; Walt, D. R.; Milanovich, F. P.; Klainer, S. M. *Anal. Chem.* **1986**, *58*, 1427-1430.

48) Janata, J. *Anal. Chem.* **1987**, *59*, 1351-1356.

49) Fuh, M. S.; Burgess, L. W.; Hirschfeld, T.; Christian, G. D. *Analyst* **1987**, *112*, 1159-1163.

50) Jordan, D. M.; Walt, D. R.; Milanovich, F. P. *Anal. Chem.* **1987**, *59*, 437-439.

51) Edmonds, T. E.; Flatters, N. J.; Jones, C. F.; Miller, J. N. *Talanta* **1988**, *35*, 103-107.

52) Jones, T. P.; Porter, M. D. *Anal. Chem.* **1988**, *60*, 404-406.

53) Stole, S. M.; Jones, T. P.; Chau, L.; Porter, M. D. In *Chemical Sensors and Microinstrumentation*; Murray, R. W., Dessy, R. E., Heineman, W. R., Janata, J. and Seitz, W. R., Eds., 1989; ACS Symposium Series No. 403, pp 283-302.

54) Jones, T. P.; Porter, M. D. *Appl. Spectrosc.* **1989**, *43*, 908-911.

55) Boisde, G.; Biatry, B.; Magny, B.; Dureault, B.; Blanc, F.; Sebille, B. *SPIE* **1989**, *1172 Chemical, Biochemical, and Environmental Sensors*, 239-250.

56) Carey, W. P.; DeGandpre, M. D.; Jorgensen, B. S. *Anal. Chem.* **1989**, *61*, 1674-1678.

57) Zhujun, Z.; Zhang, Y.; Wangbai, M.; Russel, R.; Shakhsher, Z. M.; Grant, C. L.; Seitz, W. R.; Sundberg, D. C. *Anal. Chem.* **1989**, *61*, 202-205.

58) Collison, M. E.; Meyerhoff, M. E. *Anal. Chem.* **1990**, *62*, 425A-437A.

59) Baldini, F.; Bacci, M.; Bracci, S. *SPIE* **1990**, *1368 Chemical, Biochemical, and Environmental Fiber Sensors II*, 210-217.

60) Zen, J.; Patonay, G. *Anal. Chem.* **1991**, *63*, 2934-2938.

61) Jones, T. P.; Coldiron, S. J.; Deninger, W. J.; Porter, M. D. *Appl. Spectrosc.* **1991**, *45*, 1271-1277.

62) Janata, J. *Anal. Chem.* **1992**, *64*, 196R-219R.

63) Tan, W.; Shi, Z.; Kopelman, R. *Anal. Chem.* **1992**, *64*, 2958-2990.

64) Brenci, M.; Baldini, F. *Fiber Optic Optrodes For Chemical Sensing*; 8th Optical Fiber Sensors Conference; Monterey, CA, 1992; TH4.1, pp 313-319.

65) Arnold, M. A. *Anal. Chem.* **1992**, *64*, 1015A-1025A.

66) Ding, J. Y.; Shahriari, M. R.; G. H. Sigel, J. *Porous Fiber Optical Sensors For pH Measurement*; 8th Optical Fiber Sensors Conference; Monterey, CA, 1992; TH4.3, pp 321-324.

67) Ge, Z.; Brown, C. W.; Sun, L.; Yang, S. C. *Anal. Chem.* **1993**, *65*, 2335-2338.

68) Cardwell, T. J.; Cattrall, R. W.; Deady, L. W.; Dorkos, M.; O'Connel, G. R. *Talanta* **1993**, *40*, 765-768.

69) Parker, J. W.; Laksin, O.; Yu, C.; Lau, M.; Klima, S.; Fisher, R.; Scott, I.; Atwater, B. W. *Anal. Chem.* **1993**, *65*, 2329-2334.

70) Thompson, R. B.; Lakowicz, J. R. *Anal. Chem.* **1993**, *65*, 853-856.

71) Werner, T.; Wolfbeis, O. S. *Fresenius J. Anal. Chem.* **1993**, *346*, 564-568.

72) Lee, J. E.; Saavedra, S. S. *Anal. Chim. Acta* **1994**, *285*, 265-269.

73) Shakhsher, Z.; Seitz, W. R.; Legg, K. D. *Anal. Chem.* **1994**, *66*, 1731-1735.

74) Himebaugh, R. H.; Smith, M. J. *Anal. Chem.* **1979**, *51*, 1085-1087.

75) Gibbs, C. R. *Introduction to Chemical Oxygen Demand*; Hach Company: Loveland, 1993; Booklet No. 8.

76) Moore, W. A.; Kroner, R. C.; Ruchhoft, C. C. *Anal. Chem.* **1949**, *21*, 953-957.

77) Moore, W. A.; Ludzack, F. J.; Ruchhoft, C. C. *Anal. Chem.* **1951**, *23*, 1297-1300.

78) Moore, W. A.; Walker, W. W. *Anal. Chem.* **1956**, *28*, 164-167.

79) Dobbs, R. A.; Williams, R. T. *Anal. Chem.* **1963**, *35*, 1064-1067.

80) Baumann, F. J. *Anal. Chem.* **1974**, *46*, 1336-1338.

81) Jirka, A. M.; Carter, M. J. *Anal. Chem.* **1975**, *47*, 1397-1402.

82) Canelli, E.; Mitchell, D. G.; Pause, R. W. *Wat. Res.* **1976**, *10*, 351-355.

83) Ryding, S.-O.; Forsberg, A. *Wat. Res.* **1977**, *11*, 801-805.

84) Lloyd, A. *Analyst* **1982**, *107*, 1316-1319.

85) Ballinger, D.; Lloyd, A.; Morrish, A. *Analyst* **1982**, *107*, 1047-1053.

86) Pitrebois, L.; Schepper, H. D. *Trib. Cebedeau* **1984**, *484*, 83-86.

87) deCasseres, K. E.; Best, D. G.; May, B. D. *Wat. Pollut. Control* **1984**, 416-419.

88) Jones, B. M.; Sakaji, R. H.; Daughton, C. G. *Anal. Chem.* **1985**, *57*, 2334-2337.

89) Thompson, K. C.; Mendham, D.; Best, D.; Casseres, K. E. D. *Analyst* **1986**, *111*, 483-485.

90) Gonzalez, J. F. *Envirom. Tech. Lett.* **1986**, *7*, 269-272.

91) Soto, M.; Veiga, M. C.; Mendez, R.; Lema, J. M. *Envirom. Tech. Lett.* **1989**, *10*, 541-548.

92) Dasgupta, P. K.; Petersen, K. *Anal. Chem.* **1990**, *62*, 395-402.

93) Belkin, S.; Brenner, A.; Abeliovich, A. *Wat.Res.* **1992**, *26*, 1577-1581.

94) Belkin, S.; Brenner, A.; Abeliovich, A. *Wat. Res.* **1992**, *26*, 1583-1588.

95) Wagner, V. R.; Ruck, W. *Z. Wasser Abwasser Forsch.* **1981**, *14*, 145-151.

96) Wagner, V. R.; Ruck, W. *Z. Wasser Abwasser Forsch* **1982**, *15*, 287-290.

97) Rubinstein, I.; Rishpon, J.; Sabatini, E.; Redondo, A.; Gottesfeld, S. *J. Am. Chem. Soc.* **1990**, *112*, 6135-6136.

98) Kim, Y.-T.; McCarley, R. L.; Bard, A. J. *J. Phys. Chem.* **1992**, *96*, 7416-7421.

99) Hill, W.; Wehling, B. *J. Phys. Chem.* **1993**, *97*, 9451-9455.

100) Bryant, M. A.; Crooks, R. M. *Langmuir* **1993**, *9*, 385-387.

101) Sun, L.; Johnson, B.; Wade, T.; Crooks, R. M. *J. Phys. Chem.* **1990**, *94*, 8869-8871.

102) Sun, L.; Thomas, R. C.; Crooks, R. M. *J. Am. Chem. Soc.* **1991**, *113*, 8550-8552.

103) Kajiya, Y.; Okamoto, T.; Yoneyama, H. *Chem. Lett.* **1993**, 2107-2110.

104) Deinhammer, R. S.; Ting, E.; Porter, M. D. *Anal. Chem.* **1995**, *67*, 237-246.

105) Deinhammer, R. S.; Porter, M. D.; Shimazu, K. *J. Electroanal. Chem.* **1995**, *387*, 35-46.

106) Deinhammer, R. S.; Shimazu, K.; Porter, M. D. *Anal. Chem.* **1991**, *63*, 1890-1894.

CHAPTER 2. CHROMOGENIC AND FLUOROGENIC CROWN ETHER COMPOUNDS FOR THE SELECTIVE EXTRACTION AND DETERMINATION OF Hg(II)

A paper published in Analytical Chemistry‡

Bikas Vaidya*, Jerzy Zak*†, Glenn J. Bastiaans*, and Marc D. Porter*

Johnny L. Hallman#, Nabeel A. R. Nabulsi#, Marty D. Utterback#, Bozena Strzelbicka#, and Richard A. Bartsch#

ABSTRACT

Two novel crown ether compounds, N,N'-bis(2-hydroxy-5-nitrobenzyl)-4,13-diazadibenzo-18-crown-6 (CCE) and N,N'-bis(7-hydroxy-4-methylcoumarin-8-methylene)-4,13-diazadibenzo-18-crown-6 (FCE) have been synthesized as potential reagents for the selective extraction and determination of heavy metal ions. Characterizations of the acid-base reactivity and the heavy metal ion extraction capabilities are reported. Both CCE and FCE undergo four-step ionization processes with associated tautomeric transformations and form stable complexes with divalent metal cations that can be extracted into 1,2-dichloroethane. Extraction constants for Ba(II), Ca(II), Cd(II), Cu(II), Hg(II), Pb(II), and

---

* Microanalytical Instrumentation Center, Ames Laboratory USDOE, and Department of Chemistry, Iowa StateUniversity, Ames, IA 500ii

† Permanent address: Department of Chemistry, The Silesian Technical University, 44-100 Gliwice, Poland.

Department of Chemistry and Biochemistry, Texas Tech University, Lubbock, TX 79409

Sr(II) have been determined for both reagents. For CCE, the extraction order is Hg(II) >> Pb(II) > Cu(II) > Cd(II) > Ca(II) > Sr(II) > Ba(II); whereas the order for FCE is Hg(II) >> Cu(II) > Pb(II) > Cd(II) > Ca(II) > Sr(II) > Ba(II). The selectivity of CCE for Hg(II) over the next best extracted cation, Pb(II), is ~2 x 10^7 and that of FCE for Hg(II) over next best extracted cation, Cu(II), is ~5 x 10^6. Potential applications to chemical analysis, based on the unprecedented selectivity of both reagents for Hg(II), are briefly examined.

INTRODUCTION

Since their discovery,[1] a wide variety of crown ethers have been created[2,3] for applications in solvent extraction[4-9] and isotope separation,[10] as components in ion-selective electrodes,[11,14] and for many other purposes.[15] Lipophilic crown ethers constitute an interesting subgroup of these compounds, largely because of their ability to extract selectively metal ions from an aqueous solution into an organic medium. One particularly attractive strategy couples the selective binding of metal ions by such compounds and the ability of the resulting complex to form an ion pair with a chromogenic or fluorogenic dye.[16-22] The resulting neutrally charged, ion paired complex is then partitioned into an organic phase and detected optically.

The success of these efforts has led to the construction of crown ethers with pendant proton-ionizable chromophoric or fluorophoric groups, i.e., side arms. The incorporation of such side arms eliminates the ion pairing step, which facilitates applications in chemical analysis processes (see Scheme 1). Several forms of this type of crown ether have been synthesized and evaluated for the selective determination of alkali, alkaline earth, and heavy

metal ions.[23-40] The diprotonic chromogenic and fluorogenic crown ethers **1**[23,26,27,31,37] and **2**[24,27], respectively, developed by Takagi and co-workers, have proven particularly effective as selective extraction agents for divalent metal cations. However, both **1** and **2** exhibit only marginal selectivity for Hg(II), a species of critical environmental importance.[23,24]

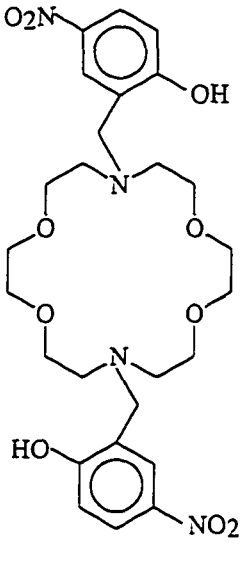

1

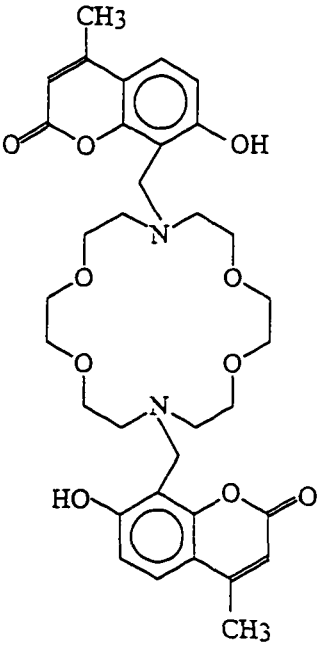

2

As part of our collective interests in this area, we initiated a joint effort to design, construct, and characterize crown ether compounds with improved selectivity for binding heavy metal cations. To this end, we have synthesized dibenzo analogs of **1** and **2**, denoted

Scheme 1

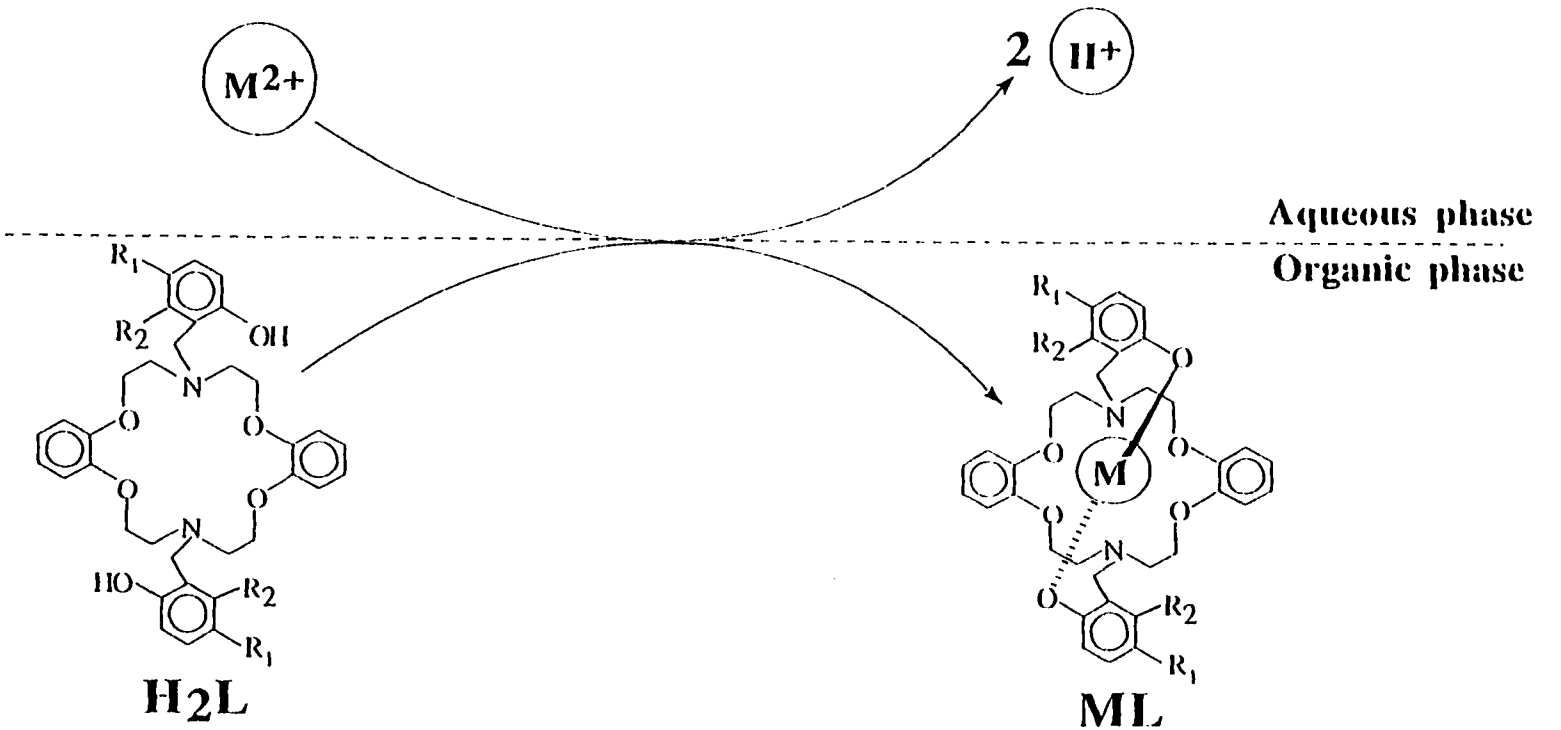

as CCE and FCE, respectively. In comparison to 1 and 2, the presence of the benzo groups in both CCE and FCE should increase the rigidity of the crown ether ring, reduce the basicity of the ring oxygens, and increase overall lipophilicity. We have found that the introduction of the benzo groups produces ligands with an unprecedented selectivity for Hg(II). The following sections describe these findings along with the synthesis, ionization behavior, and divalent metal ion binding capabilities of these novel chromogenic and fluorogenic ionophores.

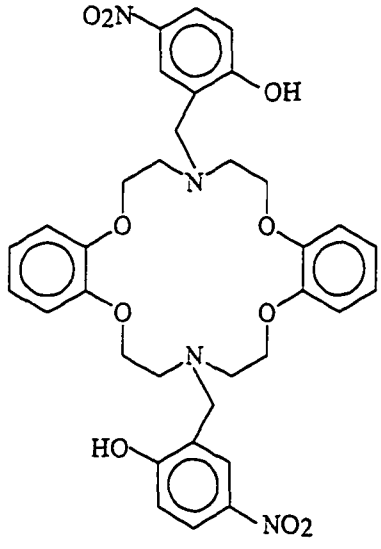

CCE

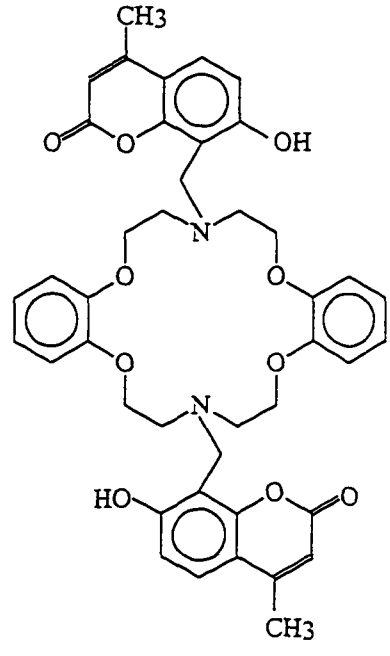

FCE

EXPERIMENTAL SECTION

Reagents and Instrumentation. Reagent-grade inorganic and organic chemicals were obtained from commercial suppliers and used without purification. THF was distilled from benzophenone ketyl and DMF was stored over 4 Å molecular sieves for at least one week. All aqueous solutions were prepared with distilled water that was subsequently deionized using a Millipore Milli-Q Water System. Buffer solutions were prepared from solutions of chloroacetic acid (for pH 2-4), 4-morpholinoethane sulfonic acid (for pH 4-8), or boric acid (for pH >8) by adding tetramethylammonium hydroxide, lithium hydroxide or sodium hydroxide solution until the desired pH was obtained.

Infrared (IR) spectra were acquired with a Perkin Elmer Model 1600 FTIR. ^{1}H NMR spectra were recorded with a Bruker AF-200 spectrophotometer with chemical shifts reported down field from TMS. Determinations of pH were performed with an Orion Research Digital Ionalyzer (Model 501) and an Orion combination glass pH electrode (Model 91-04). The pH electrode was calibrated with a set of standard aqueous buffer solutions (Fisher); all values of pH independent of solution composition are reported with respect to this calibration. Absorbance measurements were conducted with a computer-controlled Hewlett Packard diode array spectrophotometer (HP8452A) at a spectral resolution of 2 nm and integration time of 2 sec. Fluorescence measurements were performed with a 1 cm quartz cell and a SPEX double monochromator spectrofluorimeter (Fluorolog2-F112AI) equipped with a 450 W Xenon lamp; a spectral band pass of 1 nm and a scan rate of 1 nm/sec were

used. All the mathematical and graphical simulations were performed using a spread sheet program (Kaleidagraph).

Ditosylate of N-Tosyl Diethanolamine (3). N-tosyl diethanolamine[41] (92.5 g, 0.357 mol) was dissolved in 600 mL of pyridine. The solution was stirred at -10 °C in an ice-salt bath and tosyl chloride (136.1 g, 0.722 mole) was added at such a rate that the temperature was maintained below -8 °C. The reaction mixture was stirred for 1 h, refrigerated overnight, and poured into 500 mL of a slurry of ice and 6 N HCl. CH_2Cl_2 (200 mL) was added and the layers were separated. The organic layer was washed with 6 N HCl (3 x 50 mL) and water (2 x 50 mL), and evaporated in vacuo. The resultant golden oil was triturated with MeOH (~50 mL) and solidified after 0.5 h. Recrystallization from MeOH gave 153.8 g (76%) of a white solid with mp 96-98 °C (lit[42] mp 78-79 °C). ^{1}H NMR ($CDCl_3$) δ 2.33 (s, 9 H), 3.22-3.51 (t, 4 H), 3.97-4.28 (t, 4 H), 7.15-7.90 (m, 12 H).

N-Tosyl Bis-[2-(2-hydroxyphenoxy)ethyl]amine (4). To a stirred, -5 °C solution of catechol (16.80 g, 0.153 mole) and 2 drops of concentrated HCl in Et_2O (30 mL) was added 6.43 g (0.0765 mole) of dihydropyran; the solution was then stirred for 1 h at this temperature. The acid catalyst was destroyed by addition of 5% aq $NaHCO_3$, the Et_2O was evaporated in vacuo, and the aqueous layer was extracted with CH_2Cl_2 (75 mL). The organic solution was washed with 5% aq $NaHCO_3$ (2 x 50 mL) and water (2 x 50 mL), dried over $MgSO_4$, and evaporated in vacuo to give 10.31 g of a yellow oil. ^{1}H NMR analysis revealed that the oil was 50% in the mono-THP-protected catechol with the remainder being the di-THP-protected catechol.

The impure mono-THP-protected catechol was dissolved in DMF (200 mL) under nitrogen and t-BuOK (4.48 g, 40 mmol) was added. The solution was stirred at 80 °C for a 6 h period while a solution of the ditosylate of N-tosyl diethanolamine (9.80 g, 17.3 mmol) in DMF (50 mL) was added dropwise. The solution was then stirred at 80 °C for an additional 5 days and the solvent was removed in vacuo. The residue was dissolved in CH_2Cl_2 (200 mL), washed with water (3 x 50 mL), and dried over $MgSO_4$. The solvent was evaporated in vacuo and the residue was dissolved in 200 mL of 1:1 MeOH-CH_2Cl_2 (v/v). After addition of concentrated HCl (12 drops), the solution was stirred overnight at room temperature. The resulting precipitate was filtered and recrystallized from 1:1 toluene-EtOAc (v/v) to give 5.85 g (69%) of **4** as off-white needles with mp 171-173 °C. ^{1}H NMR (acetone-d_6) δ 2.32 (s, 3 H), 3.50-3.74 (t, 4 H), 4.00-4.29 (t, 4 H), 6.75 (s, 8 H), 7.12 (s, 2 H), 7.12-7.80 (q, 4 H). IR (KBr) 3438 (O-H), 1271, 1149 (SO_2) cm^{-1}. Anal. Calcd for $C_{23}H_{25}NO_6S$: C, 62.29; H, 5.68. Found: C, 62.43; H, 5.75.

Dimesylate of N-Tosyl Diethanolamine (5). Using the procedure of Crossland and Servis,[43] N-tosyl diethanolamine[41] (5.18 g, 20 mmol), Et_3N (4.64 g, 46 mmol), and mesyl chloride (5.04 g, 44 mmol) were reacted in 35 mL of CH_2Cl_2 at -5 °C. After workup, the solid was recrystallized from EtOH (200 mL) to give 6.06 g (73%) of **4** as a white solid, mp 62-64 °C. ^{1}H NMR ($CDCl_3$) δ 2.45 (s, 3 H), 3.07 (s, 6 H), 3.50 (t, 4 H), 4.41 (s, 4 H), 7.36 (d, 2 H). IR (deposit from CH_2Cl_2 on a NaCl plate) 1339, 1155 (SO_2), 1124 (C-O) cm^{-1}. Anal. Calcd for $C_{13}H_{21}NO_8S_3$: C, 37.57; H, 5.10. Found: C, 37.67; H, 5.10.

N, N'-Ditosyl 4,13-Diazadibenzo-18-crown-6 (6). Bisphenol **4** (4.00 g, 9.0 mmol) was dissolved in 500 mL of MeCN and powdered Cs_2CO_3 (9.00 g, 23 mmol) was added. The mixture was stirred at reflux for 5 h followed by the addition of a solution of dimesylate **5** (3.38 g, 8.14 mmol) in 45 mL of MeCN during a 2.2 h period. The mixture was refluxed for 3 days and filtered. The filter cake was rinsed with CH_2Cl_2. The filtrate and rinsing were combined and evaporated in vacuo. The residue was chromatographed on silica gel with CH_2Cl_2 as eluent to provide 3.01 g (55%) of **6** as a white solid with mp 225-227 °C (lit[44] 215-216 °C). ^{1}H NMR ($CDCl_3$-DMSO-D_6 *ca* 10:1) δ 2.41 (s, 6 H), 3.73 (t, 8 H), 4.12 (t, 8 H), 4.12 (t, 2 H), 6.70-7.00 (m, 8 H), 7.28 (d, 2 H).

4,13-Diazadibenzo-18-crown-6 (7). To a mixture of cyclic ditosylamide **6** (4.10 g, 6.13 mmol) and Na_2HPO_4 (1.85 g) in 410 mL of 5:1 dioxane-methanol (v/v) was added 60 g of freshly prepared, pulverized 6% Na(Hg) amalgam.[45] The mixture was stirred at 80 °C for 2 days and filtered. The solvent was removed in vacuo and the residue was dissolved in CH_2Cl_2. The solution was washed with water until the aqueous layer was neutral, dried over $MgSO_4$, and evaporated in vacuo to give 2.10 g (95%) of **7** as white needles with mp 181-183 °C (lit[44] 175-177 °C). ^{1}H NMR ($CDCl_3$) δ 2.42 (br s, 2 H), 3.13 (t, 8 H), 4.12 (t, 8 H), 6.85 (s, 8 H).

N,N'-Di(2-hydroxy-5-nitrobenzyl) 4,13-Diazadibenzo-18-crown-6 (CCE). A solution of **7** (1.00 g, 2.79 mmol) and Et_3N (1.20 g, 11.9 mmol) in 40 mL of THF was cooled to 0 °C and a solution of 2-hydroxy-5-nitrobenzyl bromide (1.28 g, 6.13 mmol) in 20 mL of THF was added over a 20-min period. The mixture was stirred at 0 °C for 8 h, refluxed for 4

h, and filtered. The filter cake was washed with cold THF and cold deionized water (3 x 20 mL) and dried with a C_6H_6 azeotrope in a Dean Stark trap. The C_6H_6 was evaporated in vacuo to provide 1.67 g (93%) of CCE as a light yellow solid with mp 225-227 °C (dec). ^1H NMR (DMSO-d_6) δ 3.17 (t, 8 H), 3.91 (s, 4 H), 4.12 (t, 8 H), 6.70-7.00 (m, 10 H), 8.00 (d, 2 H, J_o = 8.96 Hz, J_m = 2.90 Hz), 8.18 (d, 2 H, J = 2.88 Hz). IR (KBr) 3498 (OH), 1336 (NO_2), 1253, 1218, 1124 (C-O) cm^{-1}. Anal. Calcd for $C_{34}H_{36}N_4O_{10}$: C, 61.81; H, 5.49. Found: C, 61.87; H, 5.46.

N,N'-(7 -Hydroxy-4-methylcoumarin-8-methylene) 4,13-Diazadibenzo-18-crown-6 (FCE). To 0.60 g (1.67 mmol) of 7 dissolved in 53 mL of 15:1 THF-DMF (v/v) with gentle warming, 7-hydroxy-4-methylcoumarin (0.66 g, 3.74 mmol) dissolved in 3 mL of THF was added followed by 0.41 g (5.0 mmol) of formalin. The mixture was stirred for 8 days at room temperature and the solvent was removed in vacuo with heating up to 70 °C. The residue was suspended in 150 mL of C_6H_6 and refluxed in a Dean Stark trap for 2 days. The dried mixture was filtered and the filter cake was rinsed with C_6H_6. The filter cake was place in a small extraction thimble and extracted with $CHCl_3$ in a hot vapor extraction apparatus for 5 days. The $CHCl_3$ solution was filtered and the filter cake was rinsed with 3 mL of cold $CHCl_3$ to afford 0.66 g (54%) of FCE as a white solid which had very poor solubility in common organic solvents. IR (deposit from a $CDCl_3$ solution on a NaCl plate) 1706 (C=O), 1208, 1128 (C-O) cm^{-1}. Anal. Calcd for $C_{42}H_{42}N_2O_{10}$: C, 68.65; H, 5.76. Found: C, 68.49; H, 5.50. Based on its poor solubility, the white solid was suspended in 20 mL of $CHCl_3$ and 2.0 g of freshly ground K_2CO_3 was added. The mixture was stirred

overnight and filtered. The resulting yellow solution was evaporated in vacuo to give a bright yellow solid with mp 225 °C (dec). ^{1}H NMR ($CDCl_3$) δ 2.36 (s, 6 H), 2.95 (br s, 8 H), 3.80-4.30 (m, 12 H) 5.96 (s, 2 H), 6.60-6.85 (m, 8 H), 6.94 (d, 2 H, J_o = 8.74), 7.29 (d, 2 H, J_o = 8.74). Anal. Calcd for $C_{42}H_{41}N_2O_{10}K(0.5\ H_2O)$: C, 64.52; H, 5.41. Found: C, 64.65; H, 5.20.

Acid Dissociation Constants. Acid dissociation constants were determined by analysis of spectral data for CCE and FCE in buffers prepared in 7:3 MeOH-water (v/v) with hydrochloric acid, formic acid, 4-morpholinopropanesulfonic acid or boric acid and tetramethylammonium hydroxide. The ionic strength was adjusted to 0.10 M with tetramethylammonium bromide. Spectra were measured after dilution of a 50 μL sample of a 50 μM CCE or FCE solution to 5.00 mL with buffer.

Extraction Procedure. Metal ion extractions were performed by mixing 5.00 mL of a 1.0 mM metal nitrate solution with 5.00 mL of a 25 μM crown ether solution in 1,2-dichloroethane. The large excess of metal ions was used to facilitate the determination of the extraction constant by insuring a negligible change in the aqueous phase metal ion concentration after extraction. The resulting mixture was shaken for 30 min. After standing for 12 h to allow the two phases to separate, the organic phase concentrations of the free and complexed forms of CCE or FCE were determined spectroscopically. Buffer solutions were used to control the pH of the aqueous solutions.

RESULTS AND DISCUSSION

Synthesis of CCE and FCE. The routes for the synthesis of CCE and FCE are shown in Scheme 2. Although the preparation of the key intermediate 4,13-diazadibenzo-18-crown-6 (**7**) was first communicated by Högberg and Cram[44] in 1974, only a very low yield was reported. Using Scheme 2, **7** was obtained in a much higher yield in only three steps. Intermediate **7** was then converted to CCE and FCE by one-step adaptations of reactions utilized by Takagi and co-workers for the preparation of **1**[28] and **2**.[24] The final coupling of the fluorophore unit in FCE was more difficult to achieve than the chromophore coupling to give CCE. FCE had very poor solubility in common organic solvents and was transformed into a more soluble potassium monophenoxide form by reaction with K_2CO_3.

General Reactivity Considerations and Formulation for the Determination of Acid Dissociation Constants for CCE and FCE. Diazacrown ethers with two proton-ionizable chromogenic and fluorogenic side arms behave as polybasic acids.[26,27,33] As such, the stepwise acid-base equilibrium for CCE and FCE can be written as:

$$H_4L^{2+} = H_3L^{+} + H^{+} \quad (1)$$

$$H_3L^{+} = H_2L + H^{+} \quad (2)$$

$$H_2L = HL^{-} + H^{+} \quad (3)$$

$$HL^{-} = L^{2-} + H^{+} \quad (4)$$

Scheme 2[a]

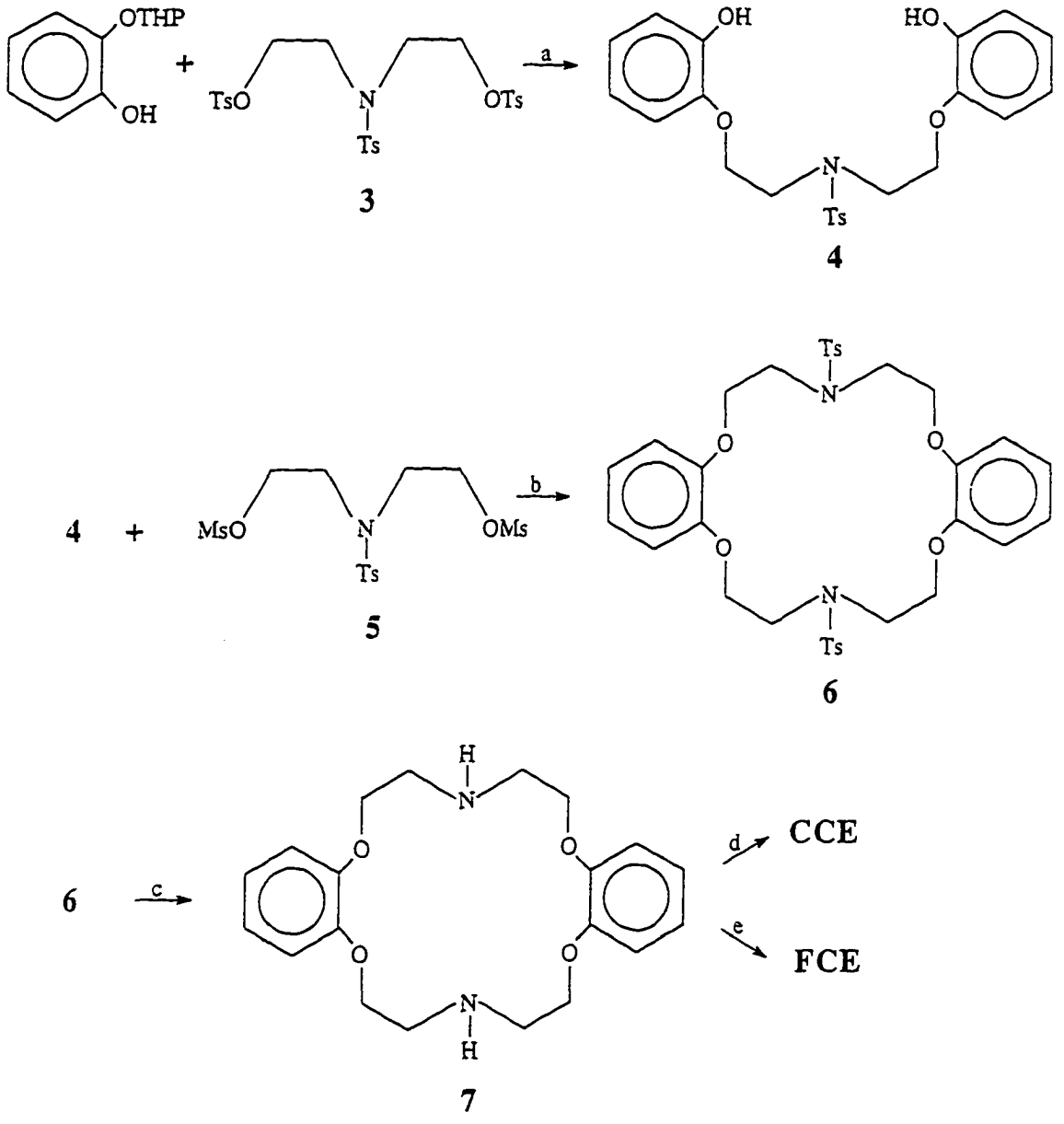

[a] (a) t-BuOK, DMF. (b) Cs_2CO_3, MeCN. (c) Na(Hg), Na_2HPO_4, MeOH. (d) 2-Hydroxy-4-nitrobenzyl bromide, Et_3N, THF. (e) 7-Hydroxy-4-methylcoumarin, formalin, THF-DMF.

Thus, the neutral form (H_2L) of CCE or FCE can be successively protonated to form mono- (H_3L^+) and di- (H_4L^{2+}) cationic forms, or successively deprotonated to produce mono- (HL^-) and di- (L^{2-}) anionic forms. The corresponding acid dissociation constants (K_{ai}) for Equations 1-4 can be formulated in terms of concentrations (assuming activity coefficients of unity) as exemplified by Equation 5.

$$K_{a1} = [H_3L^+][H^+] / [H_4L^{2+}] \qquad (5)$$

At a more detailed structural level, however, zwitterion formation is possible, which would lead to a more complex multi-component equilibrium. Zwitterion formation can occur if the phenolic groups of the side arms are stronger acids than the amine group of the crown ether ring.[46] Zwitterion formation is also influenced by solvent, whereby polar solvents promote the formation of zwitterions and non-polar solvents favor the non-ionic forms.[26] In addition, the presence of the two amine-phenol group pairs in CCE and FCE can lead to a variety of tautomeric species. Scheme 3 summarizes each of the above possibilities. Thus, the deprotonation of H_4L^{2+} to L^{2-} can pass through a host of alternate intermediates, the distribution of which is dependent on several factors, including the cation, ionic strength, and polarity of the solvent. Fully protonated CCE or FCE can then transform from H_4L^{2+} to H_3L^+ either through the loss of a proton from the ammonium or the phenolic functionalities, yielding the respective tautomeric forms $H_3L'^+$ and $H_3L''^+$. Similarly, the loss of a proton from H_3L^+ could give rise to three different forms of H_2L, i.e., H_2L', H_2L'', and H_2L'''. The loss of a third proton results in the formation of HL^-, which can exist as, HL'^- or HL''^-, and

finally, the deprotonation of HL^- yields L^{2-}. In each of these cases, the tautomeric equilibrium can be expressed with the designations given in Scheme 3 as:

$$K_{t1} = \frac{[H_3L'^+]}{[H_3L''^+]} \qquad (6)$$

$$K'_{t2} = \frac{[H_2L']}{[H_2L'']} \qquad (7)$$

$$K''_{t2} = \frac{[H_2L'']}{[H_2L''']} \qquad (8)$$

$$K_{t3} = \frac{[HL'^-]}{[HL''^-]} \qquad (9)$$

As a consequence of the tautomeric equilibria, the acid dissociation constants as exemplified by Equation 5 are the sum of the acid dissociation constants for each of the possible protonic states.[46] For example, K_{a1} is the sum of K'_{a1} and K''_{a1}, where K'_{a1} and K''_{a1} represent the dissociation of H_4L^{2+} to $H_3L'^+$ and $H_3L''^+$, respectively. Furthermore, each of the tautomeric equilibria can be related to the appropriate dissociation constants following Scheme 3 and as shown by Equation 10 for K_{t1}.

$$K_{t1} = \frac{K'_{a1}}{K''_{a1}} \qquad (10)$$

Scheme 3[a]

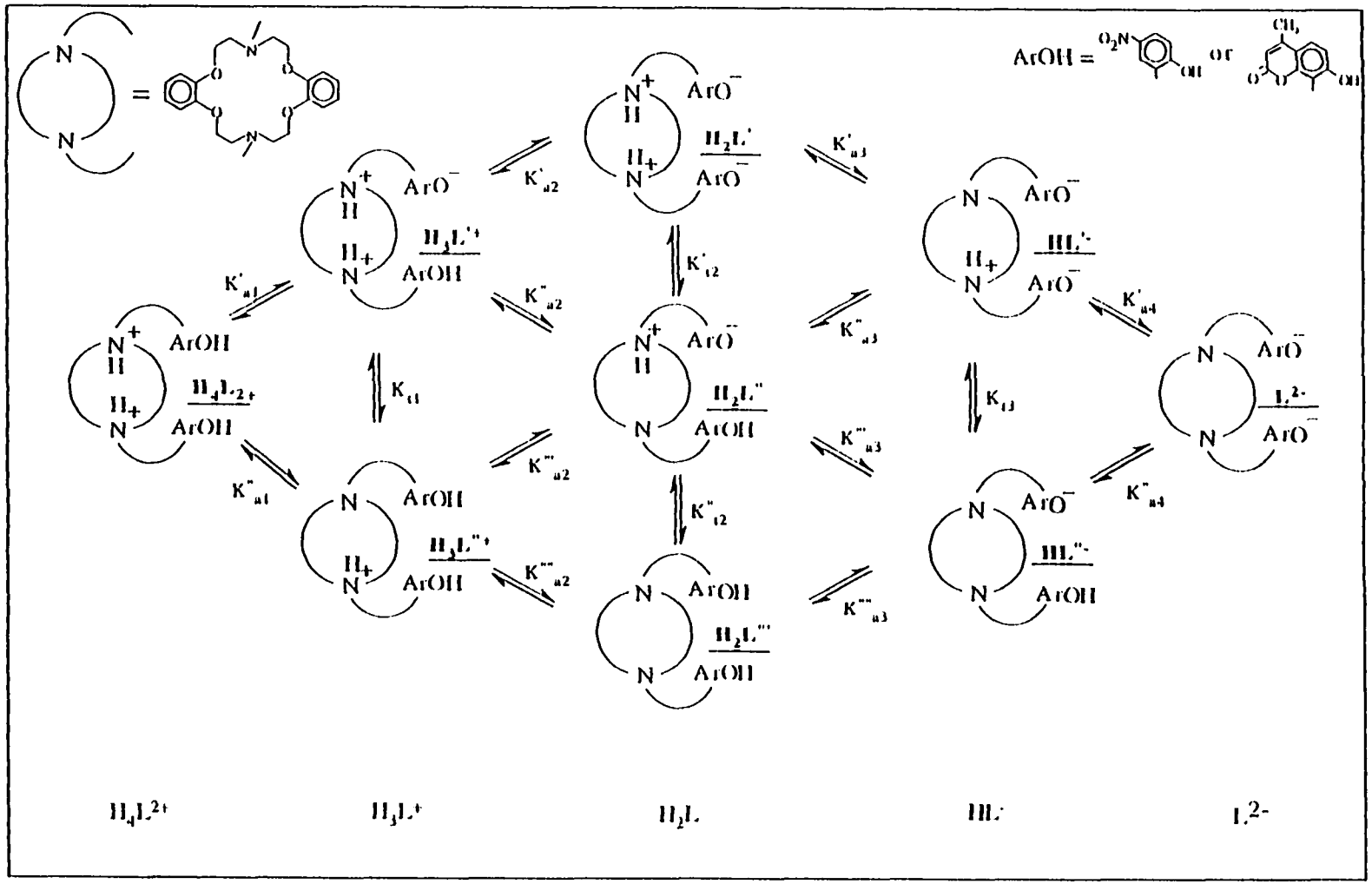

[a] Protons omitted for clarity.

To complete the development of the multi-step equilibrium for CCE and FCE, the analytical concentration of the crown ether (C_t) can be defined as the sum of the concentrations of all of their possible protonic states and is expressed by Equation 11.

$$C_t = [H_4L^{2+}] + [H_3L^{+}] + [H_2L] + [HL^{-}] + [L^{2-}] \qquad (11)$$

Combining the formulization for the acid-base equilibria for reactions 1-4 with that in Equation 11, the concentration of each protonic form of the crown ether as a function of hydrogen ion concentration can be written as represented in Equation 12 for H_4L^{2+}.

$$[H_4L^{2+}] = C_t [H^{+}]^4 / G \qquad (12)$$

where,

$$G = [H^{+}]^4 + [H^{+}]^3 K_{a1} + [H^{+}]^2 K_{a1} K_{a2} + [H^{+}] K_{a1} K_{a2} K_{a3} + K_{a1} K_{a2} K_{a3} K_{a4}$$

Finally, following the additivity law, the absorbance (A_λ) of a solution of CCE or FCE at a given wavelength (λ) can be written as:

$$A_\lambda = \left\{ [H_4L^{2+}]\varepsilon_{\lambda,H_4L^{2+}} + [H_3L^{+}]\varepsilon_{\lambda,H_3L^{+}} + [H_2L^{+}]\varepsilon_{\lambda,H_2L} + [HL^{-}]\varepsilon_{\lambda,HL^{-}} + [L^{2-}]\varepsilon_{\lambda,L^{2-}} \right\} \ell \qquad (13)$$

where $\varepsilon_{\lambda i}$ is the molar absorptivity for each of the forms of CCE or FCE at λ and ℓ is the optical path length in a transmission measurement. These formulations will be used in a subsequent section to characterize the equilibria for CCE and FCE.

Optical Properties of CCE and FCE as a Function of Solution pH and Acid Dissociation Constants. (a) Optical Properties. Figure 1 details the absorption spectra of CCE between 250 and 500 nm as a function of pH. A 7:3 MeOH-water (v/v) solution was used for solubility purposes. At pH 2 and below (Figure 1a), CCE has an absorption maximum at 312 nm. Increases in pH (Figures 1a-d) results in the appearance of a new feature at much longer wavelengths that undergoes a continuous evolution in neutral and alkaline solutions. At pH 12 and above, the absorbance maximum is at 410 nm. Over this pH range, four isosbestic points are observed: 326 nm in the pH range of 2-5 (Figure 1a), 340 nm in the pH range of 5-7 (Figure 1b), 358 nm in the pH range of 7-9 (Figure 1c) and 374 nm at pH 9-12 (Figure 1d). The existence of the four isosbestic points is consistent with the stepwise deprotonation process shown in Scheme 3. In addition, as described shortly, the continual evolution of the spectrum reflects the existence of a tautomeric equilibrium at each step in the dissociation process.

Considerations of the acid-base chemistry and the related optical properties of the parent chromophore of CCE (i.e., *p*-nitrophenol) provide insight into the structural changes that accompany the spectral changes shown in Figure 1. Based on the pH-dependent spectral data for structural analogs of the chromophoric side arms of CCE (i.e., *p*-nitrophenol and 2-hydroxy-5-nitrobenzyl alcohol[23,47]), the changes in the spectra at high pH (Figures 1c,d) primarily reflect the acid-base chemistry of the side arms. The acid-base chemistry of the amine functionalities is therefore dominant at low pH. However, the tautomeric transformation of a small amount of the chromophoric side arm gives rise to a small spectral change in the low pH region.

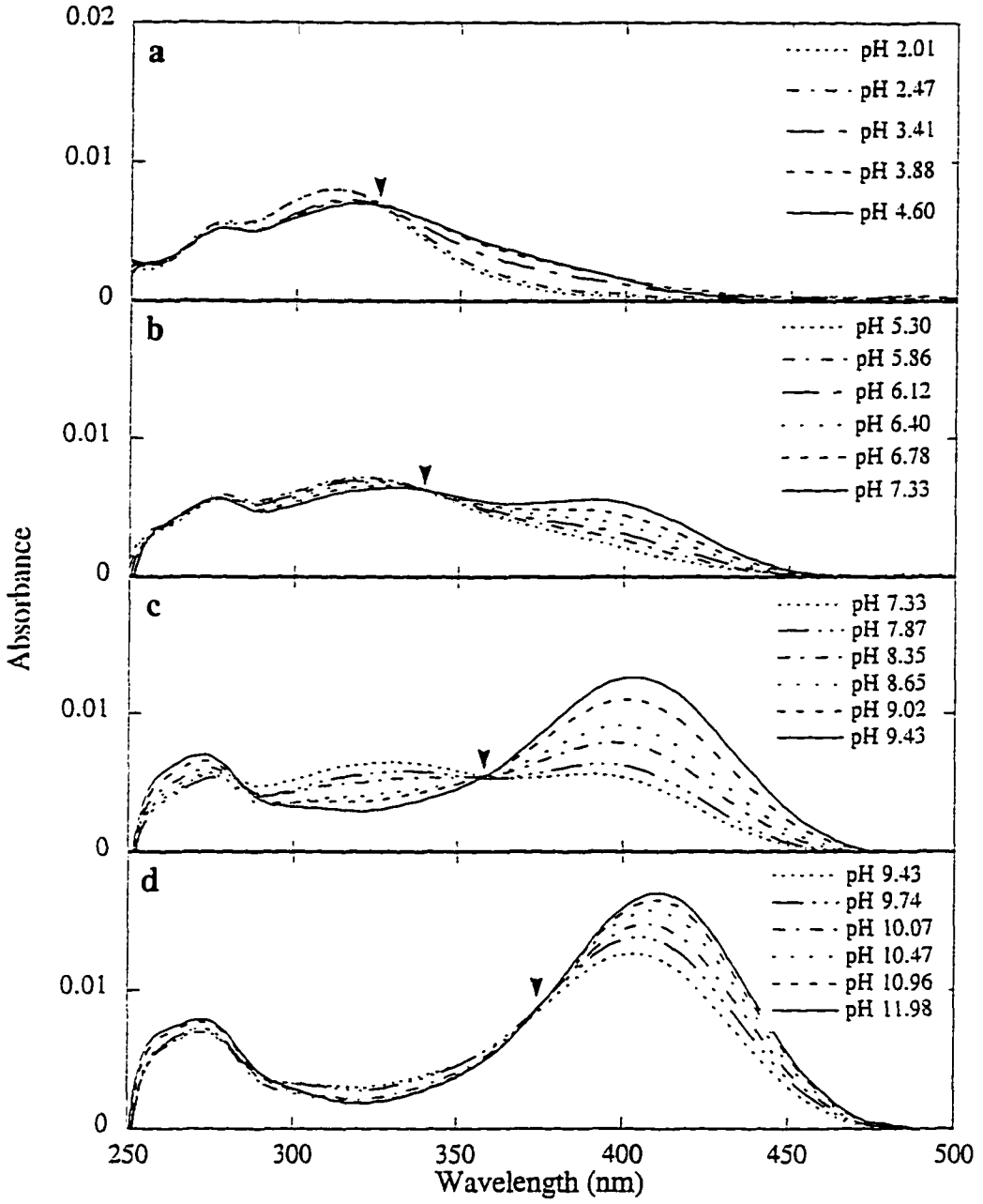

Figure 1. Absorbance spectra of CCE in 7:3 MeOH-water (v/v) as a function of pH between: a) 2.01-4.60, b) 5.30-7.33, c) 7.33-9.43, and d) 9.43-11.98. The arrows point to the isosbestic points.

Absorption spectra for FCE were also examined as a function of pH under the same experimental conditions used for Figure 1. A portion of the results is shown in Figure 2. Though the spectra lack well defined isosbestic points (an observation not at present understood), the overall behavior of FCE is similar to that of CCE, with absorbance maxima at slightly longer wavelengths at low pH and slightly shorter wavelengths at high pH. The pH range for the transformations occurs at slightly higher values (~3 to 12.5). Further, a comparison of the spectra of FCE between pH 8 and 11 (see Figure 2) with those of the parent chromophore (7-hydroxy-4-methylcoumarin) reveals that the changes in the high pH range arise primarily from the dissociation of the phenolic protons. Therefore, as with CCE, the changes in the spectra at low pH are attributed to the acid-base chemistry of the amine functionalities and the corresponding tautomeric equilibria.

(b) Determination of Acid Dissociation Constants. Based on the above observations, CCE and FCE are present predominantly in their H_4L^{2+} forms at pH 2. Thus, the absorption coefficient ($\varepsilon_{\lambda i}$) for H_4L^{2+} can be readily calculated. The same analysis can be applied to the data at the upper pH limit where CCE and FCE exist almost exclusively in their L^{2-} forms. Additionally, since the absorbance for CCE at 358 nm remains constant in the pH range 4 to 5 and 7 to 10, and the absorbance for FCE at 344 nm remains constant in the pH range 5 to 6 and above pH ~8, the values of pK_{a1} and pK_{a2} can be determined. The value of pK_{a1} is found from the absorbance data below pH 5. The value of pK_{a2} can be determined from the absorbance data between pH 5 and 7 using the method described by Albert and Serjeant,[48]

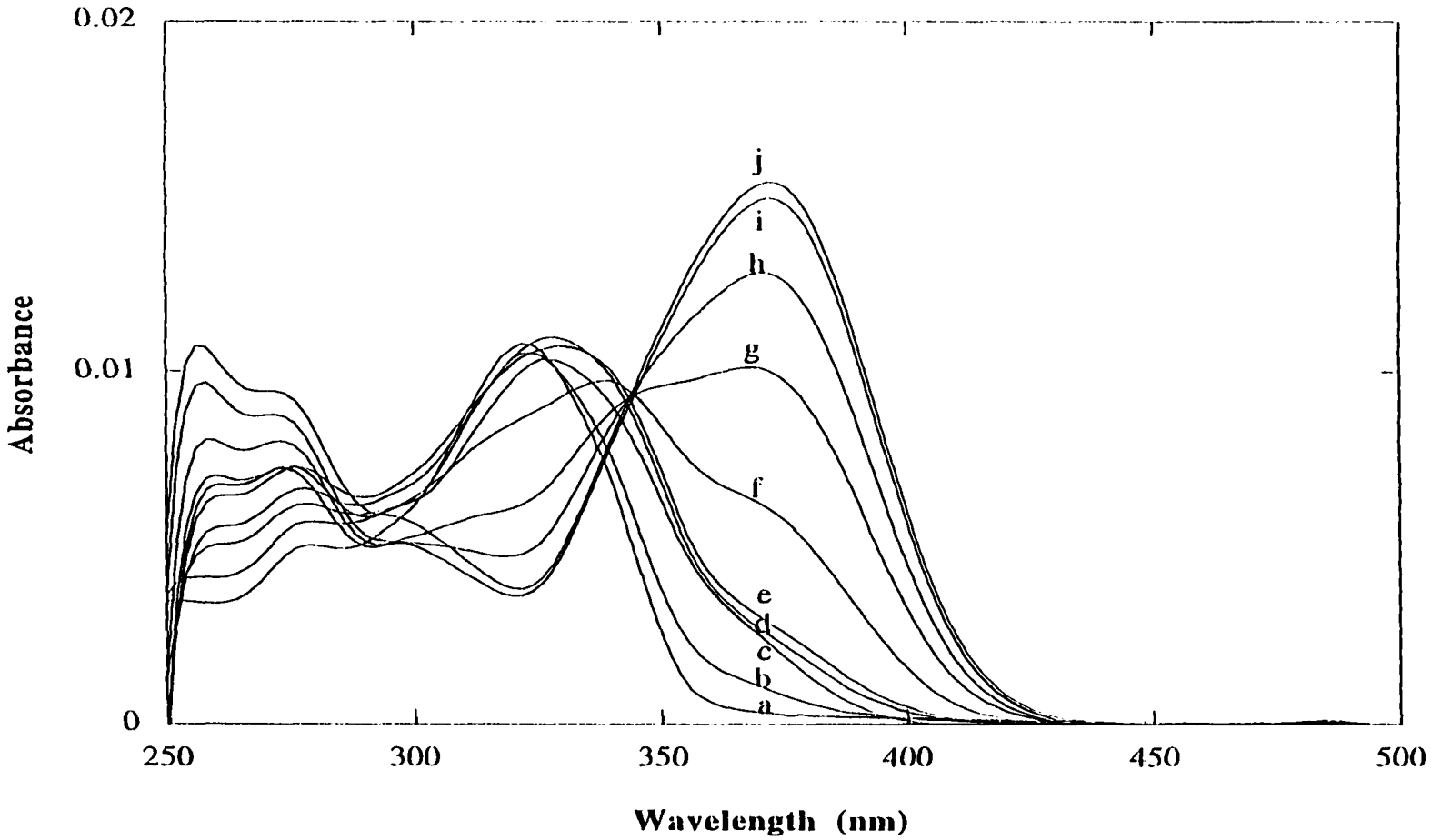

Figure 2. Absorbance spectra of FCE in 7:3 MeOH-water (v/v) as a function of pH: a) 1.9, b) 4.0, c) 6.2, d) 7.2, e) 8.2, f) 9.4, g) 9.9, h) 10.3, i) 11.2 and j) 12.0.

$$pK_a = pH + \log\frac{A_I - A}{A - A_{HI}} \qquad (14)$$

where A is the absorbance at the analytical wavelength (358 nm for CCE and 344 nm for FCE) and is the sum of the absorbances of the deprotonated species (A_I) and its conjugated acid (A_{HI}).

The remaining two pK_a values can be determined by a mathematical simulation of the equilibria using the absorption maxima for the protonated and deprotonated forms of the chromophores. This was accomplished by estimating values for $\varepsilon_{\lambda,H_3L^+}$, $\varepsilon_{\lambda,H_2L}$, $\varepsilon_{\lambda,HL^-}$, and for pK_{a3} and pK_{a4}, and then calculating absorbances using Equation 13 at all three wavelengths for the absorbance spectra shown in Figures 1 and 2. Typically, the first estimates for $\varepsilon_{\lambda,H_3L^+}$, $\varepsilon_{\lambda,H_2L}$, and $\varepsilon_{\lambda,HL^-}$ were chosen to be between the values for H_4L^{2+} and L^{2-}. The two pK_a values and absorption coefficients were changed iteratively (increments of 0.05 and 100 M^{-1} cm^{-1} for the pK_a values and absorption coefficients, respectively) until the average relative deviation between the simulated and experimental absorbance data at each of the three wavelengths was less than 5%. The simulated and measured absorbances at the three wavelengths are compared in Figure 3a for CCE and Figure 3b for FCE. The simulated data are shown by the solid lines. The agreement between the simulated and the experimental data at all three wavelengths confirms the effectiveness of the simulation. The absorption coefficients for the different ionized forms of CCE and FCE in 7:3 MeOH-water (v/v) are listed in Table 1. The pK_a values are listed in

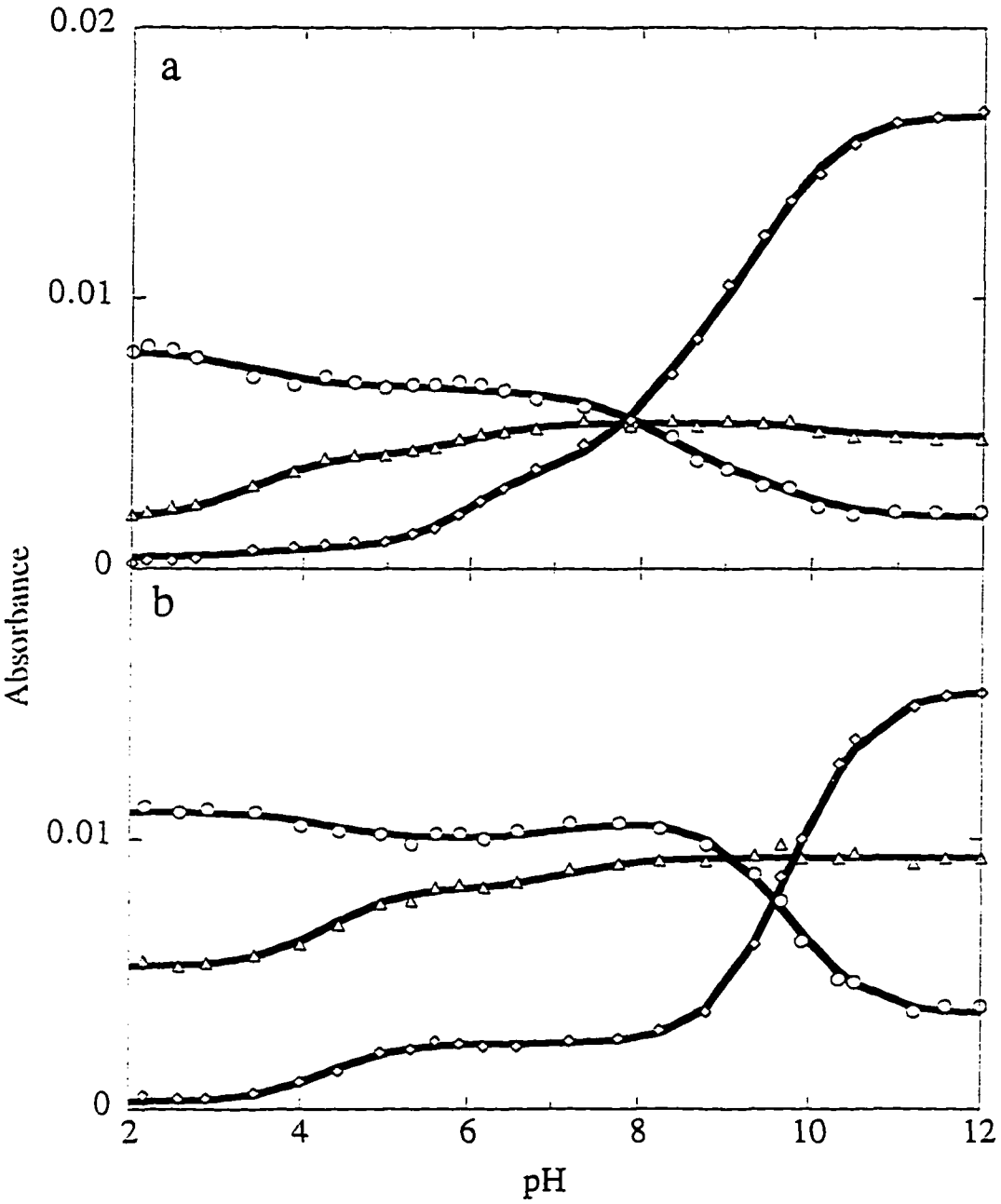

Figure 3. Measured absorbances (a) for CCE in 7:3 MeOH-water (v/v) at 312 nm (o), 358 nm (Δ), and 410 nm (◊), and (b) for FCE in 7:3 MeOH-water (v/v) at 322 nm (o), 344 nm (Δ), and 372 nm (◊) in the pH range of 2-12. Circles, triangles and diamonds represent experimental data and solid lines represent the simulated data. The uncertainty of the absorbance data is about the size of the symbols.

Table 2, which also includes the results of a study of ionic strength effects (see below) and comparison with the pK_a values for **1**, **2** and related functional analogs.

In agreement with the earlier interpretation of the optical data, the pK_a values for *p*-nitrophenol given in Table 2 support the general assignment of the processes at high pH to the transformation of the phenolic functional groups of CCE. However, the differences in the pK_a values for each of the steps indicates that a subsequent dissociative step initiates before completion of the ongoing step. These transformations, when coupled with the existence of tautomeric equilibria, hinder an overall structural description for each of the steps in the dissociation process. Nevertheless, each dissociative step can proceed through a variety of possible pathways, with the viability of each pathway dependent on the polarity and ionic strength of the solution. The existence of multiple pathways in the dissociation of CCE is evident from the spectral data shown in Figure 1a which reflects the conversion of H_4L^{2+} to H_3L^{+}. This series of spectra exhibit an increase in the absorbance at the absorbance maximum (410 nm) for the L^{2-} form of CCE that corresponds to ~10% conversion of the chromophoric side arms. This low level of conversion is inconsistent with a transformation that occurs solely through either of the two pathways in Scheme 3. Thus, the loss of the first proton from CCE yields both $H_3L''^{+}$ (~90%) and $H_3L'^{+}$ (~10%) as products.[49] These data also reveal that K_{a1}'' is greater than K_{a1}' by almost an order of magnitude and that K_{t1} is ~9.

(c) Effects of Ionic Strength and Identity of Cation. The effects of the ionic strength of the solution and of the identity of the cation on the acid-base chemistry of CCE and FCE have also been investigated. An assessment of the former provides insight into the

Table 1. Molar Absorptivities (ε x 10^{-3}, L mol^{-1} cm^{-1}) of CCE and FCE at selected wavelengths in 7:3 methanol-water (v/v).

species	CCE 312 nm	358 nm	400 nm
H_4L^{2+}	19.2	4.4	1.0
H_3L^{+}	16.2	10.0	1.8
H_2L	15.6	13.0	9.0
HL^{-}	9.0	13.0	22.2
L^{2-}	4.6	11.8	40.2
species	FCE 322 nm	344 nm	370 nm
H_4L^{2+}	25.7	12.3	0.6
H_3L^{+}	23.4	19.0	5.6
H_2L	25.1	21.7	5.6
HL^{-}	17.5	21.7	18.5
L^{2-}	8.2	21.7	36.2

possible pathways for the dissociation of the two species. A study of the latter probes the importance of cation uptake into the crown ether cavity on reactivity. The results of these experiments, which used $(CH_3)_4N^+$, Li^+, and Na^+ as cations and focused primarily on CCE, are summarized in Table 2.

The ionic strength dependences of the acid-base chemistry were examined using two different cations: $(CH_3)_4N^+$ and Li^+. In both cases, the pK_a values in the first, second and fourth dissociative steps exhibited an increase as the ionic strength of the methanolic solution increased, whereas the value for pK_{a3} remained essentially constant. The trends in the pK_{a1}, pK_{a2}, and pK_{a4} values can be qualitatively attributed to the relative stabilization of each of

Table 2. Acid Dissociation Constants for CCE, FCE, and Related Compounds in Solutions of Varied Ionic Strength and Cation Content.

compd	solvent	ionic strength (M)	cation	pK_{a1}	pK_{a2}	pK_{a3}	pK_{a4}
CCE	70%MeOH	.01-.035	$(CH_3)_4N^+$	3.42	6.00	8.15	9.65
CCE	70%MeOH	0.1	$(CH_3)_4N^+$	3.90	6.30	8.20	10.10
CCE	70%MeOH	0.1	Na^+	3.50	6.00	8.00	8.90
CCE	70% MeOH	0.01-0.1	Li+	3.60	6.20	8.15	9.75
CCE	70%MeOH	0.5-0.7	Li^+	3.95	6.48	8.10	10.15
1[a]	10%Dioxane	0.1	$(CH_3)_4N^+$	4.03	5.52	9.80	-
p-nitrophenol[b]	Water			7.15	-	-	-
p-nitrophenol[c]	70%MeOH	0.1	$(CH_3)_4N^+$	8.03	-	-	-
FCE	70%MeOH	.01-.035	$(CH_3)_4N^+$	4.30	7.21	9.35	10.05
FCE	70%MeOH	0.1	Na^+	4.80	6.40	8.30	10.00
FCE	70%MeOH	0.01-0.1	Li^+	4.40	7.00	9.65	10.40
2[d]	10%Dioxane			4.28	7.23	10.38	-
7-hydroxy-4-methylcoumarin[e]	Water			7.84	-	-	-
7-hydroxy-4-methyl coumarin[c]	70%MeOH	0.1	Na^+	8.80	-	-	-

[a] Reference 26. [b] Reference 46, p145. [c] Vaidya, B.; Porter, M., unpublished results. [d] Reference 33. [e] Moriya, T. *Bull. Chem. Soc. Jpn.* **1983**, 56, 6-14.

the possible species in each of the dissociative steps from microscopic charge considerations.[50] Thus, in agreement with the analysis of the optical data shown in Figure 1a, the transformation of H_4L^{2+} to H_3L^{+} leads primarily to $H_3L''^{+}$ (as opposed to $H_3L'^{+}$) as the more stable product. That is, the increase in the pK_{a1} with the increase in the ionic strength as observed for CCE in Table 2 argues that the higher ionic strength favors the protonated form (H_4L^{2+}) more than the deprotonated form (H_3L^{+}). Since $H_3L'^{+}$ has larger relative charge separation than H_4L^{2+}, $H_3L''^{+}$ should be the major species formed.

The second dissociative step, $H_3L^{+} \rightarrow H_2L$, can be analyzed in a similar, but more qualitative, manner. From the ionic strength dependences, there are two possible dominant pathways: $H_3L^{+'} \rightarrow H_2L''$ and $H_3L^{+''} \rightarrow H_2L'''$. Both pathways are expected to exhibit an increase in pK_a values with increasing ionic strength. The spectroscopic data reveal that ~30% of the chromogenic side arms have been affected by the transformation at the completion of the second dissociation step. Therefore, a large fraction (~70%) of H_2L must be present as H_2L'''. These data, together with the shift of tautomeric equilibria toward species with a lower charge as ionic strength decreases, indicate that H_2L''' and H_2L'' are present to a greater extent than H_2L'. These conclusions are consistent with the pathways predicted by the ionic strength dependences, although small contributions from the other two pathways are also possible.

The development of a description of the pathways for the third dissociative step is also hampered by the complexities affecting the above treatments. Based on the large relative amounts of H_2L''' and H_2L'' prior to dissociation and the virtual absence of an ionic

strength dependence of the pK_a values, it is likely that all three of the possible conversions are of importance. The collective result of these conversions yields roughly equal amounts of HL'^- and HL''^-, with HL''^- present at a marginally (a few percent) larger amount over HL'^-.

Lastly, the ionic strength dependences for the conversion of HL^- to L^{2-} indicate that the favored pathway is the conversion of HL'^- to L^{2-}. This finding suggests that the tautomeric conversion of HL''^- to HL'^- plays an obvious role in the process by the resupply of HL'^- when converted to L^{2-}.

The cation dependences reveal that the acid strengths of the ionizable protons in each of the steps are affected by Na^+, but not notably so by Li^+ and $(CH_3)_4N^+$. Comparisons of the sizes of each of these species to the cavity diameters of CCE and FCE reveal that Li^+ has an ionic diameter (1.80 Å[51]) smaller than that required for strong interactions within the cavity and that steric effects block the movement of $(CH_3)_4N^+$ (ionic diameter of 4.30 Å[51]) into the cavity. On the other hand, the uptake of Na^+ (ionic diameter of 2.32 Å[51]) is driven in part by a more favorable size match up with the cavity of the parent crown ether, 18-crown-6 (diameter 2.68-2.86 Å[52]). This added driving force results in the uptake of Na^+ by CCE, which induces an effective decrease in the pK_a value. Thus, the pK_a data obtained using Li^+ and $(CH_3)_4N^+$ more accurately reflect the intrinsic reactivity of each of the dissociative steps. We believe that similar arguments apply to an acid-base reactivity description of FCE.

In closing this section, we note that only three acid-base transitions have been reported for **1** and **2**, and structurally related compounds.[26,27,33] It is not yet clear whether these differences reflect the inherent reactivity of the compounds or the properties of the

solvent system (e.g., the 7:3 MeOH-water solvent system used herein and the 1:9 dioxane-water solvent system utilized in the studies of **1**[26] and **2**[33]).

Metal Ion Extraction. (a) Equilibrium Formulation. Capabilities of CCE and FCE for extraction of divalent metal cations into 1,2-dichloroethane were tested. As a starting point, the overall equilibrium for the extraction of a metal ion by a proton-ionizable crown ether is considered. A generalized description of the overall process is shown in Scheme 4, which depicts the transfer of the neutral extractant from the organic phase to the aqueous phase, the multi-step ionization and metal ion complexation in the aqueous phase, and the movement of the neutral complex (ML) into the organic phase. The equilibrium between H_2L in an organic phase and a divalent metal cation, M^{2+}, in aqueous phase can then be described as:

$$[H_2L]_o + [M^{2+}]_{aq} = [ML]_o + 2[H^+]_{aq} \qquad (15)$$

where $[H_2L]_o$ and $[ML]_o$ are the equilibrium concentrations of H_2L and ML in the organic phase and $[M^{2+}]_{aq}$ and $[H^+]_{aq}$ are the equilibrium concentrations of M^{2+} and H^+ in the aqueous phase, respectively. The extraction constant for this equilibrium, K_{ex}, is written as:

$$K_{ex} = \frac{[ML]_o [H^+]_{aq}^2}{[H_2L]_o [M^{2+}]_{aq}} \qquad (16)$$

This equation can be recast to give:

$$\log K_{ex} = \log q - 2\,pH - \log[M^{2+}]_{aq} \qquad (17)$$

Scheme 4

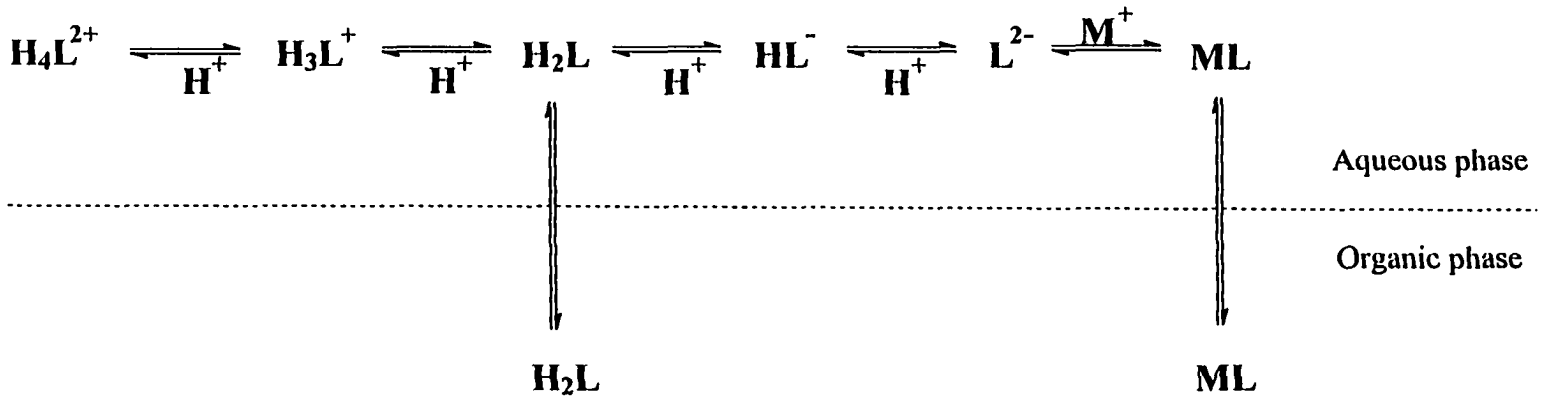
H_4L^{2+}
H^+
H_3L^+
H^+
H_2L
H^+
HL^-
H^+
L^{2-}
M^+
ML
Aqueous phase
Organic phase
H_2L
ML

where $q = [ML]_o / [H_2L]_o$.

(b) Metal Ion Extraction. Figures 4-6 summarize the extraction data of CCE and FCE for Ba(II), Ca(II), Cd(II), Cu(II), Hg(II), Pb(II), and Sr(II). Figure 4 shows the absorption spectra of CCE in 1,2-dichloroethane before (spectrum a) and after extraction of Hg(II) (spectra b-i) as a function of the pH of the aqueous solution. The pH was varied incrementally between 2 and 4. Formation of the complex results in a bathochromic shift in the spectrum and an increase in molar absorptivity as compared to the spectrum of uncomplexed CCE. Increasing the pH of the aqueous solution enhances formation of the complex, which reaches a maximum at ~pH 4. The absorbance maximum of the complex is 388 nm and has an ε of 4.1×10^4 L mol^{-1} cm^{-1}. An isosbestic point at 348 nm confirms the existence of only two forms of CCE in the organic phase as well as the negligible loss of CCE to the aqueous phase during the extraction process.

The complexes formed by CCE and FCE with the other metal ions exhibit similar spectral characteristics, but have different pH dependences. For example, Figure 5 presents the pH dependent absorption spectra of FCE in 1,2-dichloroethane before and after the extraction of Cd(II). Changes in the spectra are similar to those noted in Figure 4. In the case of Cd(II), however, the uptake by FCE as well as by CCE (see below) occurs at higher pH values, which translates to lower values for K_{ex}.

Figures 6a and 6b summarize the pH dependences of the metal complexation for CCE and FCE, respectively. For each of the cations, the plots of log q exhibit a linear dependence on pH with a nominal slope of 2. This dependence confirms the general applicability of

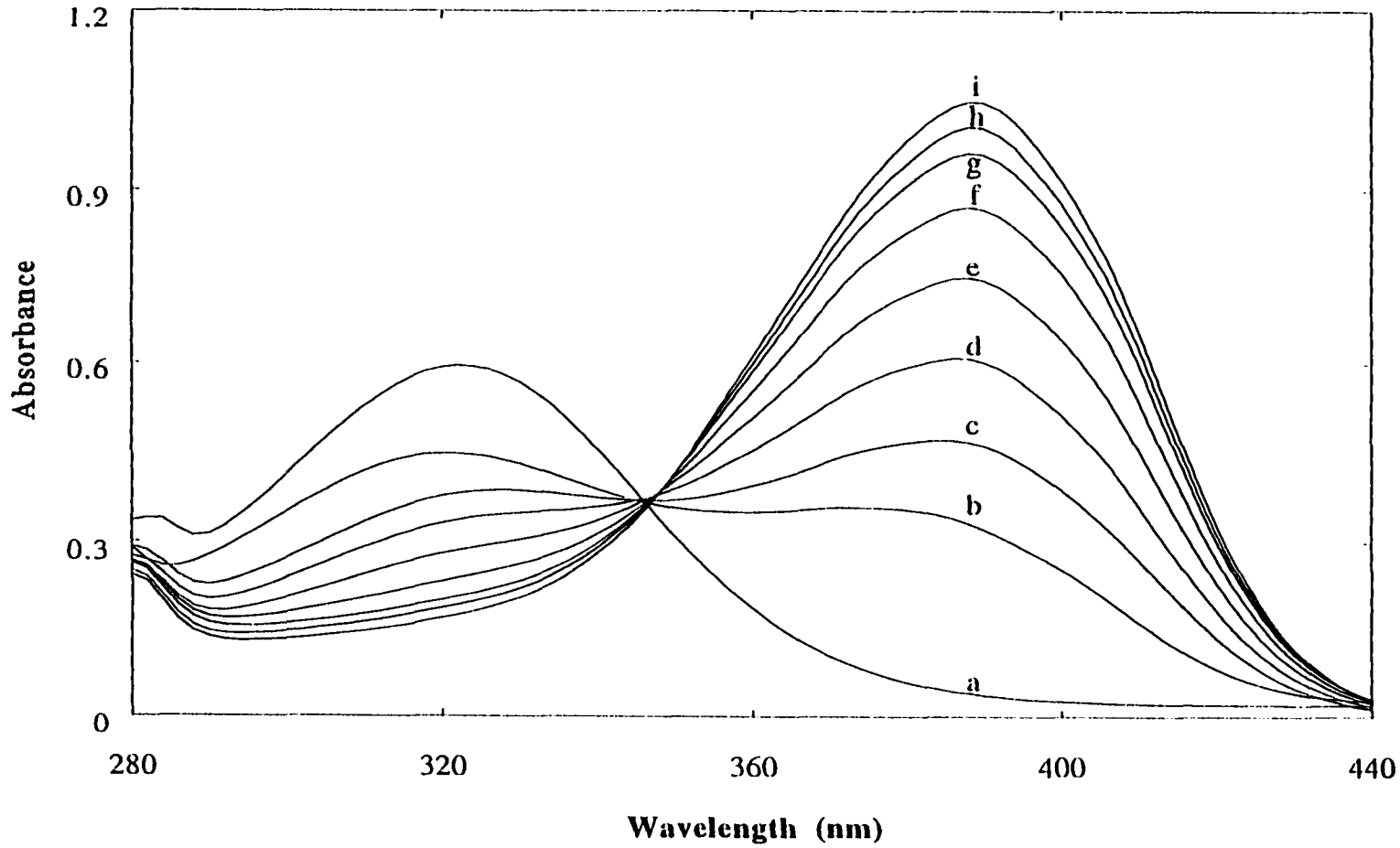

Figure 4. Absorbance spectra for 25 μM CCE solutions in 1,2-dichloroethane before (a) and after extraction of Hg(II) from an aqueous 1.0 mM Hg(II) solution at pH: 2.0 (b), 2.2 (c), 2.5 (d), 2.7 (e), 3.0 (f), 3.2 (g), 3.4 (h) and 3.9 (i).

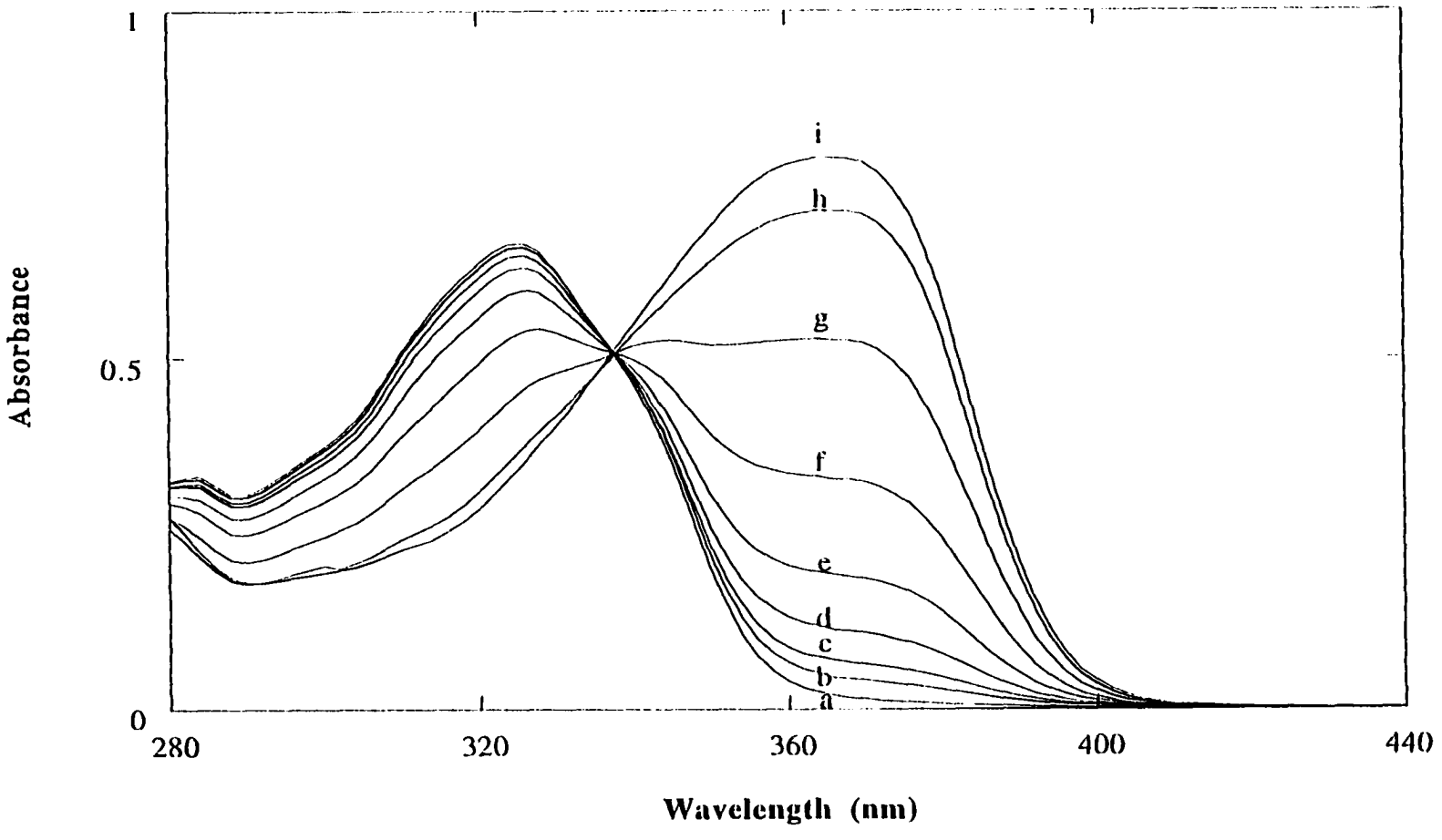

Figure 5. Absorbance spectra for 25 μM FCE solutions in 1,2-dichloroethane before, (a) and after extraction of Cd(II) from aqueous 1 mM Cd(II) solution at pH: 5.8(b), 6.0(c), 6.3(d), 6.5 (e), 6.8 (f), 7.0 (g), 7.3 (h) and 7.6 (i).

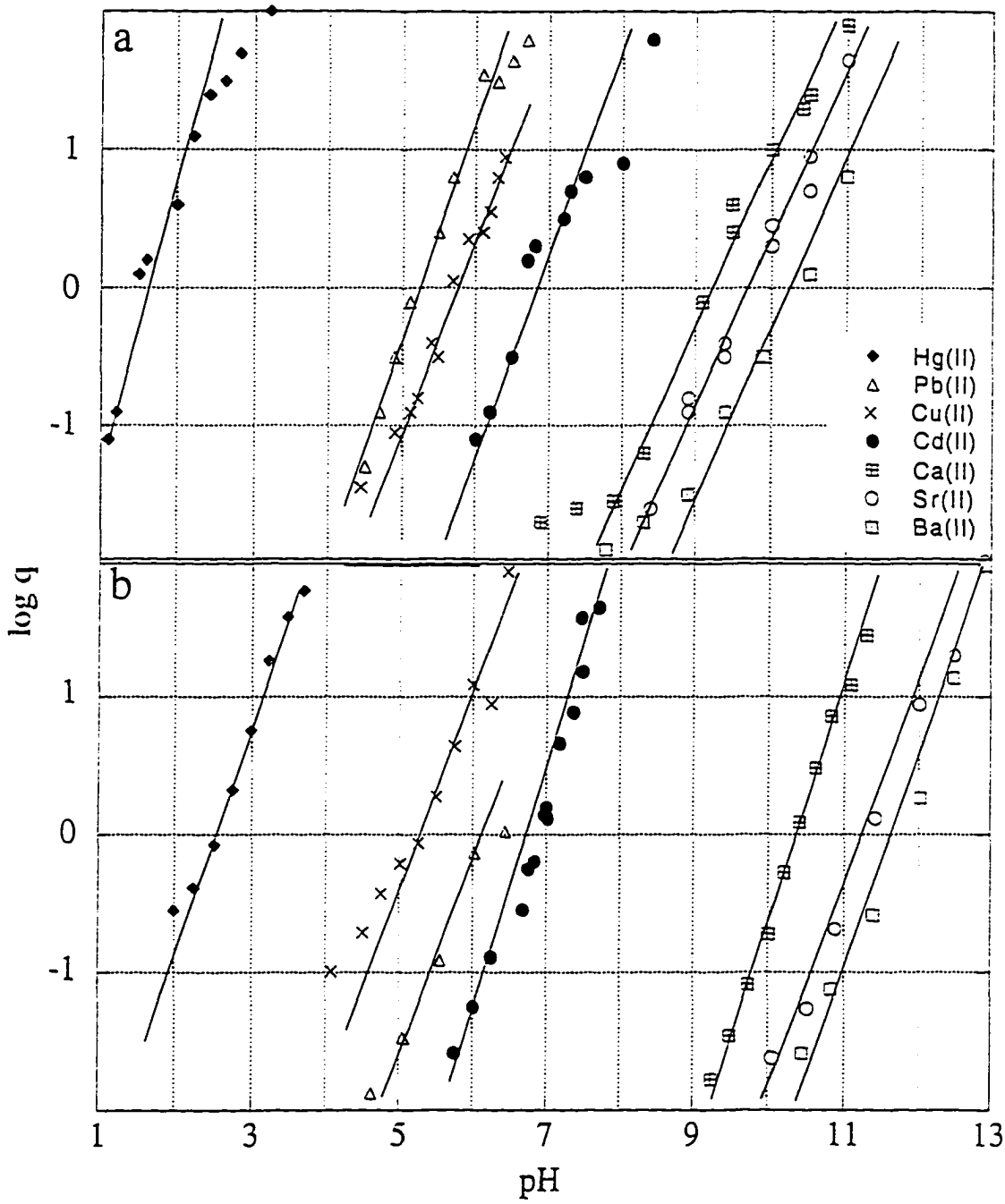

Figure 6. Selectivity of CCE (a), and FCE (b) shown by log ($[ML]_o/[H_2L]$) vs. pH plots where, M(II) is Hg(II), Pb(II), Cu(II), Cd(II), Ca(II), Sr(II), Ba(II).

Equation 15 in describing the extraction process. The changes in the spectral properties of the chelates upon complexation, which are similar to those observed for the dissociation of the phenolic protons of H_2L to L^{2-} in Figures 1 and 2, are consistent with this conclusion.

The pH dependences of log q shown in Figure 6 can be used to calculate the values of K_{ex} for each of the metal ions with CCE and FCE. These data are presented in Table 3, together with reported values for **1**[31] and **2**.[35] CCE and FCE display similar, but not identical binding preferences. For CCE, the order is Hg(II) > Pb(II) > Cu(II) > Cd(II) > Ca(II) > Sr(II) > Ba(II). The order for FCE is Hg(II) > Cu(II) > Pb(II) > Cd(II) > Ca(II) > Sr(II) > Ba(II). The selectivity of CCE for Hg(II) over the next best extracted cation, Pb(II), is 2 X 10^7 and that for FCE for Hg(II) over the next best extracted cation, Cu(II) is 5 X 10^6. Both values reflect unprecedented selectivities for Hg(II). Comparisons to the K_{ex} values for **1** and **2** further reveal that both CCE and FCE have significantly greater binding strengths for Hg(II), suggesting an opportunity for these novel crown ethers in chemical analysis (see below).

Insights into the complexation properties of CCE and FCE towards Hg(II) can be developed by comparison with those of **1** and **2**. With the important exception of Hg(II), the orders of preference toward metal ion binding for CCE and **1** are the same. However, the binding by CCE of cations other than Hg(II) is notably weaker than that of **1**. The same conclusion, based on a more limited comparison of divalent metal ion species, is applicable for FCE relative to **2**. These differences in binding reflect a complex mixture of chemical and structural effects[37] which include the relative sizes of the crown ether ring and the cation, the size and spatial orientation of the side arms, and the relative hardness/softness of the

Table 3. Extraction Constants and selectivity Factors of CCE, FCE, 1, and 2 for Ba(II), Ca(II), Cd(II), Cu(II), Hg(II), Pb(II), and Sr(II).

	-log K_{ex}				Selectivity Factor[a]		
Metal Ion	CCE	1[b]	FCE	2[c]	CCE	FCE	1
Hg(II)	0.28	5.8	2.20	d	1	1	1
Pb(II)	7.58	5.4	8.92	d	2.0×10^7	5.2×10^6	0.4
Cu(II)	8.52	5.6	7.94	d	1.7×10^8	8.7×10^5	0.6
Cd(II)	10.50	8.4	10.80	d	1.6×10^{10}	4.0×10^8	4.0×10^2
Ca(II)	15.30	12.5	16.70	14.7	6.8×10^{15}	3.2×10^{14}	5.0×10^6
Sr(II)	16.40	13.5	19.10	16.1	1.3×10^{16}	7.9×10^{16}	5.0×10^7
Ba(II)	17.70	15.1	20.70	17.1	2.7×10^{17}	3.2×10^{18}	2×10^{10}

[a] Selectivity factor = K_{ex} (Hg) /K_{ex} (M(II)). [b] Reference 31. [c] Reference 35. [d] Data not available.

interactions of the active groups in the cavity. We attribute the generally lower K_{ex} values of CCE and FCE relative to **1** and **2**, respectively, to the increased rigidities of the cavities of CCE and FCE that result from the incorporation of the two benzo groups into the ring. This stiffening represents a barrier to the adaptation of a structural arrangement favorable for interaction of CCE and FCE with metal ions. On the other hand, the reduction of electron density at the four alkyl-aryl ether oxygens due to delocalization by resonance into the benzo group substituents of CCE and FCE provides for softer ring oxygen binding sites that enhance the extraction of the soft metal Hg(II). Together, these effects result in the *remarkable selectivity* of CCE and FCE towards Hg(II).

The differences in the K_{ex} values of CCE and FCE can also be ascribed to steric effects that are coupled with chemical affinity issues. With the exception of Cu(II), the K_{ex} values of CCE for all of the metal ions examined are larger than those of FCE. The differences for each metal ion reflect contributions from the steric hindrance imposed by the more bulky side arms and the weaker acidity of the phenol functional groups of the side arms of FCE. We attribute the favored uptake of Cu(II) by FCE (as opposed to Pb(II)) to the smaller size of Cu(II), which reduces the steric barrier for complexation.

Potential Applications. The extraction data suggest the potential application of CCE and FCE as reagents for the selective detection of Hg(II) ion. With CCE, such an application would be developed using absorbance-based measurements, whereas FCE offers the possibility of fluorescence detection. In the latter case, we envisioned the selective extraction of the Hg(II):FCE species, which has its absorbance maximum shifted to longer wavelength

by ~60 nm from that of unbound FCE. Such a strategy could then take advantage of the enhanced detection capabilities of fluorescence as opposed to absorbance based technique . Unfortunately, as is usually the case,[53,54] we have found that the fluorescence of FCE is quenched by the uptake of Hg(II), as well as by Pb(II) and Cu(II). In contrast, the fluorescence is not quenched by the complexation of Cd(II), Ca(II), Sr(II), and Ba(II). Based on these observations, it is likely that the quenching of fluorescence by Hg(II), Pb(II), and Cu(II) results from the heavy atom effect via spin orbital coupling.[54] Although, FCE could still be used in a determination of Hg(II) by absorbance measurements, it was more difficult to synthesize than CCE. However, FCE could be used in determination of Cd(II) and the alkaline earth cations by fluorescence in the presence of Hg(II), Pb(II), and Cu(II) since the complexes of the latter do not fluoresce. Figure 7 shows excitation and emission spectra of FCE solution in 1,2-dichloroethane before and after extraction of Cd(II) from aqueous solutions at different pH values. The limit of detection of Cd(II) calculated using standard solutions buffered at pH 8.0 at a signal-to-noise ratio of 3, is 6 ppb.

Studies of the use of CCE for the selective extraction of Hg(II) into an organic phase like 1,2-dichloroethane revealed a linear calibration curve between 0.2 and 5.0 ppm Hg(II). These tests were conducted using a 25 μM CCE solution to extract Hg(II) from a solution buffered at pH 5.0. Estimated detection limits are ~0.2 ppm at a signal to noise ratio of 3:1. Under this condition, even millimolar Ca(II), Sr(II), and Ba(II) did not exhibit a detectable interference at the detection limit. However, as expected from Figure 6b, the presence of 100 μM Cd(II) and Pb(II) lead to an increase in absorbance by ~20% for a 0.2 ppm Hg(II)

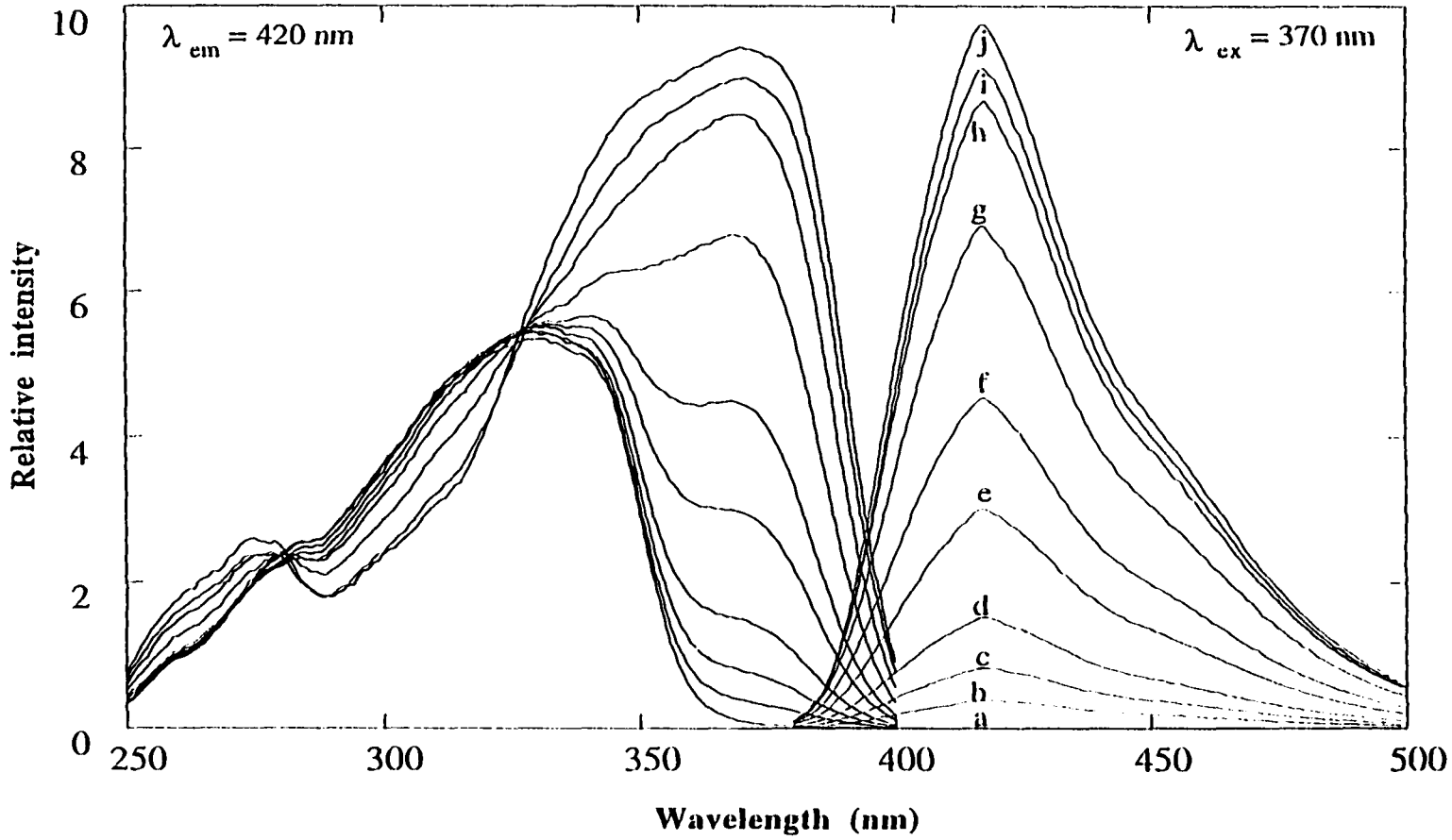

Figure 7. Excitation and emission spectra for 25 μM solutions of FCE before, (a), and after extraction of Cd(II) from aqueous solutions at pH: 5.6 (b), 5.8 (c), 6.0 (d), 6.3 (e), 6.5 (f), 6.8 (g), 7.0 (h), 7.3 (i) and 7.6 (j). Both the excitation and emission spectra of FCE equilibrated with aqueous solution buffered in the pH range of 5-8 were identical.

solution. These contributions however, can be reduced by performing the extraction at a lower pH of the aqueous sample. In addition to other metal ions, some anions are potential interferants for the determination of Hg(II) with CCE. Chloride ion at 100 μM resulted in a decrease in absorbance of ~30% in the determination of 0.2 ppm (1 μM) Hg(II).

CONCLUSIONS

This joint effort has demonstrated that the novel crown ether compounds, CCE and FCE, exhibit a remarkable selectivity in the binding of Hg(II) over a host of other divalent metal cations (i.e., Pb(II), Cu(II), Cd(II), Ca(II), Sr(II), and Ba(II)). These improved selectivities are attributed to the reduced basicity of the ring oxygen and enhanced rigidity of the crown ether ring through the incorporation of benzo groups in the ring structure. Efforts are presently underway to harness this selectivity for the development of new methods for Hg(II)-determinations based on conventional solvent extraction principles. Possible extensions to chemical sensor applications are also under consideration.

ACKNOWLEDGMENT

Research conducted at Iowa State University was supported by the Office of Basic Energy Research-Chemical Sciences Division of the U.S. Department of Energy-Ames Laboratory, Center for Advanced Technology Development and by the Microanalytical Instrumentation Center of ISU. Research conducted at Texas Tech University was supported by the Division of Chemical Sciences of the Office of Basic Energy Sciences of the U.S. Department of Energy (Grant DE-FG03-94ER14416 and earlier grants). RAB expresses his appreciation to Professor Makoto Takagi of Kyushu University for sharing the experimental

details for the synthesis of **2**. The Ames Laboratory is operated for the U.S. Department of Energy by ISU under contract No. W-7405-eng-82.

REFERENCES AND NOTES

(1) Pedersen, C. J. *J. Am. Chem. Soc.* **1967**, *89*, 7017-7036.

(2) Bradshaw, J. S. In *Synthetic Multidentate Macrocyclic Compounds*; R. M. Izatt and J. J. Christensen, Eds.; Academic Press: New York, 1978, pp 53-109.

(3) Gokel, G. W.; Korzeniowski, S. H. *Reactivity and Structure Concepts in Organic Chemistry*; Springer-Verlag: New York, 1982; Vol. 13.

(4) Frensdorff, H. K. *J. Am. Chem. Soc.* **1971**, *93*, 4684-4688.

(5) Pannell, K. H.; Hambrick, D. C.; Lewandos, G. S. *J. Organometal. Chem.* **1975**, *99*, C21-C23.

(6) Danesi, P. R.; Meider-Gorican, H.; Chiarizia, R.; Scibona, G. *J. Inorg. Nucl. Chem.* **1975**, *37*, 1479-1483.

(7) Danesi, P. R.; Chiarizia, R.; Saltelli, A. *J. Inorg. Nucl. Chem.* **1978**, *40*, 1119-1123.

(8) Sadakane, A.; Iwachido, T.; Toei, K. *Bull. Chem. Soc. Jpn.* **1975**, *48*, 60-63.

(9) Bartsch, R. A.; Czech, B. P.; Kang, S. I.; Stewart, L. E.; Walkowiak, W.; Charwicz, W. A.; Heo, G. S.; Son, B. *J. Am. Chem. Soc.* **1985**, *107*, 4997-4998.

(10) Katalnikov, S. G.; Mysheltsov, I. A. *Tr. Inst.-Mosk. Khim.-Tekhnol. Inst. im. D. I. Mendeleeva* **1989**, *156*, 3-24.

(11) Ryba, O.; Petranek, J. *Talanta* **1976**, *23*, 158-159.

(12) Rechnitz, G. A.; Eyal, E. *Anal. Chem.* **1972**, *44*, 370-372.

(13) Patranek, J.; Ryba, O. *Anal. Chim. Acta* **1974**, *72*, 375-380.

(14) Mascini, M.; Pallozzi, F. *Anal. Chim. Acta* **1974**, *73*, 375-382.

(15) Hiroka, M. *Crown Compounds: Their Characteristics and Applications*; Elsevier: Amsterdam, 1982; Vol. 12, pp 151-213.

(16) Sanz-Medel, A.; Gomis, D. B.; Alvarez, J. R. G. *Talanta* **1981**, *28*, 425-430.

(17) Sanz-Medel, A.; Gomis, D. B.; Fuente, E.; Jimeno, S. A. *Talanta* **1984**, *31*, 515-519.

(18) Nazarenko, A. Y.; Pyatnitskii, I. V.; Stolyarchuk, T. A. *Zhur. Anal. Khim.* **1981**, *36*, 1719-1721.

(19) Sumiyoshi, H.; Nakahara, K.; Ueno, K. *Talanta* **1977**, *24*, 763-765.

(20) Pyatnitskii, I. V.; Nazarenko, A. Y. *Russian J. Inorg. Chem.* **1980**, *25*, 592-594.

(21) Abrodo, P. A.; Gomis, D. B.; Sanz-Medel, A. *Microchem. J.* **1984**, *30*, 58-70.

(22) Jawaid, M.; Ingman, F. *Talanta* **1978**, *25*, 91-95.

(23) Nishida, H.; Tazaki, M.; Takagi, M.; Ueno, K. *Mikrochim. Acta* **1981**, *1*, 281-287.

(24) Nishida, H.; Katayama, Y.; Katsuki, H.; Nakamura, H.; Takagi, M.; Ueno, K. *Chem. Lett.* **1982**, 1853-1854.

(25) Nakamura, H.; Nishida, H.; Takagi, M.; Ueno, K. *Anal. Chim. Acta* **1982**, *139*, 219-227.

(26) Shiga, M.; Nishida, H.; Nakamura, H.; Takagi, M.; Ueno, K. *Bunseki Kagaku* **1983**, *32*, E293-E300.

(27) Takagi, M.; Ueno, K. *Top. Curr. Chem.* **1984**, *121*, 39-65.

(28) Katayama, Y.; Nita, K.; Ueda, M.; Nakamura, H.; Takagi, M. *Anal. Chim. Acta* **1985**, *173*, 193-209.

(29) Sasaki, K.; Pacey, G. *Anal. Chim. Acta* **1985**, *174*, 141-149.

(30) Kimura, K.; Tanaka, M.; Kitazawa, S.; Shono, T. *Chem. Lett.* **1985**, 1239-1240.

(31) Sakai, Y.; Kawano, N.; Nakamura, H.; Takagi, M. *Talanta* **1986**, *33*, 407-410.

(32) Katayama, Y.; Fukuda, R.; Takagi, M. *Anal. Chim. Acta* **1986**, *185*, 295-306.

(33) Takagi, M.; Nakamura, H. *J. Coord. Chem.* **1986**, *15*, 53-82.

(34) Kimura, K.; Tanaka, M.; Shono, T. *Bull. Chem. Soc. Jpn.* **1987**, *60*, 3068-3070.

(35) Katayama, Y.; Fukuda, R.; Iwasaki, T.; Nita, K.; Takagi, M. *Anal. Chim. Acta* **1988**, *204*, 113-125.

(36) Czech, B. P.; Babb, D. A.; Czech, A.; Bartsch, R. A. *J. Heterocyclic Chem.* **1989**, *26*, 199-203.

(37) Takagi, M. In *Cation Binding by Macrocycles*; Y. Inoue and G. W. Gokel, Eds.; Dekker: New York, 1990; pp 465-495.

(38) Brown, P. R.; Bartsch, R. A. In *Topics in Inclusion Science*; T. Osa and J. L. Atwood, Eds.; Kluwer Academic Publishers: Dordrecht, 1991; Vol. 2; pp 1-57.

(39) Wilcox, K.; Pacey, G. E. *Talanta* **1991**, *38*, 1315-1324.

(40) Blair, T. L.; Desai, J.; Bachas, L. G. *Anal. Lett.* **1992**, *25*, 1823-1834.

(41) Graf, E.; Lehn, J. M. *Helv. Chim. Acta* **1981**, *64*, 1051-1065.

(42) Pettit, G. R.; Chamberland, M. R.; Green, B. *Can. J. Chem.* **1967**, *45*, 1555-1560.

(43) Crossland, R. K.; Servis, K. L. *J. Org. Chem.* **1970**, *35*, 3198-3196.

(44) Högberg, S. A. G.; Cram, D. J. *J. Org. Chem.* **1975**, *40*, 151-152.

(45) Feiser, L. F.; Feiser, M. In *Reagents for Organic Synthesis*; Wiley: New York, 1970; Vol. 1, pp 1030-1033.

(46) Albert, A.; Serjeant, E. P. *The Determination of Ionization Constants: A Laboratory Manual;* 3rd ed.; Chapman and Hall: New York, 1984, pp 126-134.

(47) Koshland, D. E., Jr.; Karkhanis, Y. D.; Latham, H. G. *J. Am. Chem. Soc.* **1964**, *86*, 1448-1450.

(48) Albert, A.; Serjeant, E. P. *The Determination of Ionization Constants: A Laboratory Manual;* 3rd ed.; Chapman and Hall: New York, 1984, pp 70-73.

(49) We also attempted to investigate the structural detail of these transformations using infrared Fourier-transform spectroscopy. Unfortunately, the low solubility of both CCE and FCE precluded detection of any N-H vibrational modes, features which would have aided our assessment.

(50) Finston, H. L.; Rychtman, A. C. *A New View of Current Acid-Base Theories*; Wiley: New York, 1982.

(51) Huheey, J. E. *Inorganic Chemistry*; Harper & Row: New York, 1983, pp 73-78.

(52) Lamb, J. D.; Izatt, R. M.; Christensen, J. J. In *Progress in Macrocyclic Chemistry*; R. M. Izatt and J. J. Christensen, Ed.; Wiley: New York, 1981; Vol. 2; pp 41-90.

(53) Becker, R. S.; Allison, J. B. *J. Phys. Chem* **1963**, *67*, 2662-2669.

(54) McGlynn, S. P.; Azumi, T.; Kinoshita, M. In *Molecular Spectroscopy of The Triplet State* Prentice-Hall: Englewood Cliffs, New Jersey, 1969; pp 261-283.

CHAPTER 3. SELECTIVE DETERMINATION OF CADMIUM IN WATER USING A CHROMOGENIC CROWN ETHER IN A MIXED MICELLAR SOLUTION

A paper submitted to *Analytical Chemistry*

Bikas Vaidya*, Marc D. Porter*, Marty D. Utterback† and Richard A. Bartsch†

ABSTRACT

The chromogenic crown ether *N,N'*-bis(2-hydroxy-5-nitrobenzyl)-4,13-diazadibenzo-18-crown-6 (CCE) has been solubilized in a mixed micellar solution of sodium dodecyl sulfate (SDS) and cetyl pyridinium chloride (CPC) and tested for selective determination of heavy metal ions. The optical properties, acid-base equilibria, and metal ion binding capabilities of the micellar solubilized CCE for Ba(II), Ca(II), Cd(II), Cu(II), Hg(II), Pb(II), and Sr(II) are reported. Results show that the micellar solubilized CCE binds Hg(II) ~ Cd(II) > Ca(II) > Sr(II), whereas the presence of Pb(II) and Ba(II) leads to precipitate formation. There was no detectable binding with Cu(II). Based on these results, a spectrophotometric determination for Cd(II) that utilizes chloride ions to mask Hg(II) has been devised and evaluated.

---

* Microanalytical Instrumentation Center, Ames Laboratory USDOE, and Department of Chemistry, Iowa StateUniversity, Ames, IA 50011

† Department of Chemistry and Biochemistry, Texas Tech University, Lubbock, TX 79409

INTRODUCTION

We have recently demonstrated the application of the chromogenic crown ether *N,N'*-bis(2-hydroxy-5-nitrobenzyl)-4,13-diazadibenzo-18-crown-6 (CCE) and the fluorogenic crown ether *N,N'*-bis(7-hydroxy-4-methylcoumarin-8-methylene)-4,13-diazadibenzo-18-crown-6 (FCE) for the extraction and determination of heavy metals.[1] Using 1,2-dichloroethane as the organic phase in a two-phase extraction process, we found that both CCE and FCE formed stable complexes with a range of divalent metal cations, including Ba(II), Ca(II), Cd(II), Cu(II), Hg(II), Pb(II), and Sr(II). Importantly, the selectivities of CCE and FCE for Hg(II) over the next best extracted cations (i.e., Pb(II), Cu(II), and Cd(II)) were greater than 10^6.

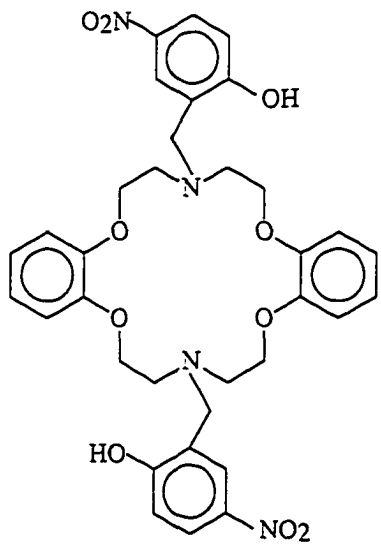

CCE

This paper reports on our exploration of different surfactant-derived micelles as solubilization carriers for CCE and its corresponding metal ion complexes in aqueous solutions. The main objective of this study was to facilitate the use of CCE for metal ion determinations by reducing the lengthy processing associated with the above two-phase extraction process. To this end, we tested the utility of single-component and two-component micelles formed from cationic (cetyl pyridinium chloride, CPC), anionic (sodium dodecyl sulfate, SDS), and nonionic (Triton X-100, TTN) surfactants as solubilizing agents for CCE and the resulting metal complexes in aqueous solutions. This paper presents these findings, including the ionization behavior and metal ion binding capabilities for CCE solubilized by the different micelles and a comparison of the reactivities of the micellar solubilized CCE to those found in our earlier two-phase extraction study.

EXPERIMENTAL SECTION

Reagents and Instrumentation. The synthesis of CCE has been described previously.[1] Reagent-grade inorganic and organic chemicals were obtained from commercial suppliers and used without purification. All aqueous solutions were prepared with distilled water that was subsequently deionized using a Millipore Milli-Q Water System.

Determinations of pH were performed with an Orion Research Digital Ionalyzer (Model 501) and an Orion combination glass pH electrode (Model 91-04). Absorbance measurements were conducted with a computer-controlled Hewlett Packard diode array spectrophotometer (HP8453) at a spectral resolution of 1 nm and integration time of 2 s.

Synthesis of CCE Disodium Salt. CCE[1] (1.88 g) was stirred in 0.05 N aqueous NaOH followed by extraction with 1,2-dichloroethane (5 x 50 mL), drying of the organic layer with sodium sulfate, and evaporation of the solvent in vacuo to give 1.70 g (86%) of the disodium salt of CCE with mp 170-172 °C (decomp.). IR (KBr): 1333 (NO_2), 1126 (C-O) cm^{-1}. ^1H NMR (DMSO-d_6): δ 2.98(br s, 8H0, 3.69 (br s, 4H), 4.12 (br s, 8H), 6.31 (d, 2H, J=9.2Hz), 6.7-7.0 (m, 8H), 7.72 (d of d, 2H, J_o=9.2 Hz, J_m=2.9 Hz), 7.98 (d, 2H, J_m=2.7 Hz). Anal. Calcd for $C_{34}H_{34}N_4Na_2O_{10}$: C, 57.96; H, 4.86. Found: C, 57.93; H, 4.98.

Determination of Equilibrium Constants. Acid dissociation constants (K_{ai}) were determined by an analysis of the spectral data for CCE in the aqueous micellar solutions buffered with hydrochloric acid, citric acid, and boric acid, each present at a concentration of 0.01 M. In all cases, the pH of the solution was adjusted by addition of either lithium hydroxide or sodium hydroxide.

Formation constants (K_{fi}) for metal ion binding were determined in the micellar solutions from the spectroscopically-derived concentrations of the metal complexes and unbound CCE as a function of pH using the same buffer systems employed in the determination of the values of K_{ai}. These measurements were conducted with a large excess of each metal ion, ensuring that changes in the concentrations of uncomplexed metal ions were negligible.

RESULTS AND DISCUSSION

Micellar Solubilization Characterizations. As a starting point, we tested the ability of CPC, TTN, and SDS to form single-component micelles that were effective in solubilizing

the neutral form of CCE as well as in supporting the metal ion binding capabilities of the solubilized CCE. These tests were conducted using the divalent metal cations Ba(II), Ca(II), Cd(II), Cu(II), Hg(II), Pb(II), and Sr(II) at surfactant concentrations (i.e., 0.01 to 0.10 M) well above the critical micelle concentration (cmc) for each surfactant.[2] Of the three surfactants, only the micellar solution composed of SDS was effective in solubilizing CCE and the resulting metal ion complexes in aqueous solution; there were no detectable enhancements in the concentration of CCE using either the CPC- or TTN-derived micelles in comparison to aqueous solutions devoid of surfactants. We also found that the solutions prepared at SDS concentrations between ~10 and 50 mM exhibited the most reproducible extent of metal ion binding by solubilized CCE. However, precipitates were formed in these solutions within 4-6 hours after preparation.

In an attempt to alleviate the above instability, the applicability of mixed micelles prepared from different binary combinations of SDS, CPC, and TTN was explored, drawing on earlier literature precedents.[3-12] This investigation revealed that a mixed micelle of CPC and SDS resulted in a CCE-solubilized solution that was stable for several days, effectively bound most of the noted divalent metal ions, and reached equilibrium with the metal ions within a few seconds after mixing the metal ion solutions with the micellar solutions. This mixed micelle was formed first by solubilizing the disodium salt of CCE (5-10 μM) in a CPC-containing (0.10 M) solution of chloroform, and then adding a small aliquot of the resulting solution to an aqueous SDS (50 mM) solution. Dilutions in the last step were generally ~50-fold. Interestingly, the solubilized form of the disodium salt of CCE, which

was prepared in a CPC-containing chloroform solution that was subsequently added as a small aliquot to an aqueous micellar CPC solutions, was ionizable via acid-base chemistry, but did not detectably bind metal ions. We do not yet have an explanation as to why the CPC/SDS mixed micelle proved more viable for our application than the micelles prepared from only SDS or CPC.

Based on the above findings, the remainder of this paper evaluates the utility of CCE solubilized in CPC/SDS mixed micelles for determination of divalent metal ions. The next sections describe the optical characteristics and acid-base properties of the micellar solubilized CCE, the results from the metal ion binding evaluations, and comparisons to the reactivities of CCE reported in our earlier two-phase extraction study.[1] In the last section, a spectrophotometric determination of Cd(II) using CCE solubilized in mixed micelles is devised and evaluated.

Acid-Base Equilibria and Optical Characteristics. We previously reported that CCE behaves as a polybasic acid, existing in dicationic, cationic, neutral, anionic, and dianionic protonic states.[1] The stepwise acid-base equilibria for CCE can be written as shown in eqs 1-4.

$$H_4L^{2+} = H_3L^{+} + H^{+} \qquad (1)$$

$$H_3L^{+} = H_2L + H^{+} \qquad (2)$$

$$H_2L = HL^{-} + H^{+} \qquad (3)$$

$$HL^- = L^{2-} + H^+ \quad (4)$$

Thus, the neutral form (H_2L) of CCE can be successively protonated to its mono- (H_3L^+) and di- (H_4L^{2+}) cationic forms, or successively deprotonated to its mono- (HL^-) and dianionic (L^{2-}) forms. The corresponding acid dissociation constants (K_{ai}) for eqs 1-4 can be formulated in terms of concentrations (assuming activity coefficients of unity) as:

$$K_{a1} = [H_3L^+][H^+] / [H_4L^{2+}] \quad (5)$$

$$K_{a2} = [H_2L][H^+] / [H_3L^+] \quad (6)$$

$$K_{a3} = [HL^-][H^+] / [H_2L] \quad (7)$$

$$K_{a4} = [L^{2-}][H^+] / [HL^-] \quad (8)$$

At a more detailed structural level, however, the formation of zwitterions is possible, a situation that would lead to a more complex multi-component equilibrium. Zwitterions can arise if the phenolic groups of the side arms are stronger acids than the amine groups of the diazacrown ether portion of CCE.[13] In addition, the presence of the two pairs of amine-phenol groups in CCE can lead to a variety of tautomeric species. As a consequence of the tautomeric equilibria, the acid dissociation constants defined by eqs 5-8 are the sum of the acid dissociation constants for the tautomers involved in each of the possible protonic states.[1,13] The formation of both zwitterions and tautomers have been examined in detail in our earlier study of CCE.[1]

Figure 1 presents a series of spectra for CCE in the mixed CPC/SDS micellar solution in the pH range from 2 to 12. At pH 2 and below (Figure 1a), CCE has an absorption maximum at 310 nm. Increases in pH result in the appearance of new features at longer wavelengths that undergo a continuous evolution up to a pH of ~12, a finding that reflects the existence of a tautomeric equilibrium for each of the protonic states (see below). At pH 12 and above, the absorbance maximum is 414 nm. Between these pH extremes, three readily identifiable isosbestic points are observed: 326 nm (pH range: 3.0-5.5), 364 nm (pH range: 9.4-12.0), and 393 nm (pH range: 8.0-8.8). A fourth isosbestic point, which is not as clearly defined as the other three, is present at ~344 nm (pH range: 6.2-7.2). The existence of the four isosbestic points is consistent with the stepwise deprotonation processes in eqs 1-4. The positions of the absorbance maxima, as well as those of the isosbestic points, differ by only a few nanometers from those for CCE dissolved in 70% aqueous methanol (i.e., a solution 70% in methanol and 30% in water);[1] these similarities further support the uptake of CCE by the CPC/SDS mixed micelle.[14,15]

The results from an analysis of the spectroscopic data in Figure 1 for determinations of the pK_{ai} values for CCE solubilized in CPC and CPC/SDS micelles are presented in Table 1, along with the values found for CCE dissolved in 70% aqueous methanol.[1] This analysis is described in our earlier work.[1] For the CPC micellar solution, all four values of pK_{ai} are less than those found in 70% aqueous methanol; these differences are consistent with expected destabilization of H_4L^{2+} and H_3L^{+} as well as the stabilization of HL^{-} and L^{2-} in the cationic microenvironment of the CPC micelle.[16] The uptake of CCE by the CPC/SDS

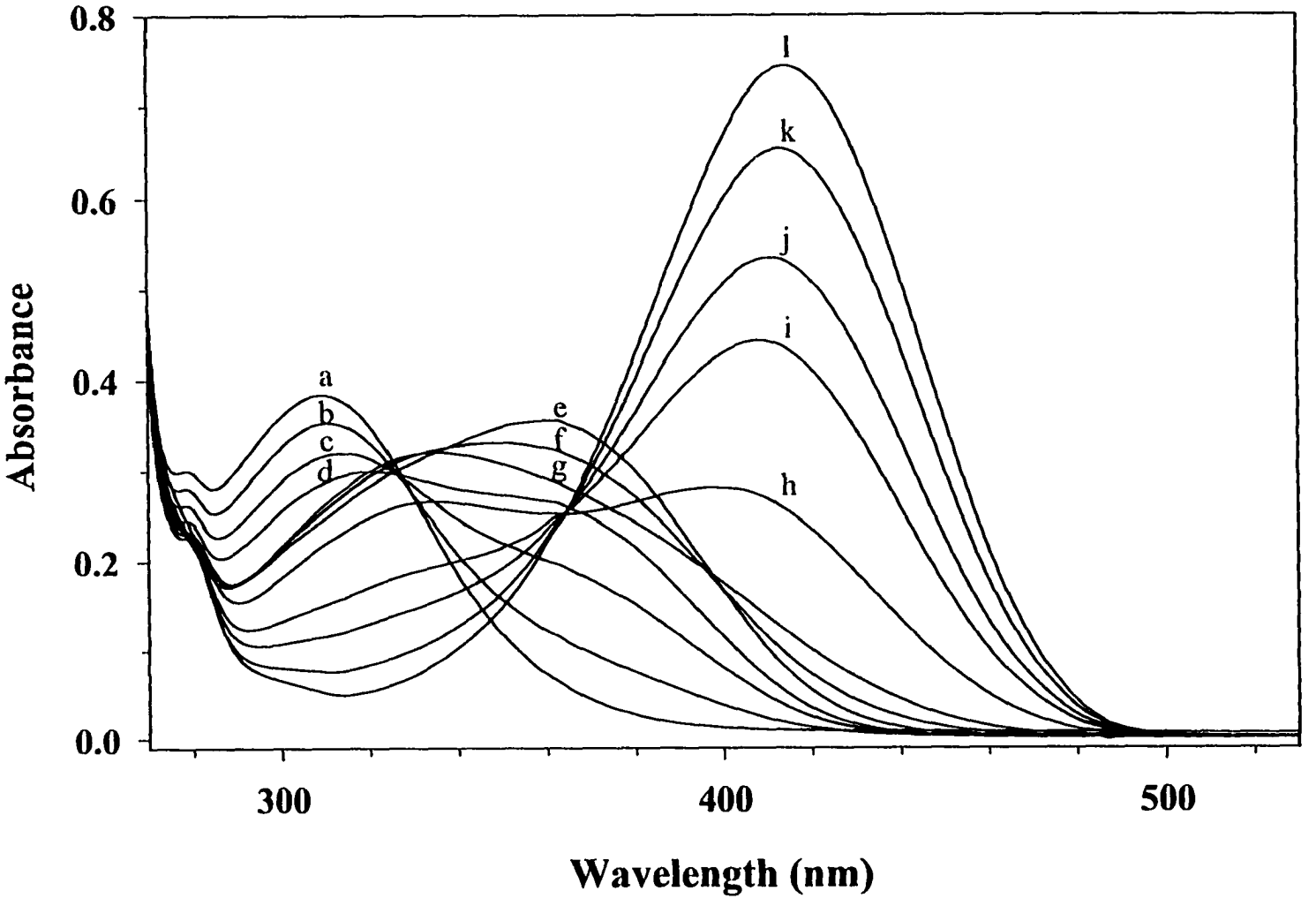

Figure 1. Absorbance spectra of 25 μM CCE in the micellar solution (50 mM SDS and 0.4 mM CPC) as a function of pH: (a) pH 2.24, (b) 3.53, (c) 4.20, (d) 4.61, (e) 7.20, (f) 8.09, (g) 8.60, (h) 9.38, (i) 9.87, (j) 10.13, (k) 10.60, and (l) 11.98.

Table 1. Acid Dissociation Constants for CCE in Micellar Solutions of Varied Composition and in a Mixed Solvent System.

Solvent	Ionic strength (M)	Cation	pK_{a1}	pK_{a2}	pK_{a3}	pK_{a4}
50 mM CPC[a]	0.01-0.1	Li^+	3.20	4.90	6.95	7.70
50 mM SDS + 0.40 mM CPC[a]	0.01-0.1	Li^+	4.25	6.45	8.25	9.80
70% MeOH[b]	0.01-0.1	Li^+	3.60	6.20	8.15	9.75

[a] The micellar systems were prepared using the disodium salt of CCE. See text for preparative details.

[b] Reference 1.

mixed micelle results, in contrast, in higher values for pK_{a1} and pK_{a2} in comparison to the mixed solvent system; these changes are diagnostic of a stabilization of H_4L^{2+} and H_3L^+ in the mixed micelle. The effects of such a microenvironment are, however, negligible for the deprotonation steps leading to HL^- and to L^{2-}. We have not yet attempted to develop further insights into correlations between the differences in acid strengths of CCE and the predominantly anionic micro-environment of the CPC/SDS mixed micelle.[17]

The spectroscopic data also provide insights into the structural changes that accompany the acid-base transformations. Based on our earlier examination of the pH-dependent spectral data for a structural analog of the chromogenic side-arm of CCE (i.e., *p*-nitrophenol and 2-hydroxy-5-nitrobenzyl alcohol),[18,19] the changes at high pH in the spectra

of the mixed micelle-solubilized CCE largely reflect the acid-base transformations of the phenolic groups of the side arms. The acid-base chemistry of the amine groups therefore plays a dominant role in the transformations at low pH, with the small change in the observed spectrum at low pH indicative of a minor contribution from a tautomeric transformation. The tautomeric conversion also appears to contribute to a small extent to the spectral changes at high pH. Further insights into the favored pathways of the protonation-deprotonation processes will require a more in-depth study of ionic strength effects.[1]

Metal Ion Binding Equilibria and Optical Characteristics. Based on the five possible protonic states of CCE, the equilibria between a dicationic metal ion (M^{2+}), CCE and the corresponding metal-ligand complex (ML) can be described as:

$$[H_4L^{2+}]_m + [M^{2+}]_{aq} = [ML]_m + 4[H^+]_{aq} \quad (9)$$

$$[H_3L^{+}]_m + [M^{2+}]_{aq} = [ML]_m + 3[H^+]_{aq} \quad (10)$$

$$[H_2L]_m + [M^{2+}]_{aq} = [ML]_m + 2[H^+]_{aq} \quad (11)$$

$$[HL^{-}]_m + [M^{2+}]_{aq} = [ML]_m + [H^+]_{aq} \quad (12)$$

$$[L^{2-}]_m + [M^{2+}]_{aq} = [ML]_m \quad (13)$$

where $[H_4L^{2+}]_m$, $[H_3L^{+}]_m$, $[H_2L]_m$, $[HL^{-}]_m$, $[L^{2-}]_m$, and $[ML]_m$ are the equilibrium concentrations of H_4L^{2+}, H_3L^{+}, H_2L, HL^{-}, L^{2-}, and ML in the micellar phase and $[M^{2+}]_{aq}$ and $[H^+]_{aq}$ are the equilibrium concentrations of M^{2+} and H^+ in the aqueous phase, respectively. The formation constants for these equilibria, K_{fi}, are written as:

$$K_{f1} = \frac{[ML]_m[H^+]_{aq}^4}{[H_4L^{2+}]_m[M^{2+}]_{aq}} \quad (14)$$

$$K_{f2} = \frac{[ML]_m[H^+]_{aq}^3}{[H_3L^{+}]_m[M^{2+}]_{aq}} \quad (15)$$

$$K_{f3} = \frac{[ML]_m[H^+]_{aq}^2}{[H_2L]_m[M^{2+}]_{aq}} \quad (16)$$

$$K_{f4} = \frac{[ML]_m[H^+]_{aq}}{[HL^-]_m[M^{2+}]_{aq}} \quad (17)$$

$$K_{f5} = \frac{[ML]_m}{[L^{2-}]_m[M^{2+}]_{aq}} \quad (18)$$

Equations 14-18 can be recast to give:

$$\log K_{f1} = \log q_4 - 4pH - \log [M^{2+}] \quad (19)$$

$$\log K_{f2} = \log q_3 - 3pH - \log [M^{2+}] \quad (20)$$

$$\log K_{f3} = \log q_2 - 2pH - \log [M^{2+}] \quad (21)$$

$$\log K_{f4} = \log q_1 - pH - \log [M^{2+}] \quad (22)$$

$$\log K_{f5} = \log q_0 - \log [M^{2+}] \quad (23)$$

where $q_4 = \frac{[ML]_m}{[H_4L^{2+}]_m}$; $q_3 = \frac{[ML]_m}{[H_3L^{+}]_m}$; $q_2 = \frac{[ML]_m}{[H_2L]_m}$; $q_1 = \frac{[ML]_m}{[HL^-]_m}$; and $q_0 = \frac{[ML]_m}{[L^{2-}]_m}$.

The formulations in eqs 9-23 are used in the remainder of this section to evaluate the metal ion binding properties of CCE solubilized in the CPC/SDS mixed micellar solution.

Figures 2 and 3, and Table 2 summarize the complexation capabilities of CCE in the CPC/SDS mixed micellar phase for the binding of Ba(II), Ca(II), Cd(II), Cu(II), Hg(II), Pb(II), and Sr(II). Figure 2 presents a portion of these results by showing the absorption spectra of the micellar solubilized CCE in the absence and in the presence of differing concentrations of Cd(II) (0.4 μM-75 μM) at a pH of 8.0 under which CCE exists mainly in its H_2L form. As evident, the formation of the Cd(II):CCE complex produces a bathochromic shift of ~70 nm (absorbance maximum: 395 nm) and an increase in molar absorptivity when compared to the spectrum of uncomplexed CCE. An isosbestic point at 352 nm confirms that metal ion binding under this condition involves only two forms of CCE. The positions of the spectral features and the pH of the solution further reveal that the metal ion binding process is represented by eq 11. We note that the complexes formed by CCE in the CPC/SDS mixed micellar phase with Hg(II), Ca(II), and Sr(II) exhibit similar spectral characteristics, but have different pH dependences; the addition of Pb(II) or Ba(II) to the micellar solution, however, resulted in precipitate formation even at pH ~2.

Figure 3 presents a few examples of the pH dependences for the complexation of divalent metal ions (i.e., Ca(II) in Figure 3a and Cd(II) in Figure 3b) by the micellar solubilized CCE in its various protonic states. The plots are presented as log q_i vs. pH, where i denotes the number of protons present on the uncomplexed form of CCE. All of the plots in Figure 3a exhibit a linear dependence on pH. The slope of each plot agrees well with that

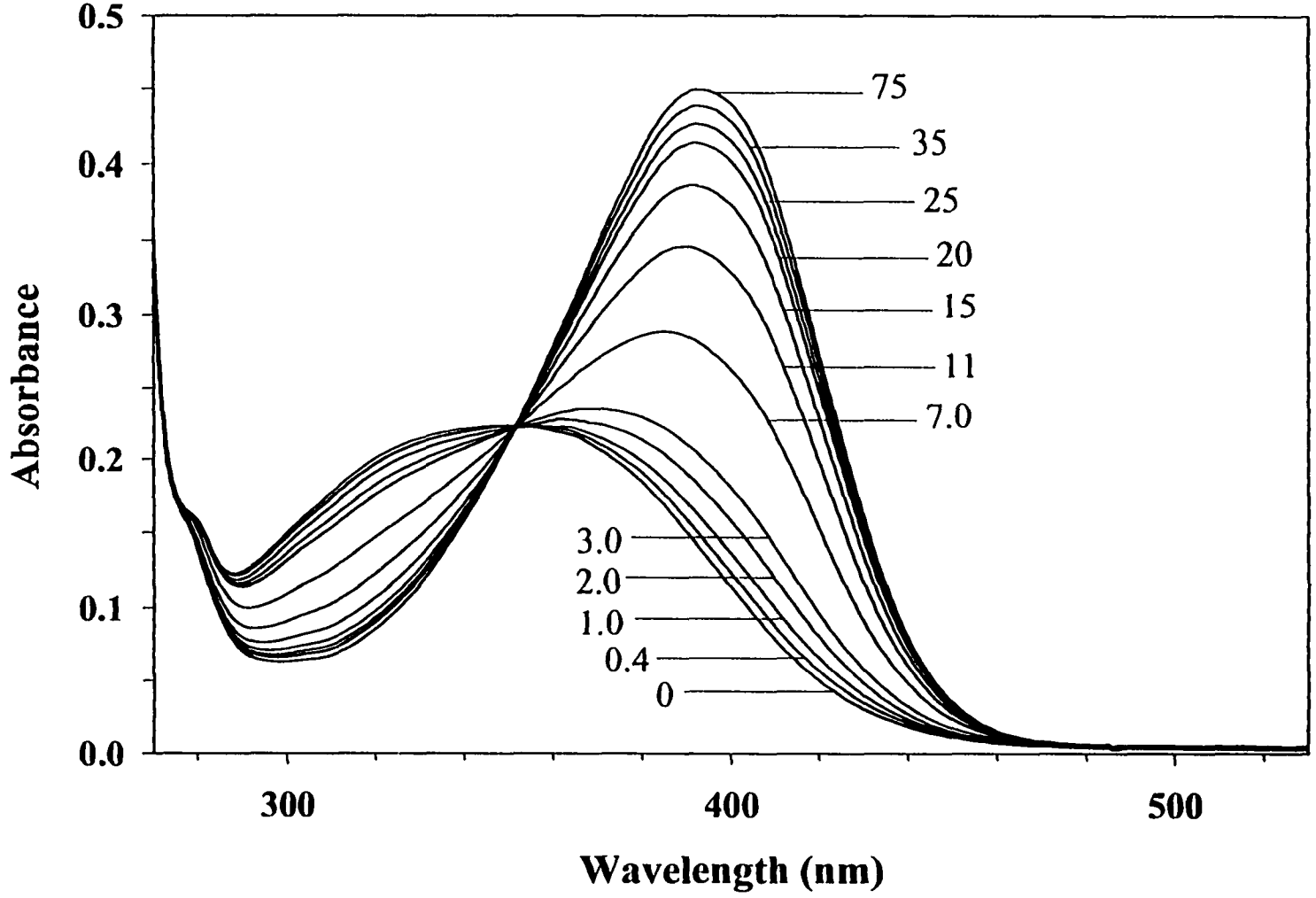

Figure 2. Absorbance spectra of 20 μM CCE in the micellar solution (50 mM SDS and 0.4 mM CPC) as a function of Cd^{2+} concentration in the range of 0 to 75 μM Cd^{2+}.

Figure 3. Plots of the log of q_i for the binding of (a) Ca(II) and (b) Cd(II) by CCE in a mixed micellar solution (1.0 mM Ca(II) or Cd(II), 25 μM CCE, 0.4 mM CPC and 50 mM SDS): q_4 (O), q_3 (∇), q_2 (□), q_1 (◊) and q_0 (Δ) as a function of pH. The symbols represent the experimental data, and solid lines represent slopes of 4, 3, 2, 1 and 0, as predicted from eqs 19-23 for each of the q_i. The uncertainties of the absorbance data are slightly smaller than the size of the symbols.

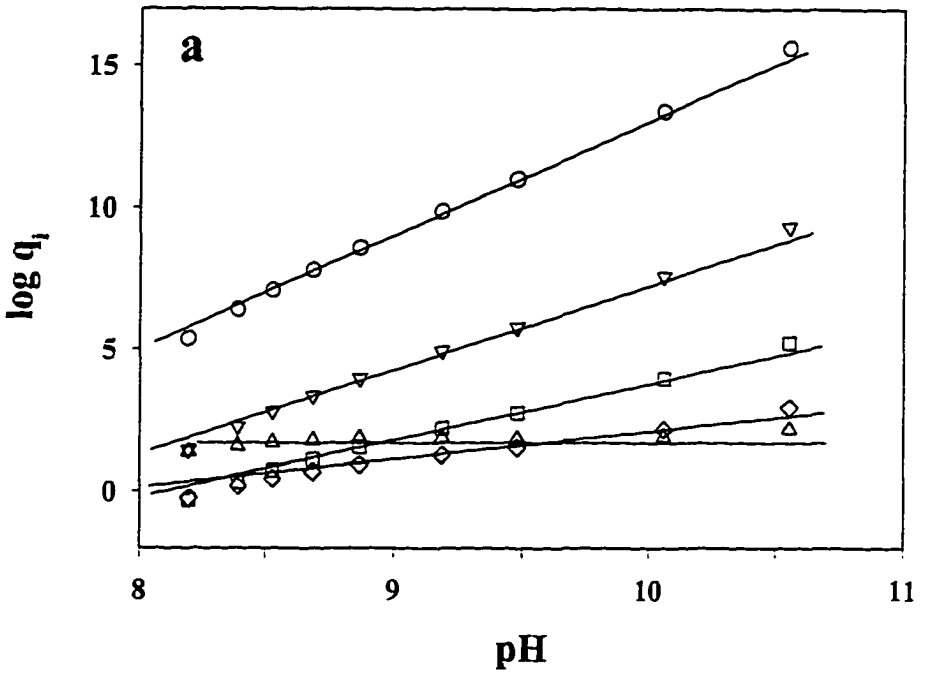
a
15
10
5
0
8
9
10
11
log qi gol
pH

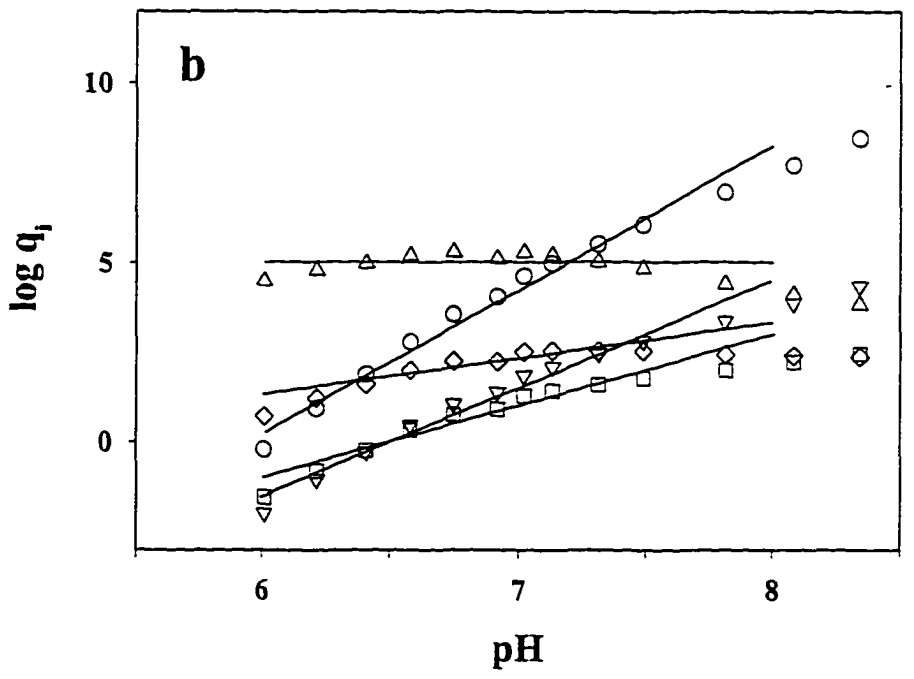
b
10
5
0
6
7
8
log qi gol
pH

expected from eqs 19-23, confirming the general applicability of the formulations in eqs 14-18 for describing the complexation of Ca(II) by CCE in the mixed micellar phase. Though not as well defined, plots for the other divalent metal ions, like that for Cd(II) presented in Figure 3b, show the same general dependences but over different pH ranges.

Table 2. Formation and Extraction Constants of CCE for Ba(II), Ca(II), Cd(II), Cu(II), Hg(II), Pb(II), and Sr(II) in a CPC/SDS Mixed Micellar Solution and in a Mixed Solvent System.

Metal Ion	-log K_{f3} [a]	-log K_{ex} [b]
Hg(II)	9.44 ± 0.59 (8)	0.28
Pb(II)	ppt.[c]	7.58
Cu(II)	>16[d]	8.52
Cd(II)	10.04 ± 0.19 (6)	10.50
Ca(II)	13.89 ± 0.06 (5)	15.30
Sr(II)	14.49 ± 0.09 (5)	16.40
Ba(II)	ppt.[c]	17.70

[a] The K_{fi} values are related to each other by the acid dissociation constants (K_{ai}) and can be transformed from one to another by division with the corresponding K_{ai} value. For example, $K_{f4} = K_{f3} / K_{a3}$ and $K_{f5} = K_{f3} / K_{a3} K_{a4}$. The uncertainties in the values of K_{f3} are given as standard deviations and the numbers in parenthesis are number of data points used in the analysis.

[b] Reference 1.

[c] The presence of this metal ion resulted in the formation of a precipitate.

[d] CCE does not complex Cu(II) to any detectable extent in CPC/SDS solution.

In addition to confirming the reaction stoichiometries of the complexation equilibria, the results in Figure 3 can be used to calculate the K_{fi} values for Ca(II) and Cd(II) with each of the protonic states of CCE. We note that the equilibrium represented by K_{f3} is analogous in formulation to the solvent extraction constant (K_{ex}) for the neutral form of CCE. Data for both K_{f3} and K_{ex} are presented in Table 2. As is evident, the metal ion binding capabilities of CCE solubilized in the mixed micelle are in some ways similar and in some ways different from those reported in our solvent extraction study.[1] That is, where measurable for the micellar system, the general order of the preferences for metal ion binding in the two cases is the same: Hg(II)>Cd(II)>Ca(II)>Sr(II). However, the magnitudes of the equilibrium constants are markedly different. For example, the values of K_{f3} for Cd(II), Ca(II), and Sr(II) are all higher than the analogous values of K_{ex}, whereas the value of K_{f3} for Hg(II) is significantly less than the corresponding value of K_{ex}. More importantly, the changes in the metal ion binding strengths of CCE that arise from solubilization in the CPC/SDS mixed micelle result in a loss of the marked selectivity of CCE for binding Hg(II) that was observed in the solvent extraction process. We presently attribute these differences, along with precipitate formation in the case of Pb(II) and Ba(II) and the undetectable binding of Cu(II), to the competitive binding by the sulfate end groups in the SDS component of the mixed micelles.

These results clearly dictate a reevaluation of the utility of CCE for divalent metal ion determinations found in our solvent extraction study when a micellar solubilization procedure is employed. Table 2 shows that there is an insufficient difference in the selectivity of the

micelle-solubilized CCE to discriminate Hg(II) (pK_{f3} = 9.44) from Cd(II) (pK_{f3} = 10.04), but that there is a sufficient difference in selectivity to discriminate Hg(II) and Cd(II) from Ca(II) (pK_{f3} = 13.89). Utilizing a masking agent for Hg(II) (e.g., chloride ion),[20] it is conceivable that an effective approach for a spectrophotometric determination of Cd(II) can be devised.

Determination of Cd(II). This section examines the potential application of the micelle-solubilized CCE for the determination of Cd(II). To this end, we used an aqueous buffer system (pH=8.0) composed of 0.1 M tris-(hydroxymethyl)aminomethane (THAM) and 0.1 M HCl. This solution composition was selected to include a high concentration of chloride ion for the masking of Hg(II) and to employ a buffer system at a pH ~8 with high capacity (pK_a of THAM = 8.06).[21]

Figure 4 shows the calibration curve obtained at 395 nm under the above conditions in the range of 0-75 μM Cd(II). As is evident, the absorbance at 395 nm increases with the concentration of Cd(II), approaching a maximum value at the upper limit of the Cd(II) concentration range. The response is linear, as shown by the inset, up to ~7 μM Cd(II). The estimated detection limit is ~6 ppb at a signal-to-noise ratio of 3. This estimated limit of detection compares favorably with that for the more commonly used complexing agent dithizone.[22] Furthermore, the procedure using micelle-solubilized CCE is more facile and less time consuming than the dithizone-based solvent extraction process. We also note that the generated wastes from our micelle-process are less hazardous than those from the dithizone method, which requires the use of potassium cyanide as a masking agent.[23] Finally, the interference of a 1000-fold of excess of Ca(II), which is the next best complexed metal

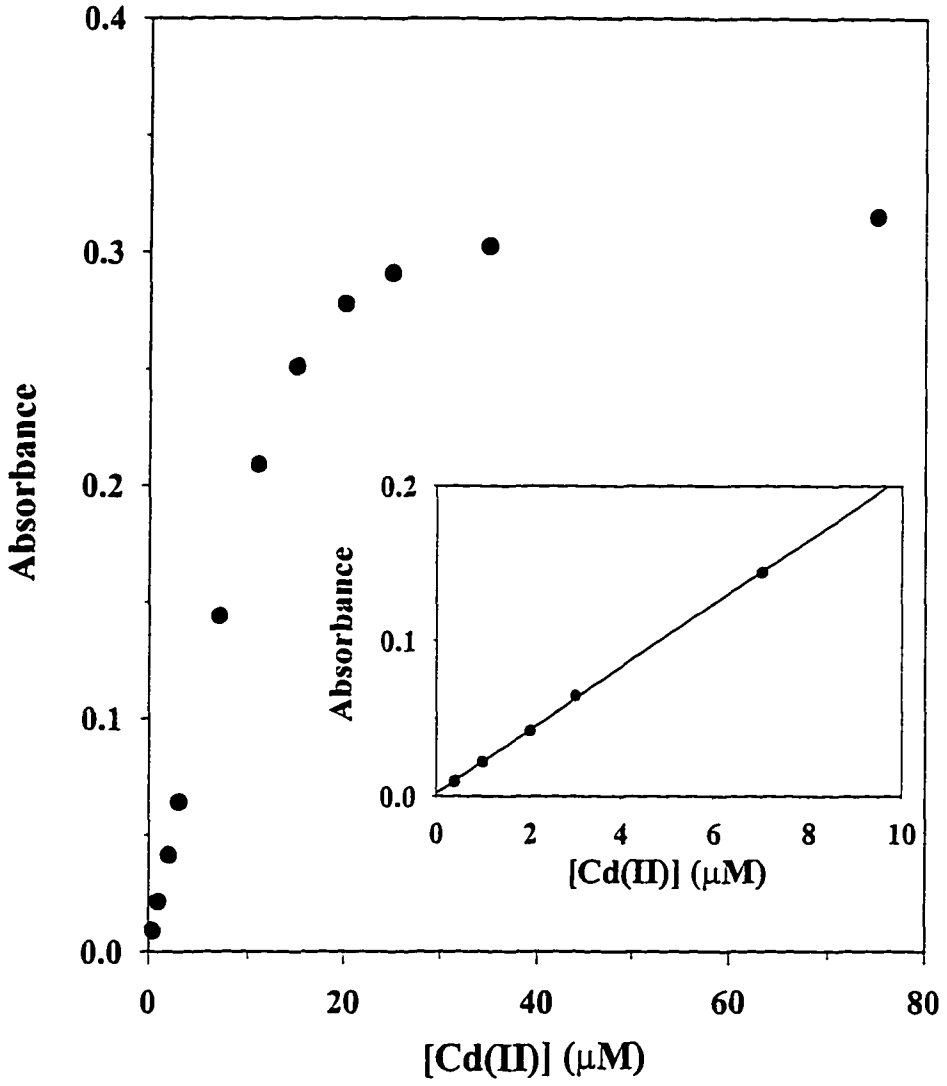

Figure 4. Calibration curve at 395 nm for Cd(II) in the range of 0-75 μM concentration using 17 μM CCE in the mixed micellar solution (0.4 mM CPC and 50 mM SDS) in pH 8.0 THAM/HCl buffer. The absorbance of a blank sample has been subtracted from the measured absorbances at each Cd(II) concentration. The inset shows the linear range, 0-7 μM, of the calibration curve (correlation coefficient = 0.9996).

ion under this analysis condition, in the determination of 1 μM Cd(II) results in ~14% increase in absorbance.

CONCLUSIONS

This paper has demonstrated that CCE can be used in a mixed micelle solubilization procedure for the low level detection (~6 ppb) of Cd(II). The main advantages of our procedure in comparison to that of solvent extraction with dithizone are ease of use and the reduction of hazardous wastes. We are presently devising experiments aimed at delineating further the factors that cause the differences in the metal ion binding capabilities when CCE is solubilized in CPC/SDS micelles in comparison to our earlier findings for a solvent extraction process.

ACKNOWLEDGMENTS

Insightful discussions with Monzir S. Abdel-Latif on the use of micelles are gratefully acknowledged. The work at Iowa State University was supported by the Office of Basic Energy Research-Chemical Sciences Division of the U.S. Department of Energy-Ames Laboratory, and by the Microanalytical Instrumentation Center of the Iowa State University. The work at Texas Tech University was supported by the Division of Chemical Sciences of the Office of Basic Energy Research of the U.S. Department of Energy (Grant DE-FG03-94ER14416). The Ames Laboratory is operated for the U.S. Department of Energy by the Iowa State University under contract No. W-7405-eng-82.

REFERENCES AND NOTES

1) Vaidya, B.; Zak, J.; Bastiaans, G. J.; Porter, M. D.; Hallman, J. L.; Nabulsi, N. A. R.; Utterback, M. D.; Strzelbicka, B.; Bartsch, R. A. *Anal. Chem.* **1995**, *67*, 4101-4111.

2) Klopf, L. L.; Nieman, T. A. *Anal. Chem.* **1984**, *56*, 1539-1542.

3) Malliaris, A.; Binana-Limbele, W.; Zana, R. *J. Colloid Interface Sci.* **1986**, *110*, 114-120.

4) Jana, P. K.; Moulik, S. P. *J. Phys. Chem.* **1991**, *95*, 9525-9532.

5) Amante, J. C.; Scamehorn, J.; Harwell, J. H. *J. Colloid Interface Sci.* **1991**, *144*, 243-253.

6) Mehreteab, A. In *Mixed Surfactant Systems*; Holland, P. M. and Rubingh, D. N., Ed.; American Chemical Society: Washington, DC, 1992; pp 402-415.

7) Scamehorn, J. F.; Harwell, J. H. In *Mixed Surfactant Systems*; Ogino, K. and Abe, M., Ed.; Marcel Dekker: New York, 1993; pp 283-315.

8) Herrington, K. L.; Kaler, E. W. *J. Phys. Chem.* **1993**, *97*, 13792-13802.

9) Abdel-Latif, M. S. *Anal. Lett.* **1994**, *27*, 2341-2353.

10) Szajdzinska-Pietek, E.; Gebicki, J. L. *J. Phys. Chem.* **1995**, *99*, 13500-13504.

11) Yatcilla, M. T.; Herrington, K. L.; Brasher, L. L.; Kaler, E. W.; Chiruvolu, S.; Zasadzinski, J. A. *J. Phys. Chem.* **1996**, *100*, 5874-5879.

12) Karukstis, K. K.; Suljak, S. W.; Waller, P. J.; Whiles, J. A.; Thompson, E. H. Z. *J. Phys. Chem.* **1996**, *100*, 11125-11132.

13) Albert, A.; Serjeant, E. P. *The Determination of Ionization Constants: A Laboratory Manual*; 3rd ed.; Chapman and Hall: New York, 1984.

14) Bakshi, M. S.; Crissantino, R.; Lisi, R. D.; Milioto, S. *Langmuir* **1994**, *10*, 423-431.

15) Caponetti, E.; Martino, D. C.; Floriano, M. A.; Triolo, R.; Wignall, G. D. *Langmuir* **1995**, *11*, 2464-2470.

16) Finston, H. L.; Rychtman, A. C. *A New View of Current Acid-Base Theories*; Wiley: New York, 1982.

17) As discussed by Szajdzinska-Pietek (ref. 10), the pyridinium ring of CPC is sequestered near the head group region of SDS micelle. Bakshi et al. (ref. 14) have shown that the crown ether 18-crown-6 distributes between the aqueous and micellar phases based on the observed decrease in both the micellar size and the cmc with the increase in the 18-crown-6 concentration. Caponetti et al. (ref. 15), using small angle neutron scattering, concluded that the crown ethers were localized in the SDS micellar phase, but were unable to establish the exact distribution within the micelle.

18) Koshland, D. E., Jr.; Karkhanis, Y. D.; Latham, H. G. *J. Am. Chem. Soc.* **1964**, *86*, 1448-1450.

19) Nishida, H.; Tazaki, M.; Takagi, M.; Ueno, K. *Mikrochim. Acta* **1981**, *1*, 281-287.

20) Ringbom, A. J. *Complexation in Analytical Chemistry*; Interscience Publishers: New York, 1963.

21) Perrin, D. D. *Buffers for pH and Metal Ion Control*; Chapman and Hall: New York, 1974.

22) APHA *Standard Methods For The Examination of Water and Wastewater*; 18th. ed.; American Public Health Association: Washington, DC, 1992.

23) Saltzman, B. E. *Anal. Chem.* **1953**, *25*, 493-496.

CHAPTER 4. REDUCTION OF CHLORIDE INTERFERENCE IN CHEMICAL OXYGEN DEMAND (COD) DETERMINATION WITHOUT USING MERCURY SALTS

A paper to be submitted to *Analytica Chimica Acta*

Bikas Vaidya, Steve W. Watson, Shelley J. Coldiron, and Marc D. Porter

ABSTRACT

An efficient method for the reduction of chloride interference in the determination of chemical oxygen demand (COD) without the use of Hg(II) as a masking agent is described. Chloride ion is removed as hydrochloric acid gas from acidified sample solutions at 150 °C in a closed reaction tube and captured by a bismuth-based adsorbent held in a specially designed Teflon-basket above the solution. The effects of adsorbent composition, basket design, sulfuric acid concentration, reflux time, chloride concentration, and silver(I) catalyst on the efficiency of the removal of chloride ion and the COD determination are discussed.

INTRODUCTION

Oxygen demand is an important delimiter for the effect of organic pollutants in aqueous environmental systems.[1] As these pollutants are consumed by microorganisms, the oxygen content of water is depleted. This loss can have adverse effects on the balance of natural ecosystems if the oxygen content falls below the level necessary to support aquatic life. Chemical oxygen demand (COD), biological oxygen demand (BOD) and total organic carbon (TOC) are the three main methods used to assess organic pollution in aqueous

systems.[2,3] However, because of the tedious nature of BOD and TOC determinations, COD is the predominant method of choice.[1,3]

For COD determinations, a wide range of chemical reagents have been used as oxidizing agents, including acidic dichromate, acidic permanganate, iodate, and persulfate.[1,4] However, dichromate has been found to be the most broadly effective oxidant when used in strongly acidic solutions and with a Ag(I) catalyst.[1-3,5-23] The standard COD determination adds an oxidant ($Cr_2O_7^{2-}$), a catalyst (Ag(I)), and sulfuric acid to an aqueous sample that is then heated for ~ 2 hours.[1,2] This process results in the oxidation of organic compounds, as shown in Equation 1 for the often used COD-calibration compound potassium hydrogen phthalate ($KC_8H_5O_4$ or KHP). This reaction is the equivalent of that in Equation 2 where oxygen and not $Cr_2O_7^{2-}$ is used as the oxidant. Thus, each mole of $Cr_2O_7^{2-}$ oxidizes the same amount of KHP as 1.5 moles of O_2. By determining spectroscopically the amount of $Cr_2O_7^{2-}$ consumed or the amount of Cr^{3+} generated by these reactions, the amount of oxygen that would be required to complete the parallel conversion in Equation 2 can be calculated.

$$2\ KC_8H_5O_4 + 10\ K_2Cr_2O_7 + 41\ H_2SO_4 \rightarrow$$
$$16\ CO_2 + 46\ H_2O + 10\ Cr_2(SO_4)_3 + 11\ K_2SO_4 \qquad (1)$$

$$2\ KC_8H_5O_4 + 15\ O_2 + H_2SO_4 \rightarrow 16\ CO_2 + 6\ H_2O + K_2SO_4 \qquad (2)$$

The primary focus of this study rests with the removal of chloride ion from water samples prior to a COD determination. This step is necessary because chloride ion interferes

with a COD determination though the consumption of $Cr_2O_7^{2-}$, as shown in Equation 3.[24] The presence of chloride ion can therefore result in a positive deviation in a COD determination. In addition, the product of the reaction in Equation 3, Cl_2, can be converted in the presence of ammonia back to chloride ion via the net reaction in Equation 4,[24] thereby amplifying the effect of the interference of chloride ion. Thus, the effect of chloride ion on a COD determination cannot be quantitatively accounted for, a situation requiring the removal of chloride ion prior to the addition of $Cr_2O_7^{2-}$.

$$6\ Cl^- + Cr_2O_7^{2-} + 14\ H^+ \rightarrow 2Cr^{3+} + 3\ Cl_2 + 7\ H_2O \qquad (3)$$

$$2\ NH_4^+ + 3\ Cl_2 \rightarrow N_2 + 6\ HCl + 2\ H^+ \qquad (4)$$

$$HgSO_4 + 2\ Cl^- \rightarrow HgCl_2 + SO_4^{2-} \qquad (5)$$

Almost all of the methods used in COD determinations mask chloride ion by the addition of a mercury salt (e.g., $HgSO_4$).[1-3,8,10,11,17,21-23] The masking reaction, shown in Equation 5, yields an unreactive complex with respect to oxidation by $Cr_2O_7^{2-}$. Other approaches that attempt to manage the problem of chloride ion interference in COD include the addition of silver salts to mask chloride ion,[13-16] the addition of chromium(III) to lower the oxidation potential of the reaction in Equation 3,[18] and the determination of the amount of chloride ion oxidized by iodometric titration with a subsequent correction to the COD determination for chloride ion.[9]

The results described herein pursue an alternative pathway for the removal of chloride ions from samples in COD determination. The goal is to develop a facile method for the effective removal of chloride ion that negates the need of the hazardous masking agent like Hg(II). At 10 mg/L, the interference of chloride ion is below the uncertainty of COD determinations for most types of samples (e.g., ground water and waste treatment system samples). Our approach derives in large part from a recent study that evaluated the capability of removing chloride ion from aqueous samples by its room temperature evolution as gaseous HCl.[24,25] The evolved HCl was then removed from the vapor phase upon passage over a calcium hydroxide adsorbent that was contained in a glass vessel with glass frits to provide access to the adsorbent. This process was, however, ineffective in reducing the concentration of chloride ion to a level sufficient to eliminate the use of Hg(II) as a masking agent. To overcome this limitation, we have explored the application of elevated temperatures to drive HCl more exhaustively from the sample solution. This approach also necessitated an investigation of alternative adsorbent materials that would be more insoluble than calcium hydroxide because of the condensation of the moisture within the adsorbent container. This paper describes our findings.

EXPERIMENTAL SECTION

Chemicals. Bismuth(III) oxide (Bi_2O_3) was purchased from Aldrich Chemical Company. Standard potassium hydrogen phthalate (KHP) solutions were received from Hach Company. Reagent grade chemicals were used throughout without further purification.

Aqueous solutions were prepared with distilled water that was subsequently deionized using a Millipore Milli-Q water system.

Instrumentation. Determinations of pH were performed with an Orion Research digital ionalyzer (Model 501) and an Orion combination glass pH electrode (Model 91-04). Chloride ion concentrations were determined potentiometrically with an Orion combination chloride electrode (Model 96-17b) and an Orion SA 720 ISE. A Hach DR2000 spectrophotometer was used for all the COD determinations. A Hach COD reactor was used for heating the samples for both the removal of chloride ion and the dichromate-based oxidation of the COD samples. Determinations of Bismuth were done by inductively coupled plasma-atomic emission spectrometry (ICP-AES) by the Ames Laboratory Analytical Services.

Adsorbent preparation. Adsorbent B1. 4.66 g of Bi_2O_3 was dissolved in 100 mL of 2.0 M HCl followed by the addition of 300 mL of 2.0 M NaOH. After one hour, the yellow precipitate was separated from solution by filtration, rinsed extensively with water, and dried at 105 °C.[26]

Adsorbent B2. Adsorbent **B1** was soaked in 3.6 M NaOH for 4 hours, rinsed with water, and dried at 105 °C.

Adsorbent S1. 18.6 g of Bi_2O_3 was added slowly to a stirred solution (500 mL) of 1.2 M sulfuric acid. Next, 2.0 M sodium hydroxide solution was added to this mixture until the pH was ~12.5. After standing for ~12 hours, the resulting precipitate is filtered, washed with copious amounts of water, and dried at 105 °C.

Basket design and preparation. A Teflon basket was designed to fit inside a standard Hach COD reaction tube,[1] and is shown in Figure 1. The basket contains the adsorbent, allows gas to flow over the adsorbent for the efficient uptake of HCl, and physically separates the adsorbent from the sample by suspension of the basket above the sample solution. The screw cap seals against the lip of the basket and tube to seal the reaction vessel. The holes in the bottom and the large vents on the sides of the basket facilitate gas and water reflux.

The basket is filled by first placing a layer of fine (~7 μm) pyrex glasswool in the bottom of the basket. The adsorbents are then added to the basket and covered with another layer of glasswool. The packed basket is soaked in deionized water for a few minutes to pre-wet the adsorbent, which is then centrifuged to remove excess water.

Procedures for removal of chloride ion and COD determinations. The overall procedure has two steps: chloride ion removal and solution digestion. For chloride ion removal, the sample solutions are prepared by adding 1.00 mL of aqueous sample and 1.00 mL of concentrated sulfuric acid to a reaction tube. A pre-wetted basket with the adsorbent is then inserted into the reaction tube, which is subsequently capped and gently shaken to mix the sample with sulfuric acid. The reaction tube is then heated at 150° C for 2 hours. Next, the reaction tubes are air-cooled and centrifuged. The baskets are then removed from the reaction tube.

For digestion, the oxidant ($K_2Cr_2O_7$) and catalyst (Ag_2SO_4) are added to the sample solution. The reaction tube is then capped, gently shaken to facilitate mixing, and reheated at

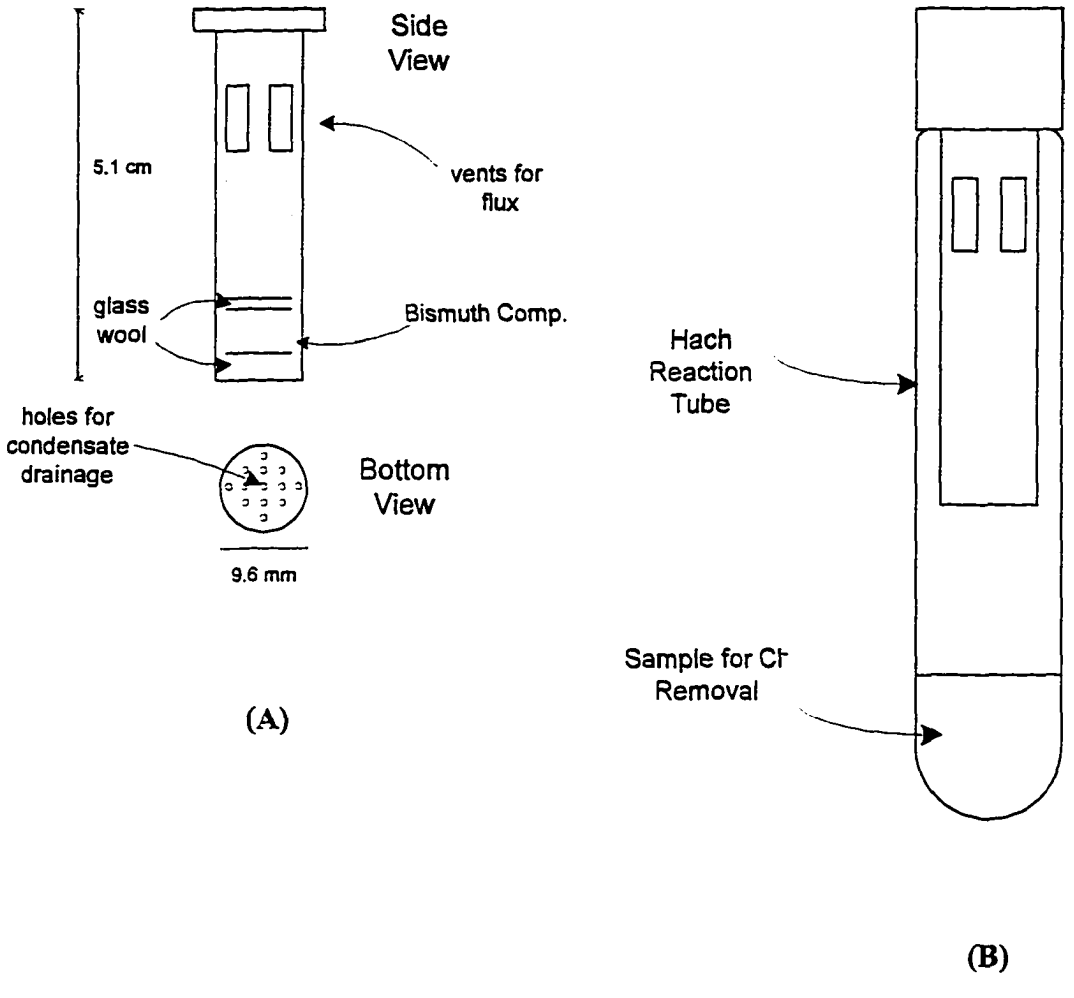

Figure 1. Teflon basket (A) and basket loaded into the reaction tube (B).

150 °C for 2 hours. After cooling to room temperature, COD is determined spectroscopically at 590 nm.

RESULTS AND DISCUSSION

In 18 N sulfuric acid, chloride ion is readily converted to molecular HCl, which is readily evolved as a gas at elevated temperatures as shown by Equations 6 and 7. However, to prevent the possible loss of volatile organic compounds in COD samples, the use of a sealed reaction tube is required. We therefore designed an inert collection basket to contain the adsorbent and collect HCl in the head space of the sealed reaction tube. The design of the basket, which is shown in Figure 1, facilitates insertion and sealing in the reaction tube. The latter characteristics are of importance because these reaction tubes have been designed to function effectively at the temperature (150 °C) used in the dichromate digestion step in the standard procedure for COD determinations. Our strategy then is to enhance thermally the removal of HCl by using conditions similar to those already part of the standard COD determination procedure, i.e., a temperature limit of 150 °C and a sulfuric acid concentration of ~18 N.[1,2]

$$Cl^-_{(aq)} + H^+_{(aq)} \rightleftharpoons HCl_{(aq)} \qquad (6)$$

$$HCl_{(aq)} \rightleftharpoons HCl_{(g)} \qquad (7)$$

As noted earlier, we explored the use of insoluble adsorbent materials. To this end, we focused upon several oxy-compounds of bismuth, since these materials and their chloride complexes are insoluble in water as exemplified by Equation 8.

$$HCl_{(g)} + BiOOH_{(s)} \rightarrow BiOCl_{(s)} + H_2O \qquad (8)$$

Four different forms of these compounds were tested: as-received Bi_2O_3, adsorbent **B1**, adsorbent **B2**, and adsorbent **S1**. We found that the as-received Bi_2O_3 and adsorbent **B1** were not effective in the extraction of HCl from the vapor phase. We then tested adsorbents that were reformulations of **B1**, which was prepared as previously described by the dissolution of Bi_2O_3 in HCl and precipitation by 2.0 M NaOH.[26] Two new formulations (i.e., adsorbent **B2** and **S1**) were used. The first involved the extraction of adsorbent **B1** in 3.6 M NaOH to yield adsorbent **B2**, the second entailed the dissolution of Bi_2O_3 in H_2SO_4 and the precipitation with NaOH to yield adsorbent **S1**. These formulations were designed to reduce the possible presence of residual chloride ion in adsorbent **B1**. The remaining portions of this paper present the results of our tests of each of the adsorbents as extraction phases for the removal of chloride ion for use in COD determinations.

Adsorbent capacity. In our initial evaluation of performance of each adsorbent, 10.0 mL of 0.0300 M (1065 ppm) HCl solution and 0.12 g of the different forms of the bismuth-based adsorbents were loaded into separate capped reaction tubes and mixed by sonication for ~2 h. After allowing the liquid and solid phases to separate, the chloride ion concentrations in the supernatant were determined with a chloride ion selective electrode.

The results of these studies are summarized in Table 1. Our findings indicate that with the exception of the as-received Bi_2O_3, each of the other three adsorbents is effective in the removal of chloride ion. In addition, the data indicate that adsorbents **B2** and **S1** were more effective in removal of chloride ion than **B1**. If then a viable approach can be

Table 1. Residual chloride ion in the solution.

Adsorbent	Final chloride concentration (ppm)[a]
Bi_2O_3	>1000
B1	18 ± 4
B2	7 ± 4
S1	7 ± 4

[a] Initial [Cl] = 1065 ppm.

developed that maintains the physical separation of adsorbent and analyte solution for the prevention of the loss of COD-related materials via adsorption on the adsorbent, the necessary reduction of chloride ion from analyte solutions may potentially be realized.

Variations of Adsorbent quantity and reflux time. In the next step of our preliminary evaluation, we tested the efficiency of the adsorbents **B2** and **S1** for the removal of HCl vapor generated from the heated, acidified solutions in a closed reaction tube. These tests were conducted first by adding 1.00 mL of the 1065 ppm chloride solution and 1.00 mL of concentrated sulfuric acid to the reaction tubes. Next, baskets with the **B2** or **S1** adsorbents were inserted into the reaction tubes, which were then capped and heated at 150 °C. In one set of experiments, the amount of adsorbent was varied (Table 2), while the reflux times were varied in the other set of experiments (Table 3). After cooling, the solution was adjusted to a pH of ~2.0 with NaOH and diluted to 25.00 mL in a volumetric flask. The chloride ion was then measured with a chloride ion selective electrode.

Table 2. Chloride ion uptake by various quantities of adsorbents B2 and S1.

Adsorbent	Amount of adsorbent (g)	Final chloride concentration (ppm)[a]	% Removal of chloride
B2	0.014	350 ± 50	33
B2	0.052	263 ± 50	50
B2	0.093	175 ± 50	67
B2	0.734	87 ± 50	83
S1	0.008	138 ± 50	75
S1	0.041	138 ± 50	75
S1	0.087	87 ± 50	83
S1	0.748	87 ± 50	83

[a] The uncertainty on the measured chloride ion concentration reflects the large dilution of the 18 N sulfuric acid required to bring the pH to ~2.0. Limit of detection of the chloride ion selective electrode is ~4 ppm.

Table 3. Chloride ion uptake by adsorbents B2 and S1 after refluxing at 150 °C for different periods of time.

Adsorbent	Reflux time (min)	Final chloride concentration (ppm)[a]	% Removal of chloride
B2	45	275 ± 50	50
B2	60	225 ± 50	58
B2	120	175 ± 50	67
S1	10	438 ± 50	17
S1	20	263 ± 50	50
S1	30	175 ± 50	67
S1	60	113 ± 50	79
S1	120	87 ± 50	83
S1	180	50 ± 50	90
S1	480	50 ± 50	90

[a] The uncertainty on the measured chloride ion concentration reflects the large dilution of the 18 N sulfuric acid required to bring the pH to ~2.0. Limit of detection of the chloride ion selective electrode is ~4 ppm.

Table 2 summarizes the results when acidified samples were heated at 150 °C for 2 hours and the amounts of each of the two adsorbents were varied. The results indicate that adsorbent **S1** is more efficient in capturing chloride ion than adsorbent **B2**. That is, adsorbent **S1** has a higher capacity for the uptake of chloride ion than adsorbent **B2**. This difference is evident, for example, by the much greater extraction capability of the 0.008 g sample of **S1** compared to the 0.014 g sample of adsorbent **B2**. One possible reason for the improved chloride ion removal efficiency of **S1** over **B2** is the difference between synthesis procedures. We suspect that, adsorbent **B2** contained residual chloride that was possibly present as BiOCl, with the residual chloride reducing the effective collection capacity. In contrast, adsorbent **S1**, while probably containing residual sulfate, could exchange sulfate for chloride.

Table 3 shows the remaining chloride ion and the fraction of the total chloride ion removed when the acidified sample was heated at 150 °C for different periods of time in the presence of the same amount (0.12 g each) of **B2**- and **S1**-adsorbents. The chloride ion removal efficiency of adsorbent **S1** after 30 minutes of refluxing was essentially the same as that for adsorbent **B2** after 120 minutes of refluxing. Results also indicate that the chloride ion removal process slowed significantly after ~60 minutes of heating. Based upon these experimental findings, we ascertained that a 2-hour heating period represented the lower limit necessary for the removal of chloride ion to the indicated levels.

Sulfuric acid concentration. We next investigated the effect of the sulfuric acid concentration on the evolution of HCl in the reaction tubes. Sulfuric acid concentrations

were varied from 1 N to 24 N. Thus, 0.667 mL aliquots of a 1600 ppm chloride solution and 1.33 mL aliquots of the solutions of differing sulfuric acid concentrations were pipetted into the reaction tubes. A Teflon basket containing 0.12 g of adsorbent **S1** was then inserted into the reaction tube, which was subsequently capped and heated at 150 °C for 2 hours. After cooling to room temperature, the pH was adjusted to ~2.0 with NaOH, the resulting solution diluted to 25.00 mL in a volumetric flask, and the residual chloride ion measured with a chloride ion selective electrode. The results are presented in Figure 2. As expected from Equations 6-8, the removal efficiency for chloride ion increases as the sulfuric acid concentration increases, reaching a limiting value at a sulfuric acid concentration of ~16 N. Based upon these results, we adopted a sulfuric acid concentration of 18 N because this concentration insures that the chloride ion removal process operates at its noted maximal efficiency, and is similar to that used in the sample digestion process.

Dissolved Bi^{3+}. The possible effects of dissolved Bi^{3+} on the measurement of COD were also investigated in view of its possible extraction from the basket by reflux condensate. Although not likely, there is a possibility that Bi^{3+} could be oxidized to Bi^{5+}, resulting in a positive contribution to the COD results. To this end, we dissolved various levels of Bi^{3+} in an aqueous matrix and added this solution to two different (175 ppm and 600 ppm) standard COD samples. The measurements of these COD samples were compared to blank solutions and the results are shown in Table 4. From this study, we concluded that levels below 100 ppm Bi^{3+} would not contribute substantially to the determined COD level. In contrast, a +10% deviation was found when Bi^{3+} was present at 1000 ppm. However, an analysis using

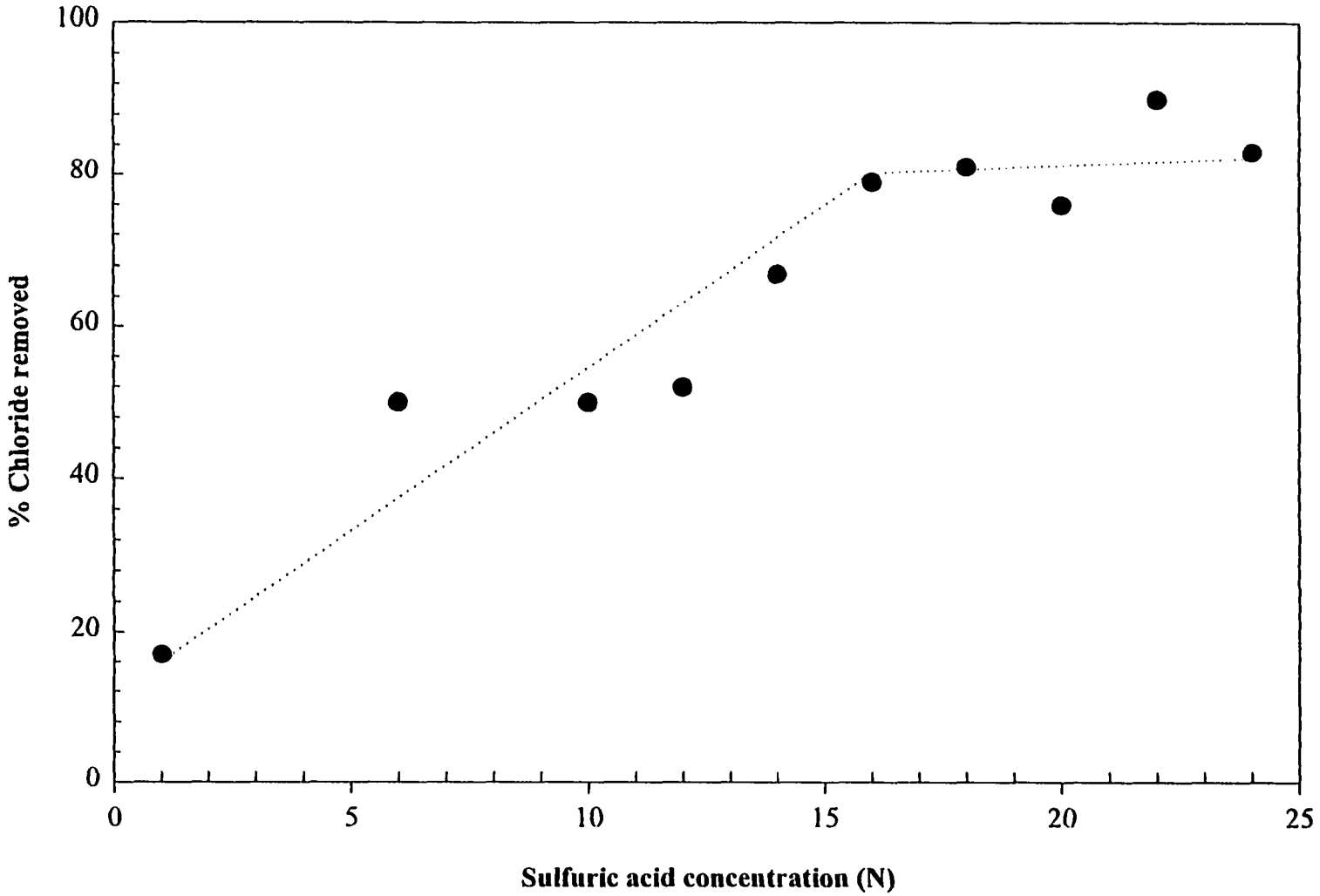

Figure 2. Effect of sulfuric acid concentration on chloride ion removal (see text for details).

ICP-AES of the samples that were subjected to refluxing at 150 °C for 2 hours in a reaction tube with a basket packed with 0.12 g of adsorbent **S1** showed the presence of 5 ppm or less of bismuth.

Initial chloride ion concentration. Another concern was the effect of the initial chloride ion concentration on removal efficiency. We tested standard samples ranging from 100 ppm to 1065 ppm chloride ion and found, as shown in Table 5, that the process removed chloride ion to effectively the same level (~75 ppm). This finding suggests that regardless of the initial chloride ion concentration, the chloride removal process reached a lower limit within a 2-hour heating period; after 2 hours, the rate of the chloride removal was not detectable. We suspect this finding reflects the finite solubility of HCl in the heated sample solution, which effectively slows the chloride removal process to an undetectable rate.

Table 4. Effect of Bismuth on COD determination.

Actual COD (ppm)	[Bi^{3+}] (ppm)	Meas. COD (ppm)[a]	% Deviation
175	0	175 ± 6 (3)	0
175	100	182 ± 2 (2)	4
175	1000	192 ± 11 (3)	10
600	0	601 ± 10 (3)	0
600	100	598 ± 8 (3)	<1
600	1000	636 ± 6 (3)	6

[a] The standard deviations were determined using replicate samples, the numbers of which are given parenthetically.

Table 5. Effect of initial chloride concentration on residual chloride after the chloride removal process.

Initial Cl^- concentration (ppm)	Measured Cl^- concentration (ppm)[a]
0	0 ± 50 (3)
100	75 ± 50 (3)
300	75 ± 50 (3)
1065	75 ± 50 (3)

[a] The uncertainty on the measured chloride ion concentration reflects the large dilution of the 18 N sulfuric acid required to bring the pH to ~2.0. Limit of detection of the chloride ion selective electrode is ~4 ppm.

Evolution of HCl vs oxidation of chloride ion. We were also interested in the possibility of combining the chloride removal process with the sample digestion step. If viable, such a combination could eliminate the time required for sample pretreatment for chloride ion removal. To investigate this possibility, we used standard (300 ppm) COD samples prepared with KHP that was spiked with known chloride ion levels. These results, including those for a series of control experiments, are summarized in Table 6. Comparisons to the two control experiments reveal that chloride ion removal by its evolution as HCl counteracts the interference to the determination by the oxidation of chloride ion by dichromate. This experiment showed clearly that the removal of chloride ion must be a pretreatment step.

Chloride ion removal and COD determination. We also examined the effects of the efficiency of the chloride ion removal process on the reliability of the COD determination. Standard COD solutions (0-500 ppm) that were spiked with 1065 ppm

Table 6. Evolution of HCl vs. oxidation of chloride during COD oxidation.

Cl^- added (ppm)	Adsorbent	COD measured[a] (ppm)
none	none	308
1065	none	> 450
1065	0.12 g S1	> 450
1065	0.12 g B2	> 450
1065	50 mg $HgSO_4$[b]	330

[a] Before refluxing, samples contained 300 ppm COD in 18 N sulfuric acid. [b] $HgSO_4$ was added to the solution, and no bismuth adsorbent was used.

chloride ion were first heated for two hours with the basket filled with 0.12 g of adsorbent **S1.** The dichromate oxidant was then added to the sample, and heated for an additional two hours. The results of this test are plotted in Figure 3. These data reveal a linear correlation with a slope of 0.997 and a y-intercept of 73.2 ppm COD (correlation coefficient = 0.995). The results indicate good agreement between the experimental and expected COD values, with the offset attributed to a fixed level of residual chloride ion as discussed above (Table 5). However, the y-intercept is higher than expected based only on the residual chloride ion listed on Table 5, which we believe reflects the presence of nitrogen-containing impurities in the preparation solutions.

Ag(I) Catalyst. Silver(I) ion is often used as a catalyst in COD determinations to insure the effective oxidation of a wide range of organic compounds by dichromate. To determine the effects of Ag(I) ion upon the chloride ion removal process, samples were prepared by mixing 1.00 mL of concentrated sulfuric acid containing 1% silver sulfate (w/v),

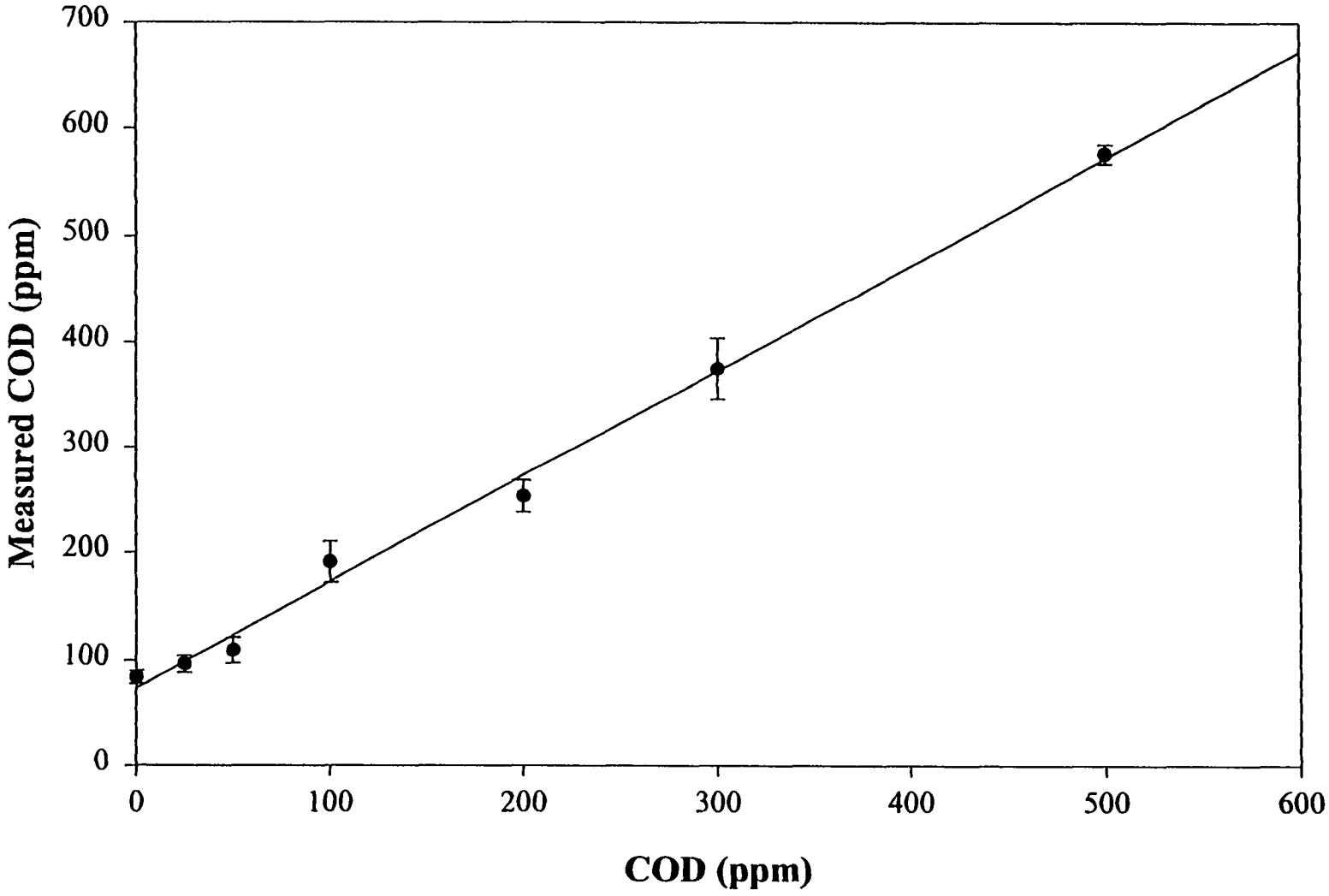

Figure 3. Effect of remaining chloride ion on the COD determination (see text for details).

and 1.00 mL of COD standard solution that were spiked with 1065 ppm chloride ion. The chloride ion pretreatment process was conducted at 150 °C for 2 hours with 0.12 g of adsorbent S1 in the basket. The basket was then removed, the oxidant added, and the reaction tube heated again at 150 °C for another 2 hours. The COD content was determined after cooling to room temperature. These findings are presented in Figure 4, which shows a linear correlation (slope: 0.862, y-intercept: 72.0 ppm COD, and correlation coefficient: 0.999) between the measured and expected COD levels. Thus, the addition of Ag(I) salt to the sample does not have a notable impact on the chloride ion removal process, as evident from a comparison to the correlation in Figure 3.

However, if Ag(I) salt is added after the chloride ion removal step and prior to oxidation of the sample by dichromate, a decrease in the background interference due to chloride ion is realized. This decrease is shown by the linear correlation (slope: 0.984, y-intercept: 11.5 ppm COD, and correlation coefficient: 0.998) presented in Figure 5. The low y-intercept of 11.5 ppm for the data, in comparison to those in Figures 3 and 4, is attributed to the increased difficulty of oxidizing chloride ion when it is bound with Ag(I) as AgCl.[13-16]

CONCLUSIONS

Our results show that the use of highly toxic mercury salts to mask the interference of chloride ion can potentially be avoided with a bismuth-based adsorbent and minor modifications in the current standard method of COD determination. The bismuth adsorbent prepared using sulfuric acid, adsorbent **S1**, proved the most effective with our basket design in the minimization of chloride ion interference in COD determinations. The majority of

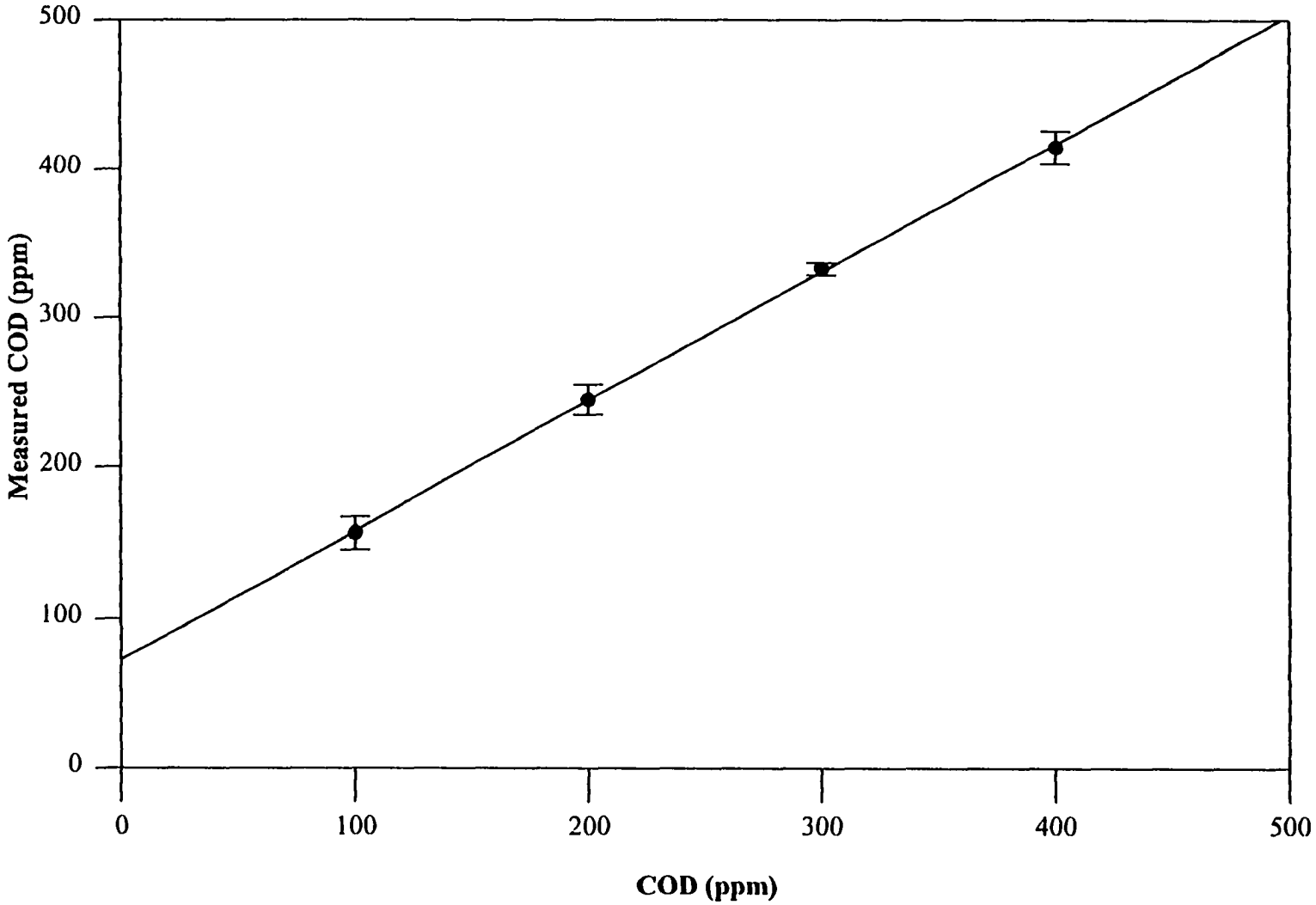

Figure 4. Chloride interference on COD determinations when Ag^{+} is present during the chloride ion removal step (see text for details).

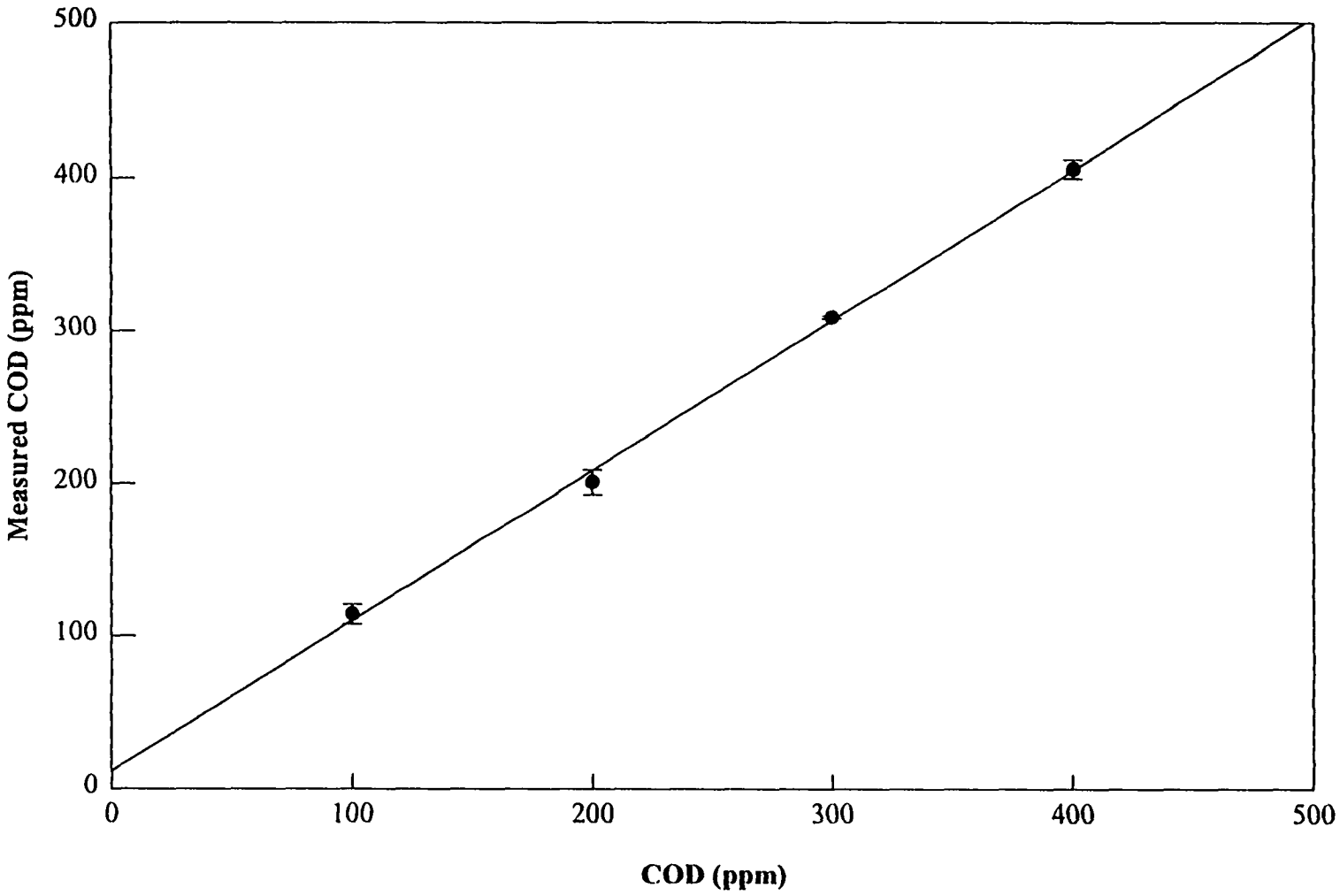

Figure 5. Chloride interference on COD determination when Ag^{+} is present only in the oxidation step (see text for details).

chloride ion in an aqueous sample is removed as HCl gas, which is captured by the bismuth adsorbent packed in the suspended basket. The residual chloride ion concentration is found to be effectively constant regardless of the initial chloride ion content of the sample. Interference in COD measurement resulting from the remaining chloride ion is further reduced by the addition of Ag(I) salt after the completion of the bismuth-based chloride ion removal step. The Ag(I) ion serves as a catalyst for the organic oxidation process with the collateral masking of residual chloride ion. Tests are underway to delineate the scope of this process in terms of the many types of COD samples often encountered in water testing laboratories.

ACKNOWLEDGMENTS

This work was supported by the Hach Company, Office of Basic Research-Chemical Sciences Division of the United States Department of Energy-Ames Laboratory, and by the Microanalytical Instrumentation Center of the Iowa State University. The Ames Laboratory is operated for the United States Department of Energy by the Iowa State University under contract No. W-7405-eng-82.

REFERENCES

1) Gibbs, C. R. *Introduction to Chemical Oxygen Demand*; Hach Company: Loveland, 1993; Booklet No. 8.

2) APHA *Standard Methods for the Examination of Water and Wastewater*; 19 th. ed.; American Public Health Association: Washington, DC, 1995.

3) Himebaugh, R. H.; Smith, M. J. *Anal. Chem.* **1979**, *51*, 1085-1087.

4) Medalia, A. I. *Anal. Chem.* **1951**, *23*, 1318-1320.

5) Moore, W. A.; Kroner, R. C.; Ruchhoft, C. C. *Anal. Chem.* **1949**, *21*, 953-957.

6) Moore, W. A.; Ludzack, F. J.; Ruchhoft, C. C. *Anal. Chem.* **1951**, *23*, 1297-1300.

7) Moore, W. A.; Walker, W. W. *Anal. Chem.* **1956**, *28*, 164-167.

8) Dobbs, R. A.; Williams, R. T. *Analytical Chemistry* **1963**, *35*, 1064-1067.

9) Baumann, F. J. *Anal. Chem.* **1974**, *46*, 1336-1338.

10) Jirka, A. M.; Carter, M. J. *Anal. Chem.* **1975**, *47*, 1397-1402.

11) Canelli, E.; Mitchell, D. G.; Pause, R. W. *Water Research* **1976**, *10*, 351-355.

12) Ryding, S.-O.; Forsberg, A. *Water Research* **1977**, *11*, 801-805.

13) Lloyd, A. *Analyst* **1982**, *107*, 1316-1319.

14) Ballinger, D.; Lloyd, A.; Morrish, A. *Analyst* **1982**, *107*, 1047-1053.

15) Pitrebois, L.; Schepper, H. D. *Trib. Cebedeau* **1984**, *484*, 83-86.

16) deCasseres, K. E.; Best, D. G.; May, B. D. *WAT. Pollut. Control* **1984**, 416-419.

17) Jones, B. M.; Sakaji, R. H.; Daughton, C. G. *Anal. Chem.* **1985**, *57*, 2334-2337.

18) Thompson, K. C.; Mendham, D.; Best, D.; Casseres, K. E. D. *Analyst* **1986**, *111*, 483-485.

19) Gonzalez, J. F. *Envirom. Tech. Lett.* **1986**, *7*, 269-272.

20) Soto, M.; Veiga, M. C.; Mendez, R.; Lema, J. M. *Envirom. Tech. Lett.* **1989**, *10*, 541-548.

21) Dasgupta, P. K.; Petersen, K. *Anal. Chem.* **1990**, *62*, 395-402.

22) Belkin, S.; Brenner, A.; Abeliovich, A. *Wat.Res.* **1992**, *26*, 1577-1581.

23) Belkin, S.; Brenner, A.; Abeliovich, A. *Wat. Res.* **1992**, *26*, 1583-1588.

24) Wagner, V. R.; Ruck, W. *Z. Wasser Abwasser Forsch.* **1981**, *14*, 145-151.

25) Wagner, V. R.; Ruck, W. *Z. Wasser Abwasser Forsch* **1982**, *15*, 287-290.

26) Fritsche, U. *Process for removing nitrate from water*; Patent No. DE 4,125,627 A1, German Patent Office, Federal Republic of Germany, 1993.

CHAPTER 5. STRUCTURAL ORIENTATION PATTERNS FOR A SERIES OF ANTHRAQUINONE SULFONATES ADSORBED AT AN AMINOPHENOL THIOLATE MONOLAYER CHEMISORBED AT GOLD

A paper to be submitted to *The Journal of Physical Chemistry*

Bikas Vaidya, Randall S. Deinhammer, and Marc D. Porter*

ABSTRACT

This paper presents the results of an investigation of the structural orientation and binding patterns for a series of anthraquinone sulfonates at the protonated monolayer spontaneously adsorbed at gold from 4-aminothiophenol (ATP). Both mono- (i.e., 2-anthraquinone sulfonate) and di-sulfonated (1,5-anthraquinone disulfonate, 1,8-anthraquinone disulfonate, and 2,6-anthraquinone disulfonate) anthraquinones with different positioning of the sulfonate groups were used. The structural and binding patterns were deduced using infrared reflection spectroscopy. These deductions relied primarily on orientational inferences from the strengths of sulfonate vibrational modes, as coupled to the infrared surface selection rule at substrates like gold with a high reflectivity. Implications to the eventual control of the structure to multi-layer organized films are discussed.

INTRODUCTION

Spontaneously adsorbed monolayer and multilayer films have several intriguing properties of value as both model and technologically relevant interfacial materials.[1-9] In the case of the former, these types of interfacial structures can be used to gain insights into the

fundamental basis of interfacial reactivity, lubrication, and related processes. This paper is aimed at exploring issues that are of importance in extending the architecture of organic monolayer films to more than a single layer. The intent is to assess some of the operational principles requisite to the growth and orientation of a second adsorbed layer.

Approaches to construct ordered multilayer films via spontaneous adsorption have, to date, focused on the use of stacked zirconium phosphonate and phosphate layers[10-13] and on bifunctional alkanethiolates.[14-20] In both cases, the strategy entailed the use of a second electrostatically-adsorbed layer that sterically matched that of the underlying layer in an attempt to translate the structural integrity of the underlying layer to the second layer. These approaches have met with varying degrees of success, with the disorder in the multilayer structure increasing as the number of layer increase.

Like many other sulfur-containing organic compounds, 4-aminothiophenol (ATP) has drawn attention of many surface scientists, mainly because of its ability to form an ordered monolayer on metal surfaces like gold[14,21-29] and silver[24,30], and the presence of a reactive amine group to serve as a site for subsequent modification.[22,28,31] Monolayers of ATP on gold (ATP/gold) has been used as a promoter for rapid heterogeneous electron transfer of cytochrome c,[32] and pyrroloquinine quinone,[29] for growing ordered polymer of aniline,[21,27] and to immobilize glucose oxidase and redox mediator in glucose selective electrode.[26] In addition, the amine group at low solution pH is protonated as shown in Scheme 1. The protonated ATP monolayer on gold is capable of electrostatically binding anionic species like 2,6-anthraquinone disulfonate.[14]

Scheme 1

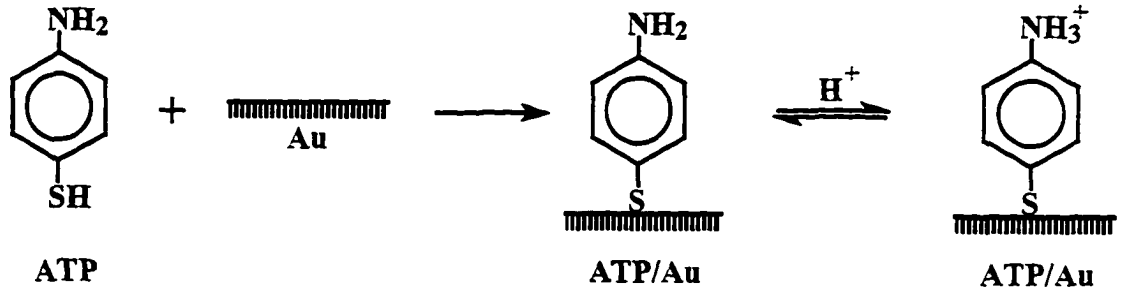

The following sections investigate the formation and characterization adsorbed anthraquinone mono- and di- sulfonates (Chart 1) at the protonated form of a gold-bound monolayer formed from 4-aminothiophenol (ATP) using infrared reflection spectroscopy. Through the use of the different structures of these adsorbates, insights into the binding and structural orientation patterns of potential use in the controlled construction of ordered multilayer films. This paper presents the results and conclusions of this study.

EXPERIMENTAL SECTION

Chemicals. 4-Aminothiophenol, and 1,8-anthraquinone disulfonate (dipotasium salt) were obtained from TCI. 2-anthraquinone monosulfonate (sodium salt), 1,5-anthraquinone disulfonate (disodium salt), and 2,6-anthraquinone disulfonate (disodium salt) were obtained from Aldrich. All the reagents were used as received. Aqueous solutions were prepared with distilled water that was subsequently deionized using Millipore Milli-Q water system.

Sample preparation. Substrates were prepared by the resistive evaporation of ~300 nm gold onto 75 mm x 25 mm glass slides primed with ~15 nm of chromium in a

Chart 1.

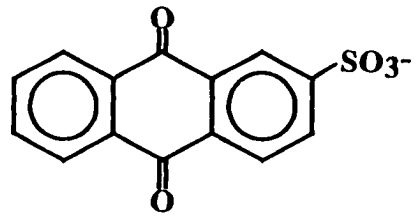

2-AQMS

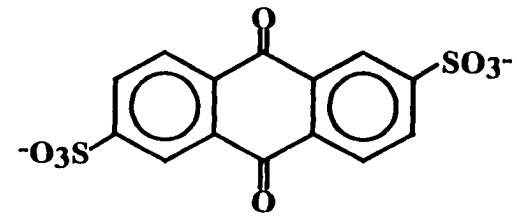

2,6-AQDS

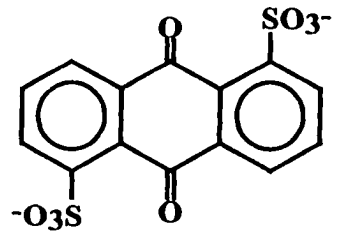

1,5-AQDS

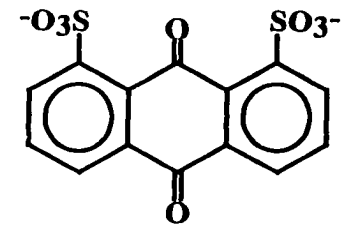

1,8-AQDS

cryogenically pumped Edwards E306A coating system. The deposition rate of gold was 0.3-0.4 nm/s.

After preparation, the gold substrates were immersed into 1-10 mM ethanolic solution of ATP for one hour unless otherwise stated. The samples were rinsed extensively with ethanol and dried on a spin coater. These samples were then immersed for one hour into 5 mM aqueous solutions of the anthraquinone derivatives composed of a pH 2.0 phosphate buffer (0.1 M H_3PO_4 and 0.1 M NaH_2PO_4). Upon immersion, the samples were lightly rinsed with buffer (devoid of any anthraquinone), 0.01 M HCl, and dried on a spin coater.

Instrumentation. Infrared spectra were acquired with a Nicolet 750 FTIR spectrophotometer and a liquid N_2 cooled HgCdTe detector. Reflection spectra were obtained using p-polarized light incident at 81° with respect to the surface normal. A home-built sample holder was used to position the substrate in the spectrophotometer.[33] The reflection spectra are reported as $-\log(R/R_0)$, where R is the reflectance of the sample and R_0 is the reflectance of a reference, octadecanethiolate-d_{37} monolayer on gold. Transmission spectra were obtained by the dispersion of the samples in KBr. The spectra were collected at 2 cm^{-1} resolution (zero filled) with Happ-Genzel apodization. Further details of these methods are given elsewhere.[34]

RESULTS AND DISCUSSION

Structural characterization of the 4-ATP monolayer at gold. As a starting point for analyzing the bindings patterns of the anthraquinone sulfonates at ATP/gold, the spectra for ATP dispersed in KBr (ATP/KBr) and for as-formed ATP/gold are presented between

1750 and 750 cm^{-1} in Figures 1a,b, respectively. Peak positions and mode assignments are summarized in Table 1. The strong correlations of the positions for several of the bands for the two different types of samples confirm the general composition of ATP/gold. This correlation is evident, for example, from the presence of the δ(N-H) band near 1620 cm^{-1}, the ν(C=C) band near 1590 cm^{-1}, and the ν(C-N) band near 1281 cm^{-1} in both spectra.

These data also provide qualitative insight into the average spatial orientation of ATP/gold. The analysis develops from the infrared surface selection rule which relies on the preferential excitation of vibrations with transition dipoles having components normal to highly reflective metallic surfaces.[35] Thus, assuming that the symmetry species for 4-ATP can be assigned to the C_{2v} point group and that the plane of the aromatic ring is in the *yz* plane and *z* is the C_2 axis, the transition dipoles for the infrared active a_1 and b_2 symmetry species are in-plane modes and the b_1 symmetry species is an out-of-plane mode.[30] Therefore, the virtual absence in the ATP/gold spectrum of the b_1 vibrational mode found at 823 cm^{-1} for ATP/KBr, coupled with the persistence of the a_1 modes at 1591 and 1178 cm^{-1}, are indicative of an average orientation of the aromatic ring along the surface normal. This assessment, which is represented in Scheme 1, is consistent with those in earlier reports on this and closely related monolayers systems.[28,30]

Infrared structural characterizations of anthraquinone mono- and di-sulfonates adsorbed at ATP/Gold. (i). General Observations. The infrared spectroscopic data for these systems are presented between 1750 and 750 cm^{-1} in Figures 2-6. Summaries of band assignments and peak positions for the bands central to the qualitative interpretation for the

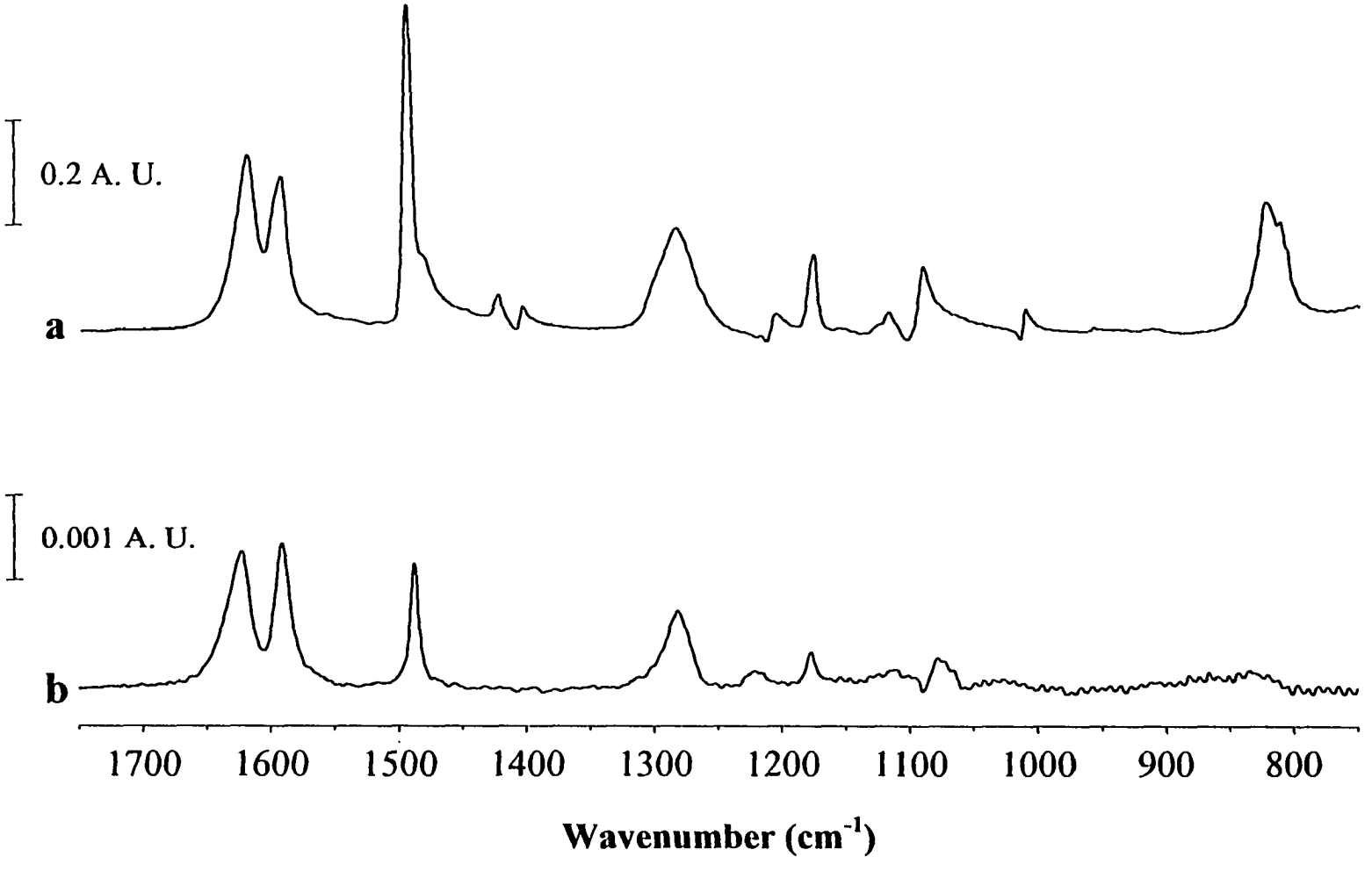

Figure 1. Infrared spectra of ATP in KBr (a) and ATP at gold (b).

Table 1. Infrared peak positions (cm^{-1}) and band assignments for 4-amino-thiophenol dispersed in KBr (4-ATP/KBr) and chemisorbed at gold (4-ATP/gold).

peak positions		
4-ATP/KBr	4-ATP/gold	band assignments[a]
1620	1623	δ(NH)
1594	1591	ν(C=C), 8a (a_1)
1495	1488	ν(C=C) + δ(C-H), 19a (a_1)
1423		ν(C=C) + δ(C-H), 19b (b_2)
1404		
1284	1281	ν(C-N)
	1222	
1205		
1176	1178	δ(C-H), 9a (a_1)
1091	1078	ν(C-S), 7a (a_1)
823		π(C-H), 11 (b_1)

a) Mode descriptions: ν, stretch; δ, bend; π, wags.

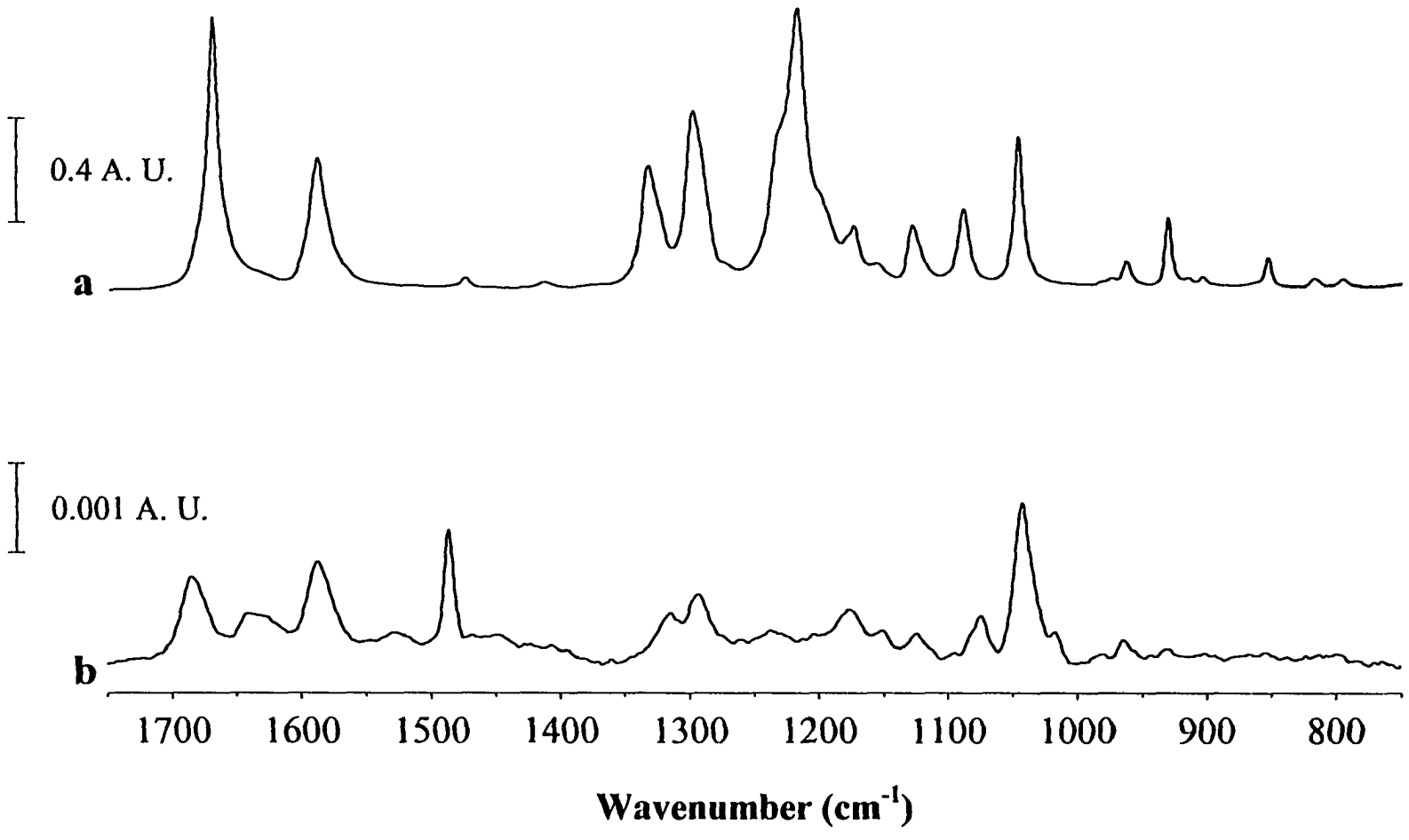

Figure 2. Infrared spectra of 2-AQMS in KBr (a) and at ATP/gold (b).

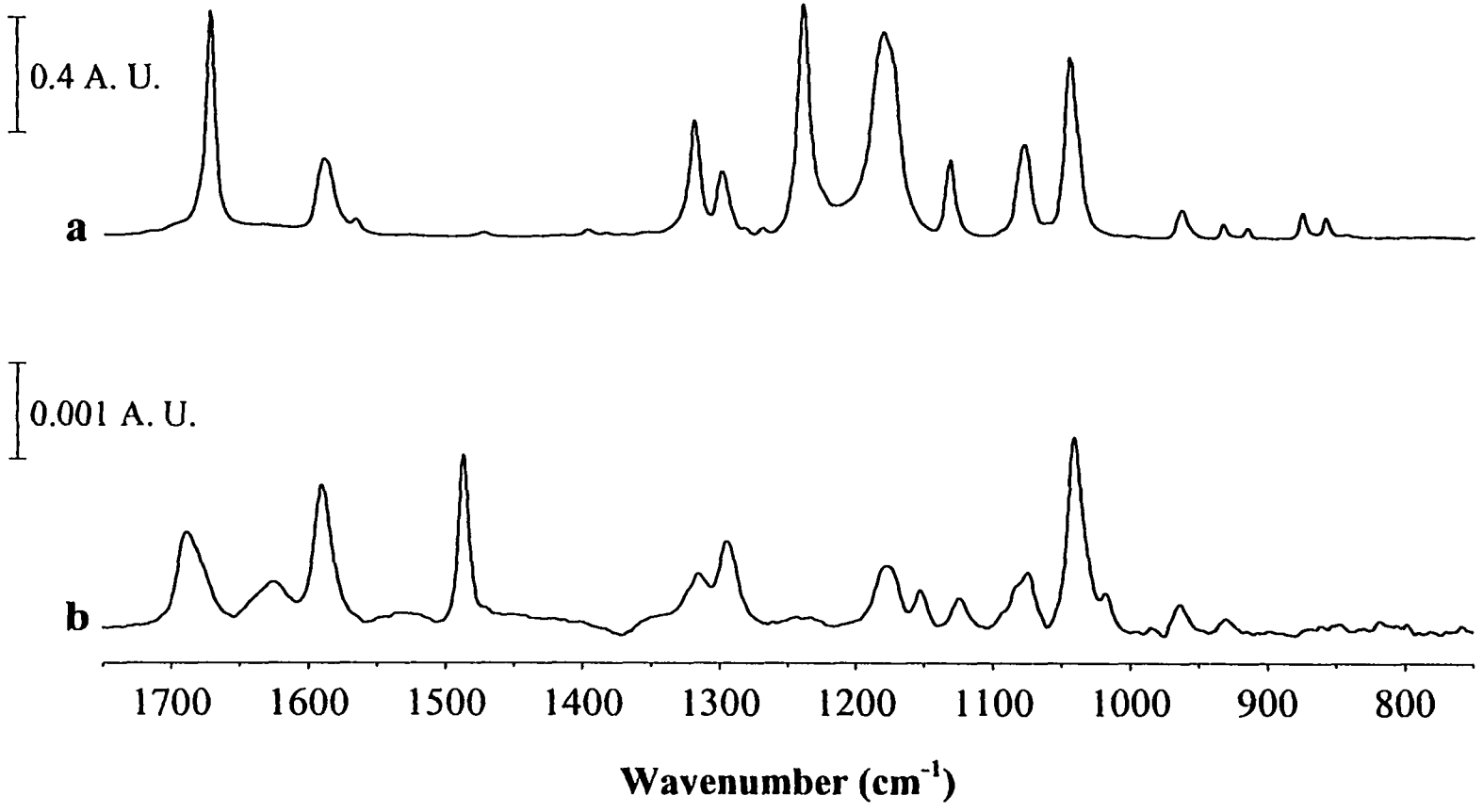

Figure 3. Infrared spectra of 2,6-AQDS in KBr (a) and at ATP/gold (b).

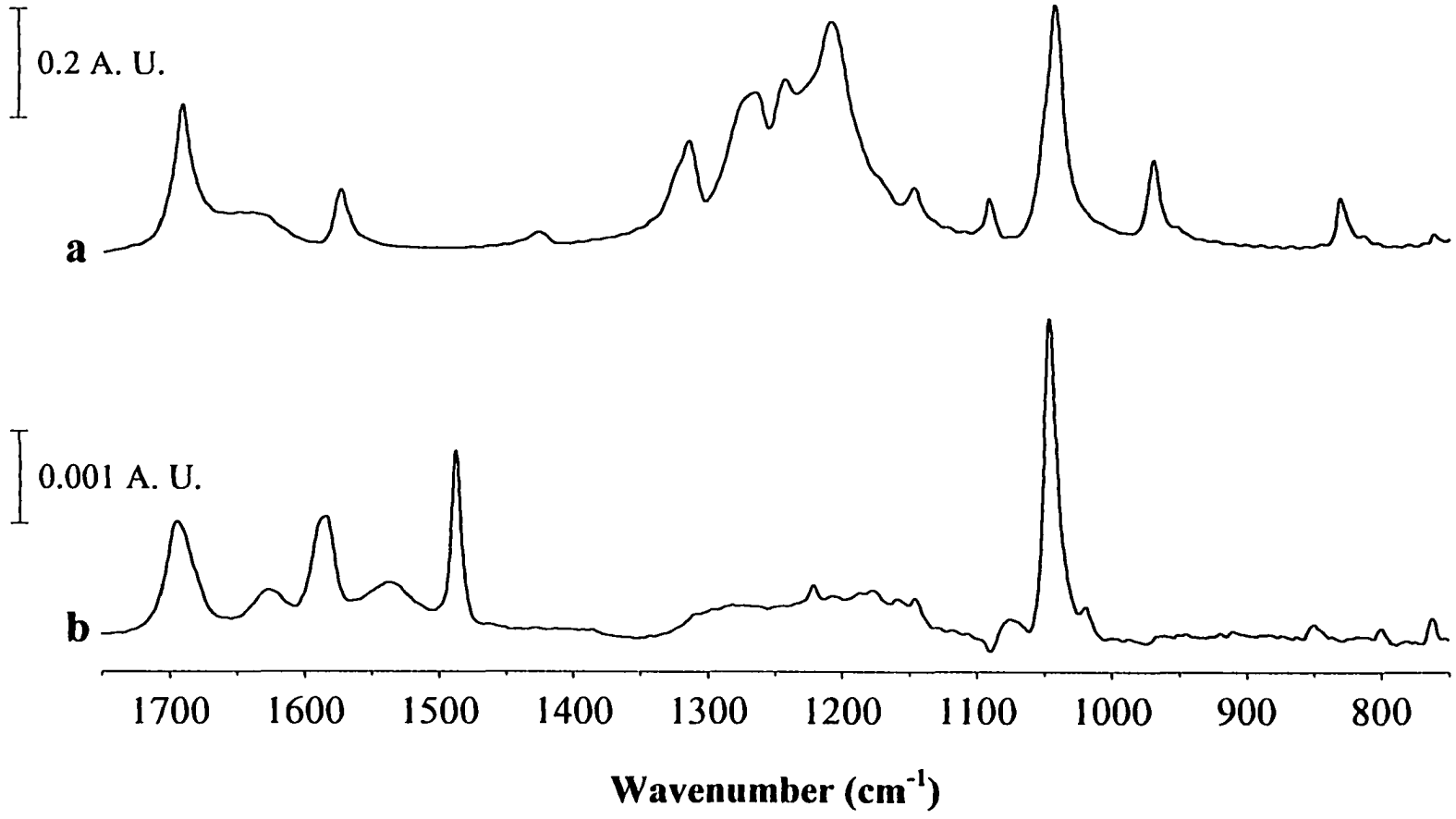

Figure 4. Infrared spectra of 1,5-AQDS in KBr (a) and at ATP/gold (b).

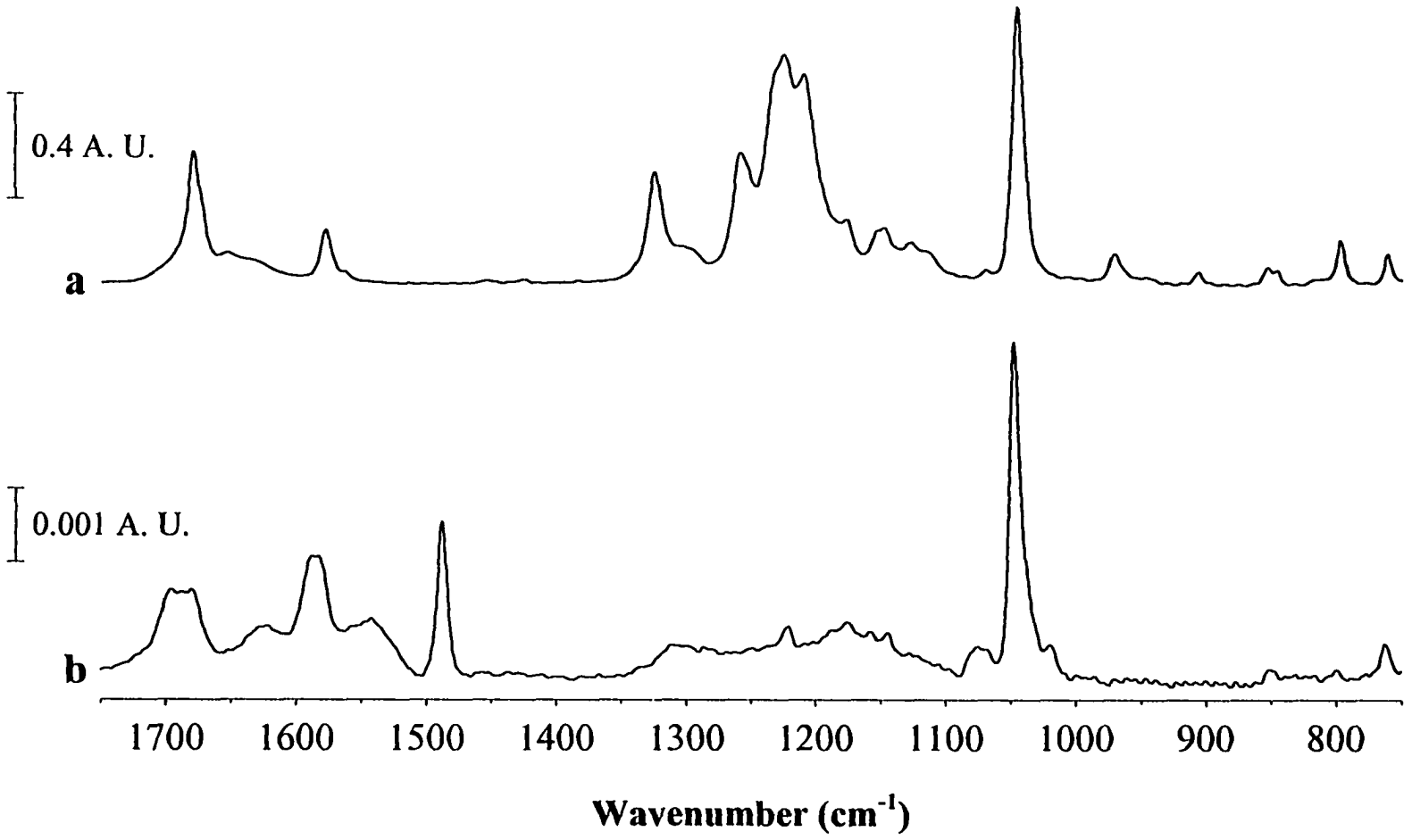

Figure 5. Infrared spectra of 1,8-AQDS in KBr (a) and at ATP/gold (b).

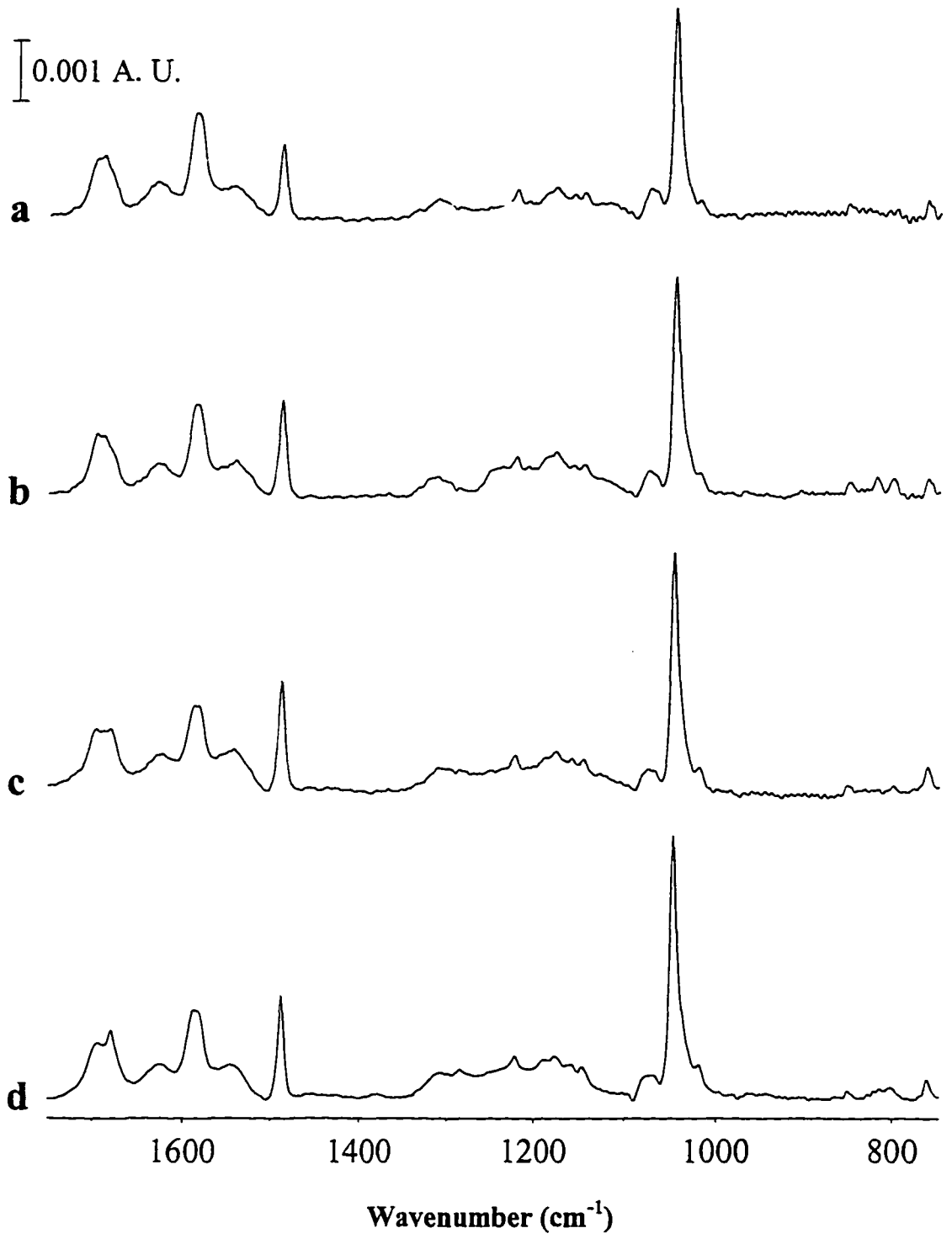

Figure 6. Infrared spectra of 1,8-AQDS at ATP/gold formed by immersing in 5 mM 1,8-AQDS in pH 2 aqueous solution for (a) 5 minutes, (b) 20 minutes, (c) 1 hour, and (d) 1 day.

binding patterns of the anthraquinone sulfonates at ATP/gold are given in Table 2. These interpretations will rely largely on the relative magnitudes of the ν(C=O), the two $\nu_{as}(SO_3)$ modes, and the $\nu_s(SO_3)$ mode of the adsorbed anthraquinone sulfonates and the perturbation of the δ(NH) and ν(CN) modes of the underlying ATP monolayer.

In general, we found that the formation of the adsorbed layers from the anthraquinone mono- and di-sulfonates was complete within one hour after immersing freshly prepared ATP/gold into the sample solutions. This conclusion was based on the observation that, with the exception of 1,8-AQDS, there were only subtle changes in the infrared spectra of these systems after ~60 min of immersion in the formation solutions. We will focus largely on the general structural interpretations of the adsorbed anthraquinone sulfonates formed with ~60 min immersion times, commenting in detail only on the much slower evolution of the 1,8-AQDS system.

We also found, as previously described,[14] that the presence of adsorbed anthraquinone sulfonates were detectable via infrared spectroscopy only when using formation solutions that insured the protonation of the amine group of ATP. Formation conditions where the amine was not protonated failed to yield a detectable adsorbed species. We were also successful in tests to adsorb small amounts of the anthraquinone sulfonates at uncoated gold films. The resulting spectra, while having bands with magnitudes near the performance limit of our instrument, aided in completing some of the vibrational mode assignments.

(ii). 2-AQMS. The spectroscopic data for 2-AQMS/KBr and for 2-AQMS adsorbed at ATP/gold are shown in Figures 2a,b, respectively. Though not quantifiable in terms of

Table 2. Infrared peak positions (cm^{-1}) and band assignments for anthraquinone mono- and di sulfonates dispersed in KBr, and adsorbed at an ATP monolayer on gold.

	Anthraquinone modes			ATP modes	
Sample	ν (C=O)	ν_{as} (SO_3)	ν_s (SO_3)	δ(NH)	ν (C=C) + δ(C-H), 19a(a_1)
2-AQMS/KBr	1670	1234 1217	1047		
2-AQMS/ATP/Au	1678	nd	1041	1625	1487
2,6-AQDS/KBr	1672	1240 1181	1045		
2,6-AQDS/ATP/Au	1686	1178	1041	1625	1487
1,5-AQDS/KBr	1691	1243 1208	1042		
1,5-AQDS/ATP/Au	1695	nd	1046	1627	1487
1,8-AQDS/KBr	1680	1210	1046		
1,8-AQDS/ATP/Au	1695 1680	nd	1047	1622	1488

coverage, the presence of the ν(C=O) band at 1678 cm^{-1} and the $\nu_s(SO_3)$ band at 1041 cm^{-1} in Figure 2b confirms the adsorption of 2-AQMS at ATP/gold. The adsorption of 2-AQMS is also demonstrated by the strong perturbations of the δ(NH) and ν(CN) modes of ATP. The former mode is at 1620 cm^{-1} for ATP/KBr, but is weakened, broadened, and shifted (~5 cm^{-1} to higher energy) for ATP/gold. The latter mode is at 1284 cm^{-1} for ATP/KBr, and is not detected for ATP/gold.

In addition, the absence of bands around 1225 cm^{-1}, a region where the two $\nu_{as}(SO_3)$ bands are found in Figure 2a, is consistent with the general structural picture given in Scheme 2. This description develops, in part from the difference in the orientations of the transition dipoles for the $\nu_{as}(SO_3)$ and $\nu_s(SO_3)$ modes. Qualitatively, the $\nu_s(SO_3)$ mode is aligned along the C-S bond of the tetrahedron formed by the C-SO_3 substructure, whereas those for both of the $\nu_{as}(SO_3)$ modes are orthogonal to the $\nu_s(SO_3)$ mode. Thus, the presence of the $\nu_s(SO_3)$ band, the absence of both of the $\nu_{as}(SO_3)$ bands, the strong perturbation of the δ(NH) band, and the absence of the ν(CN) band when 2-AQMS is adsorbed at ATP/gold points to the general structural orientation of adsorbed 2-AQMS that is depicted in Scheme 2.

Scheme 2 also suggests that adsorbed 2-AQMS interacts primarily through electrostatic interactions with the underlying protonated amine of ATP/gold. That is, the structure of the underlying ATP monolayer is not detectably affected by the adsorption of 2-AQMS. This assertion is based on the similarity in the magnitudes of the band at 1488 cm^{-1} (i.e., a ν(C=C)+ δ(C-H) mode) in Figures 2a,b, which would likely exhibit a difference in magnitude if the adsorption of 2-AQMS altered the spatial orientation of chemisorbed ATP.

Scheme 2

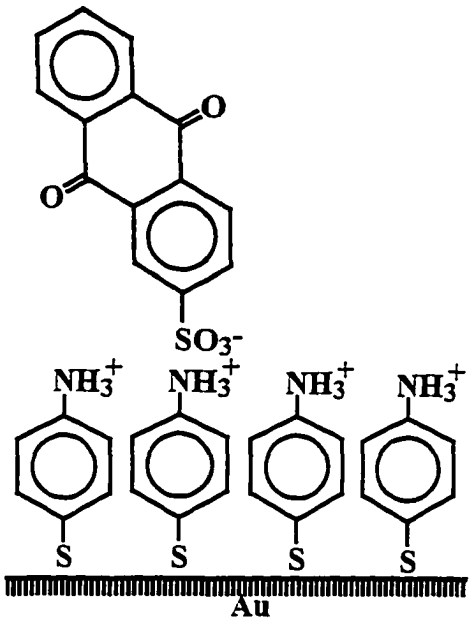

2-AQMS/ATP/Au

(iii). 2,6-AQDS. Figure 3 presents the infrared spectra for 2,6-AQDS, and follows the same labeling format used for Figure 2. Based on the location of the two sulfonates on opposite sides of the 2,6-AQDS structure, this adsorbate along with the other anthraquinone disulfonates tests in more detail the relative importance of the interactions (e.g., electrostatic interactions) between the adsorbate and underlying surface and the interactions (e.g., π-π interactions) between neighboring adsorbates on the general structural arrangement of the adsorbed layer. In contrast to the spectrum for 2-AQMS at ATP/gold, bands for the low energy $\nu_{as}(SO_3)$ (1178 cm^{-1}) mode and the $\nu_s(SO_3)$ mode (1041 cm^{-1}) are evident in Figure 3b. In addition, the larger magnitude of the $\nu_s(SO_3)$ band for 2,6-AQDS in comparison to 2-AQDS is consistent with the expectation of having two sulfonate groups aligned along the

surface normal of the underlying substrate. These signatures give rise to the general structural picture given in Scheme 3, which shows that the electrostatic interactions between the protonated amine and one of the sulfonates play a strong role in controlling the spatial orientation of adsorbed 2,6-AQDS.

Scheme 3.

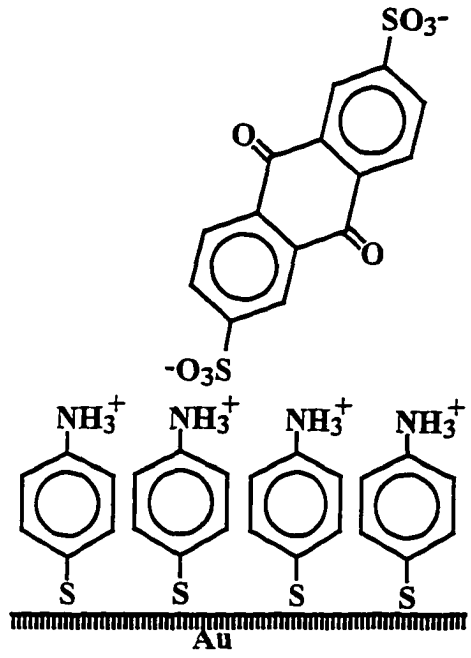

2,6-AQDS/ATP/Au

(iv). 1,5-AQDS. Like 2,6-AQDS, the structure of 1,5-AQDS tests the relative importance of the interactions between the adsorbate and substrate and between neighboring adsorbates in dictating the spatial arrangement of this adsorbate-substrate system. Indeed, there are several parallels between the two spectra for 1,5-AQDS (Figure 4a,b) and the two for 2,6-AQDS. In other words, the effect of adsorbed 1,5-AQDS on the underlying modes

(i.e., δ(NH) and ν(C-N)) of ATP reflects the electrostatic interaction between adsorbed 1,5-AQDS and the protonated amine group of the ATP monolayer.

There are, however, some additional striking differences between the spectra in Figures 4a,b. These differences are indicative of a spatial arrangement for adsorbed 1,5-AQDS that differs markedly from those of both 2-AQMS and 2,6-AQDS. Figure 4b, while exhibiting a strong band at 1046 cm^{-1} for the $\nu_s(SO_3)$ mode, is virtually devoid of any detectable vibrational modes between 1350 and 1100 cm^{-1}. This region contains several strong bands in Figure 4a, including the $\nu_{as}(SO_3)$ modes at 1243 and 1208 cm^{-1} as well as the C-(C=O)-C stretching mode[36] for the quinone substructure of the adsorbed species. While as yet uncertain as to the specific band assignment, the latter mode has a transition dipole that lies along the long axis of the anthraquinone structure. Therefore, the absence of the bands between 1350 and 1100 cm^{-1}, together with the presence of a strong $\nu_s(SO_3)$ band in Figure 4a, supports the structural arrangement presented in Scheme 4.

(v). 1,8-AQDS. The structural form of 1,8-AQDS differs from 2,6-AQDS and 1,5-AQDS by having both of the sulfonate groups on the same side of the extended ring structure. The effect of this structural variation is revealed by comparisons of Figures 5a,b. As found for adsorbed 1,5-AQDS, the bands between 1350 and 1100 cm^{-1} are notably weaker for 1,8-AQDS adsorbed at ATP/gold (Figure 5b) than for 1,8-AQDS/KBr. Indeed, the spectrum for adsorbed 1,8-AQDS is more like that of adsorbed 1,5-AQDS than of adsorbed 2-AQMS and adsorbed 2,6-AQDS. In other words, the presence of the large band for $\nu_s(SO_3)$ at 1047 cm^{-1}, coupled with the low magnitudes of the spectral features between 1350 and 1100 cm^{-1}, is

Scheme 4.

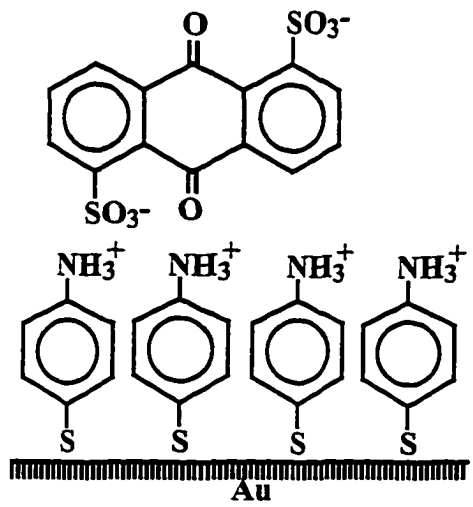

1,5-AQDS/ATP/Au

diagnostic of the general structural arrangement shown in Scheme 5 for 1,8-AQDS adsorbed at an ATP monolayer.

Interestingly, the evolution of the IR spectra for 1,8-AQDS on ATP/Au requires a more extended period of immersion than the ~60 minutes to reach an effectively unchanged spectrum for the other three adsorbates. The evolution of the spectrum for this system is presented in Figure 6. As evident, the ν(C=O) (~1695 cm^{-1}) evolves with increasing immersion time. At short immersion times (e.g., 5 min), the ν(C=O) band has a relatively undefined structure, where as the two distinct bands appear after 24 hours of immersion. Interestingly, the low energy band at 24 hours is located at the same position as that for 1,8-AQDS/KBr (1680 cm^{-1}). This evolution indicates the formation of a more ordered layer of 1,8-AQDS dispersed in KBr. We believe the trend evolution of the ν(C=O) band indicates

Scheme 5.

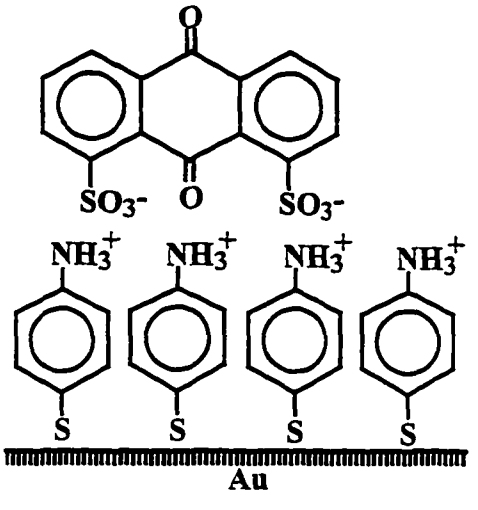

1,8-AQDS/ATP/Au

the formation of a more ordered layer of 1,8-AQDS on ATP/Au as immersion time increases. We attribute the slower ordering of 1,8-AQDS to the greater barrier to lateral movement because of having two effective linkages to the surface as opposed to the single linkages of the other three adsorbates.

CONCLUSIONS

The chemisorption of ATP forms an ordered monolayer on gold with an average orientation of the aromatic ring along the surface normal that can be protonated or deprotonated by varying the pH of the contacting solution. Anthraquinone mono- and disulfonates can be electrostatically attached to the protonated ATP monolayer on gold. The orientation of the anthraquinone mono- or disulfonate attached to the protonated ATP surface

is largely directed by the anionic sulfonate groups that bind to the surface-bound ammonium group.

ACKNOWLEDGMENTS

This work was supported by the Office of Basic Research-Chemical Sciences Division of the United States Department of Energy-Ames Laboratory, and by the Microanalytical Instrumentation Center of the Iowa State University. The Ames Laboratory is operated for the United States Department of Energy by the Iowa State University under contract No. W-7405-eng-82.

REFERENCES

1) Whitesides, G. M.; Laibinis, P. E. *Langmuir* **1990**, *6*, 87-96.

2) Chau, L.; Porter, M. D. *Chem. Phys. Lett.* **1990**, *167*, 198-204.

3) Stole, S. M.; Porter, M. D. *Langmuir* **1990**, *6*, 1199-1202.

4) Ulman, A. *An Introduction to Ultrathin Organic Films from Langmuir-Blodgett to Self-Assembly*; Academic Press: Boston, 1991.

5) Walczak, M. M.; Chung, C.; Stole, S. M.; Widrig, C. A.; Porter, M. D. *J. Am. Chem. Soc.* **1991**, *113*, 2370-2378.

6) Walczak, M. M.; Popenoe, D. D.; Deinhammer, R. S.; Lamp, B. D.; C, C.; M. D, P. *Langmuir* **1991**, *7*, 2687-2693.

7) Widrig, C. A.; Alves, C. A.; Porter, M. D. *J. Am. Chem. Soc.* **1991**, *113*, 2805-2810.

8) Zak, J.; Yuan, H.; Woo, L. K.; Porter, M. D. *Langmuir* **1993**, *9*, 2772-2774.

9) Walczak, M. M.; Alves, C. A.; Lamp, B. D.; Porter, M. D. *J. Electroanal. Chem.* **1995**, *396*, 103-114.

10) Lee, H.; Kepley, L. J.; Hong, H.; Akhter, S.; Mallouk, T. E. *J. Phys. Chem.* **1988**, *92*, 2597-2601.

11) Keller, S. W.; Kim, H.; Mallouk, T. E. *J. Am. Chem. Soc.* **1994**, *116*, 8817-8818.

12) Kaschak, D. M.; Mallouk, T. E. *J. Am. Chem. Soc.* **1996**, *118*, 4222-4223.

13) Hanken, D. G.; Naujok, R. R.; Gray, J. M.; Corn, R. M. *Anal. Chem.* **1997**, *69*, 240-248.

14) Sun, L.; Johnson, B.; Wade, T.; Crooks, R. M. *J. Phys. Chem.* **1990**, *94*, 8869-8871.

15) Evans, S. D.; Ulman, A. *J. Am. Chem. Soc.* **1991**, *113*, 5866-5868.

16) Sun, L.; Kepley, L. J.; Crooks, R. M. *Langmuir* **1992**, *8*, 2101-2103.

17) Kim, T.; Crooks, R. M.; Tsen, M.; Sun, L. *J. Am. Chem. Soc.* **1995**, *117*, 3963-3967.

18) Wells, M.; Dermody, D. L.; Yang, H. C.; Kim, T.; Crooks, R. M. *Langmuir* **1996**, *12*, 1989-1996.

19) Wells, M.; Crooks, R. M. *J. Am. Chem. Soc.* **1996**, *118*, 3988-3989.

20) Yang, H. C.; Dermody, D. L.; Xu, C.; Ricco, A. J.; Crooks, R. M. *Langmuir* **1996**, *12*, 726-735.

21) Rubinstein, I.; Rishpon, J.; Sabatini, E.; Redondo, A.; Gottesfeld, S. *J. Am. Chem. Soc.* **1990**, *112*, 6135-6136.

22) Sun, L.; Thomas, R. C.; Crooks, R. M. *J. Am. Chem. Soc.* **1991**, *113*, 8550-8552.

23) Kim, Y.-T.; McCarley, R. L.; Bard, A. J. *J. Phys. Chem.* **1992**, *96*, 7416-7421.

24) Hill, W.; Wehling, B. *J. Phys. Chem.* **1993**, *97*, 9451-9455.

25) Bryant, M. A.; Crooks, R. M. *Langmuir* **1993**, *9*, 385-387.

26) Kajiya, Y.; Okamoto, T.; Yoneyama, H. *Chem. Lett.* **1993**, 2107-2110.

27) Sabatini, E.; Redondo, A.; Rishpon, J.; Rudge, A.; Rubinstein, I.; Gottesfeld, S. *J. Chem. Soc. Faraday Trans.* **1993**, *89*, 287-294.

28) Hayes, W. A.; Shannon, C. *Langmuir* **1996**, *12*, 3688-3694.

29) Katz, E.; Lion-Dagan, M.; Willner, I. *J. Electroanal. Chem.* **1996**, *408*, 107-112.

30) Osawa, M.; Matsuda, N.; Toshii, K.; Uchida, I. *J. Phys. Chem.* **1994**, *98*, 12702-12707.

31) Vaidya, B.; Porter, M. D., Unpublished results.

32) Allen, P. M.; Hill, H. A. O.; Walton, N. J. *J. Electroanal. Chem.* **1984**, *178*, 69-86.

33) Stole, S. M.; Porter, M. D. *Appl. Spectrosc.* **1990**, *44*, 1418-1420.

34) Walczak, M. M.; Chung, C.; Stole, S. M.; Widrig, C. A.; Porter, M. D. *J. Am. Chem. Soc.* **1991**, *113*, 2370-2378.

35) Porter, M. D. *Anal. Chem.* **1988**, *60*, 1143A-1149A.

36) Silverstein, R. M.; Bassler, G. C.; Morrill, T. C. *Spectrometric Identification of Organic Compounds*; 4th ed.; John Wiley and Sons: New York, 1981.

CHAPTER 6. GENERAL CONCLUSIONS

The selectivity of a method in chemical analysis usually depends on a host of intricate interactions and equilibria between the analyte, reagent, solvent and other species present in the system. The interaction(s) can range, for example, from simple electrostatic attraction or repulsion to hydrophobic/hydrophilic, acid-base, or electron donor-acceptor interactions. These interactions depend heavily on the nature and the physical state of each of the species present in the system, as well as on the relative and/or absolute amount of each of the species. The selectivity of a method of chemical analysis can usually be enhanced by optimizing the parameters that govern the equilibria of the system.

The feasibility for the improvement of different methods of chemical analysis by manipulation of molecular structure, medium, phase and surface functionality and orientation of the molecules adsorbed on a surface has been investigated. Chapter 2 has demonstrated a remarkable enhancement in selectivity in the binding of divalent metal cations using two novel crown ether compounds. The incorporation of benzo groups in the ring structure reduced basicity of the ring oxygen and enhanced rigidity of the crown ether ring; as a result, the two novel crown compounds CCE and FCE exhibited an unprecedented selectivity in the binding of Hg(II) over a host of other divalent metal cations. Other desirable modifications on the crown ethers would be to attach a thiol, silane, or amine tether so that the crown ether could be attached to a metal, glass or carbon surface and be used as a sensor for the continuous monitoring of Hg(II).

Methods of chemical analysis can also be improved by the elimination of phase boundary, as exists between an aqueous and an organic phase, by introducing a micellar phase. Different types of micelles can be used to solubilize compounds that are otherwise insoluble in water to facilitate the determination of various analytes. In particular, two phase extractions are often tedious and the use of micellar strategies have been shown to reduce processing time. However, introduction of such a pseudo-phase can change, for better or worse, the reactivity and selectivity of the reagent. For example, as described in Chapter 3, the high selectivity of CCE for Hg(II) in a two phase extraction was almost fully attenuated upon solubilization in the mixed micelle.

Use of micellar solution with fluorogenic crown ether could result in an increase in fluorescence intensity as a result of the adsorption of the fluorophores on the micelles. In addition a zwitterionic surfactant may show more interesting changes in metal ion binding and spectral properties. Entrapment of the crown ethers using sol-gel material on an optical probe is another possibility that solves the solubility problem and conserves the reagent, and may be more suitable for continuous monitoring applications.

An improvement in a method of chemical analysis by removal of an interferrent into a different phase has been demonstrated in Chapter 4. In the method developed for the chloride removal for COD determinations, chloride ion is removed as HCl gas. HCl gas is then captured by a bismuth-based adsorbent, eliminating the use of a toxic mercury salt.

The last chapter examined fundamental issues in the control of the architecture of model surfaces to gain insight into the factors that can be explored for the construction of

ordered multilayer films. These studies may have value in guiding the design of architectures for molecular recognition purposes. ATP forms an ordered monolayer on gold with an average orientation of the aromatic ring along the surface normal and can be protonated or deprotonated by varying the pH of the contacting solution. Anthraquinone mono- and disulfonates can be electrostatically attached to the protonated ATP monolayer on gold. The orientation of the adsorbed anthraquinone mono- or disulfonate is largely directed by the anionic sulfonate group that binds to the surface bound ammonium group. The orientation of each of the four anthraquinone sulfonates studied have been determined from their respective infrared spectra. Ongoing studies should build on these results, serving as a basis of guiding principles for control of surface architectures in three dimensions.

APPENDIX. THE ROLE OF CHEMICALLY MODIFIED SURFACES IN THE CONSTRUCTION OF MINIATURIZED ANALYTICAL INSTRUMENTATION

A paper presented at 23rd International Conference on Environmental Systems†

Marc D. Porter, Shelley J. Coldiron and Bikas Vaidya

ABSTRACT

This paper describes the development of a thin-firm optical sensor for measuring pH. The indicator behaves as a polyprotic acid with differing optical properties in each of its chemical forms. Together, these properties facilitate the development of an internally calibrated sensor by calculating the ratios of the absorption maximas for each form of the indicator. The covalent immobilization procedure developed demonstrated long term stability of 4 months without recalibration.

INTRODUCTION

The development of reversible multicomponent optical sensors remains a significant challenge.[1-20] Current optical pH sensor technology is hampered by the inaccuracies resulting from variations in ionic strength.[21] Also, since most of the sensor materials are constructed from an impermeable thin film of an organic polymer, response times can be as long as 10 minutes. Such long times are not suitable for real-time monitoring. This decreases the operating efficiency of personnel through lengthy instrumental operation procedures.

In earlier work, we addressed these problems though the development of a highly selective pH sensor (pH range 0-4.5) with a response time of <2 sec.[22] The sensor was constructed by immobilizing Congo Red at a base-hydrolyzed cellulose acetate film. The rapid response results from the porous structure of the hydrolyzed polymeric support which minimizes barriers to mass transport between the analyte and immobilized indicator.

We identified other indicators for expanding the capabilities of our sensors. Brilliant Yellow, with an optical transition occurring between pH 6 to 8 in solution, was the first indicator investigated. However, upon immobilization, the optical transition occurred at higher pH values (i.e., ~2 pH units). A response shift to higher or lower pH values is an effect frequently observed as a consequence of immobilization.[14] Of the many immobilized indicators tested, fluoresceinamine demonstrated the most desirable optical transition for pH with a wide response range of 1 to 10.

Initial indicator attachment techniques with Congo Red utilized non-covalent adsorption of the dye with the cellulosic film.[22] However, to increase long term stability of the sensor, covalent coupling of the indicator with the film is strongly preferred. Several published techniques, such as coupling of the indicator through cyanuric chloride for attachment to the film,[23] crosslinking of the dye to the cellulosic film with glutaraldehyde,[24] oxidizing hydrolyzed cellulose acetate hydroxy groups to aldehyde substituents followed by amine substitution,[25] and replacing hydrolyzed cellulose acetate hydroxy groups with fosyl chloride followed by indicator attachment,[26] were investigated. However, once immobilized by these methods, most of the indicators investigated either failed to exhibit an optical

response to a change in pH, or the amount of indicator immobilized was too deficient to yield a significant signal for quantification. Ultimately, epoxy derivitized beads were identified as an immobilization intermediary for cellulose acetate film inclusion. The following sections detail research conducted to develop a pH sensing thin-film based upon covalently-bound fluoresceinamine. The films are used with a miniaturized fiber-optic photometer that was developed in our laboratory.

EXPERIMENTAL

Epoxy Bead Characteristics: Riedel-deHaen (Hannover, Germany) produces a polymer carrier (Polymer Carrier VA-Epoxy BIOSYNTH®) for the covalent immobilization of enzymes. Chemically, it is a copolymer based on vinyl acetate and divinylethylene-urea. The surface is modified with oxirane groups after hydrolysis of the acetate groups.[27] These epoxide linkages can be utilized to couple various compounds. Fluoresceinamine was immobilized on the beads through the compound's primary amine with a base catalyzed reaction (Figure 1). Advantageous properties of the beads include: high structural stability, chemical stability over a wide pH range, and negligible swelling or shrinking with changing pH or salt concentration. Particle size ranges from 50-200 μm. The epoxide equivalency for the beads is 300 μmol/g.

Immobilization: The epoxide beads were pulverized into a powder to minimize particle aggregation in solution. Fluoresceinamine was coupled to the pulverized epoxy beads by adding an excess (1:10 by weight) of indicator to beads. This mixture was

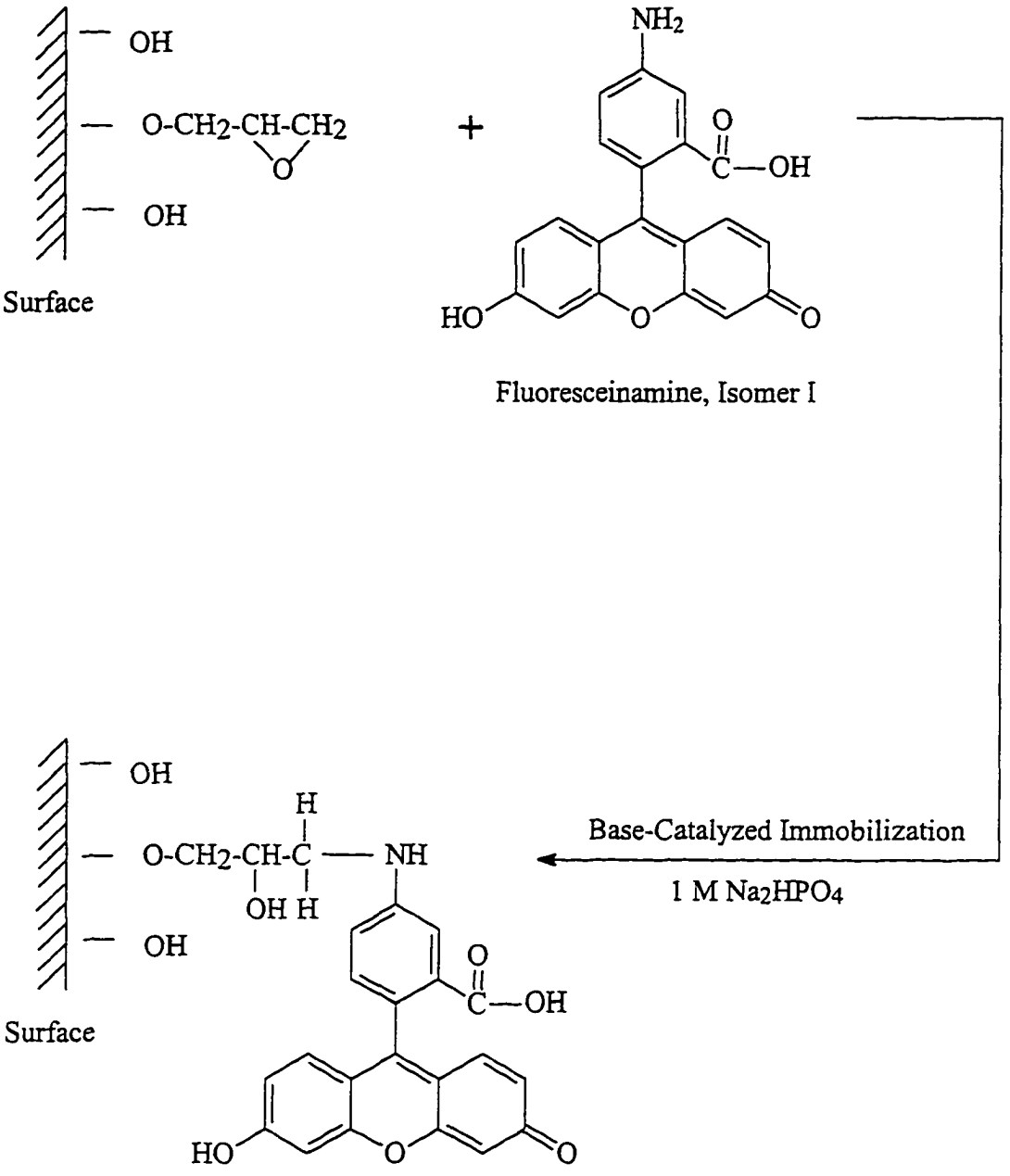

Figure 1. Base Catalyzed Immobilization of Fluoresceinamine at Epoxy Bead Surface.

immersed in 1 M Na_2HPO_4 (pH 7.5). The suspension was stirred for 2 h, and excess dye was removed by washing the beads with 0.1 M Na_2HPO_4.

Fabrication of Sensing Film: The dried immobilized product was dissolved in cyclohexanone, and cellulose acetate was added to produce a 14% w/v cellulose acetate/cyclohexanone solution. The suspension was ultrasonicated to further disperse the crushed, dyed beads within the viscous solution. The cellulosic suspension was cast onto glass slides and dried at for 70 °C for ~24 h. The dried films were then hydrolyzed with 0.1 M KOH for 24 h.

Evaluation of Sensor Response: The spectral attributes of the fluoresceinamine films were examined with a Hewlett-Packard 8452A Diode Array Spectrophotometer. The films were secured in a flow through cell (Figure 2) and positioned within the optical path of the spectrophotometer. The absorbance characteristics of the films were measured at various pH values.

Reagents: Fluoresceinamine was obtained from Aldrich and used without further purification. The pH of the solution was controlled by citric acid and disodium phosphate buffers.[28] All solutions were prepared with deionized water.

RESULTS AND DISCUSSION

In an attempt to verify the mode of immobilization shown in Figure 1, infrared (IR) spectra were taken of the dyed epoxy beads and compared to spectra from unmodified beads and the reagent dye using a Nicolet 740 Fourier transform infrared spectrometer. The samples were mixed with KBr and pressed into pellets for absorption measurements.

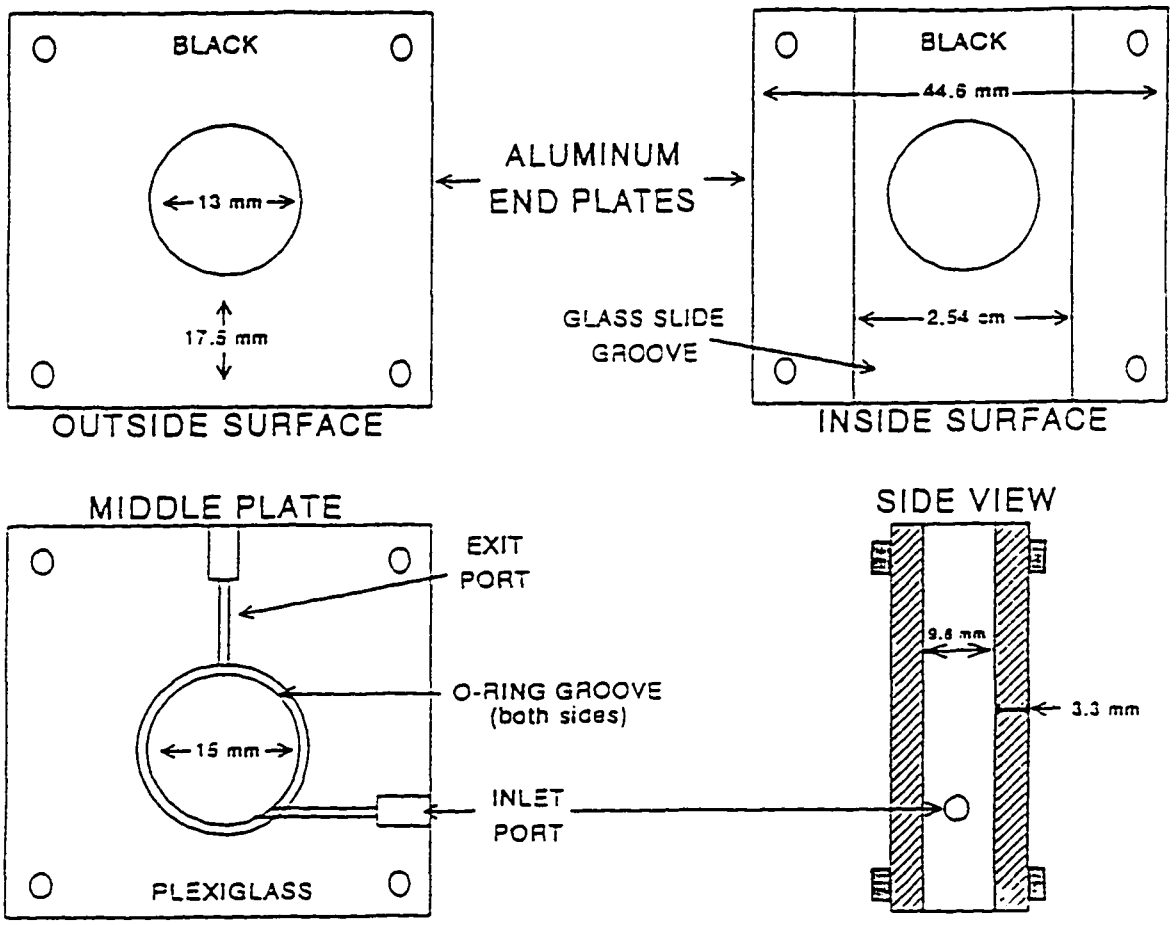

Figure 2. Flow Through Cells for Examining Absorbance Properties of Thin film Sensors.

Theoretically, with immobilization, comparative IR spectra of the dyed beads should indicate a decrease in relative intensity of the primary amine peak positions and an increase in relative intensity at the secondary amine peak positions. However, comparative spectra of the unmodified epoxy beads and the dyed beads were only slightly distinguishable. Efforts are currently underway to verify the predicted immobilization reaction from the IR data.

The films exhibit both visible and fluorescent spectroscopic transitions with changes in pH from 1 to 10. The indicator behaves as a triprotic acid with absorption maxima at 440 nm, 464 nm, and 500 nm. This property facilitates the development of an internally calibrated sensor by allowing the calculation of the ratio of the absorption maxima for each form of the indicator. Such an approach also compensates for calibration difficulties that may arise from preparative variations in the amount of immobilized indicator and for desorption loss of the indicator from the film during use.

As can be seen from Figure 3, there are tangential spikes occurring at ~485 nm and an abnormal band occurring at 570-600 nm. For visual simplicity, the plot only depicts the spectral response at the extremes (pH 1 and 10) and midpoint (pH 7). The anomalies are collectively attributed to scattering caused by the flow through cell, the beads, and the cellulosic film (Figure 4). The fluoresceinamine absorption spectra can be enhanced by subtracting this background signal (Figure 5). A calibration curve for the full pH range of 1-10 can be constructed by ratioing the peak maxima of 500 nm to 464 nm. The curve can be described by a fifth order polynomial, $Y = 6.8448 \times 10^{-1} + 1.0095X - 3.8337 \times 10^{-1} X^2 + 6.4700 \times 10^{-2} X^3 - 4.8200 \times 10^{-3} X^4 + 1.3000 \times 10^{-4} X^5$ (see Figure 6).

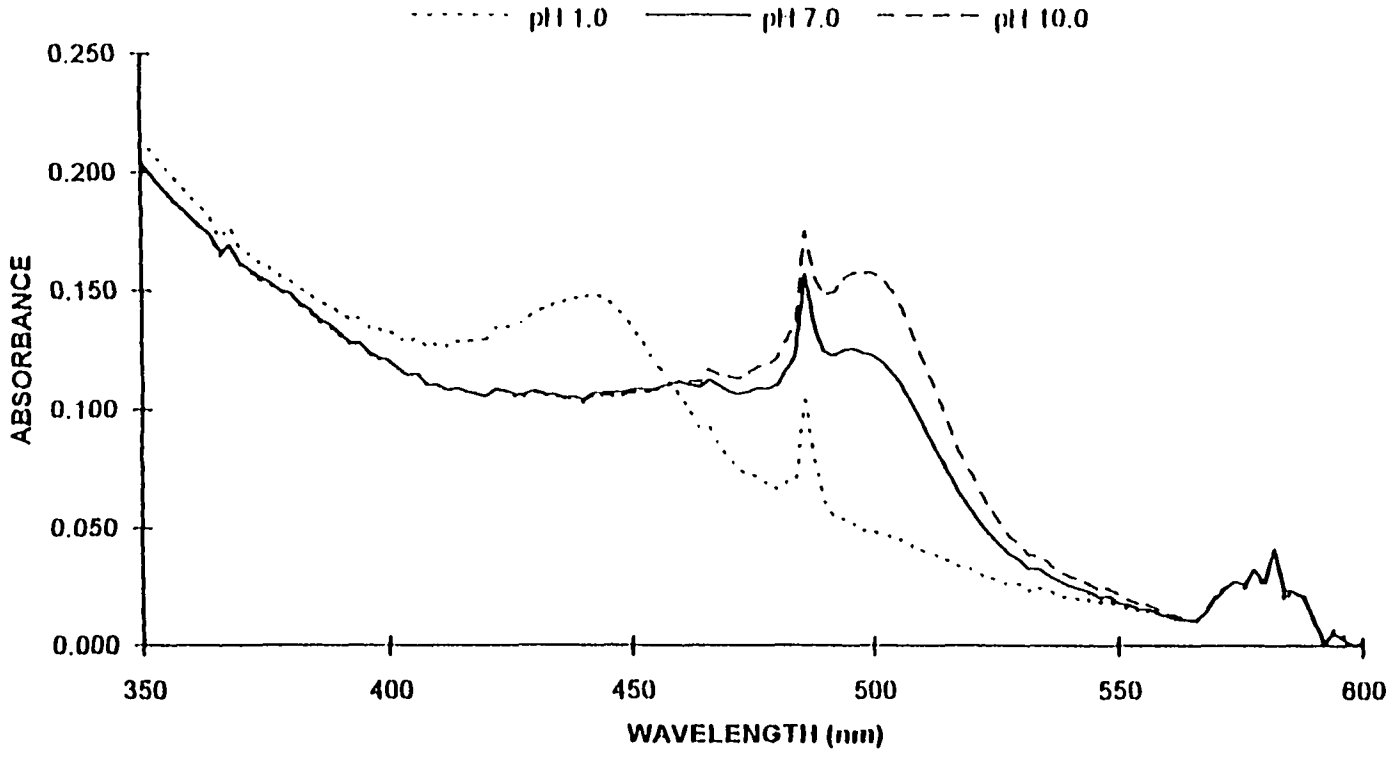

Figure 3. Absorbance Spectra of Immobilized Fluoresceinamine.

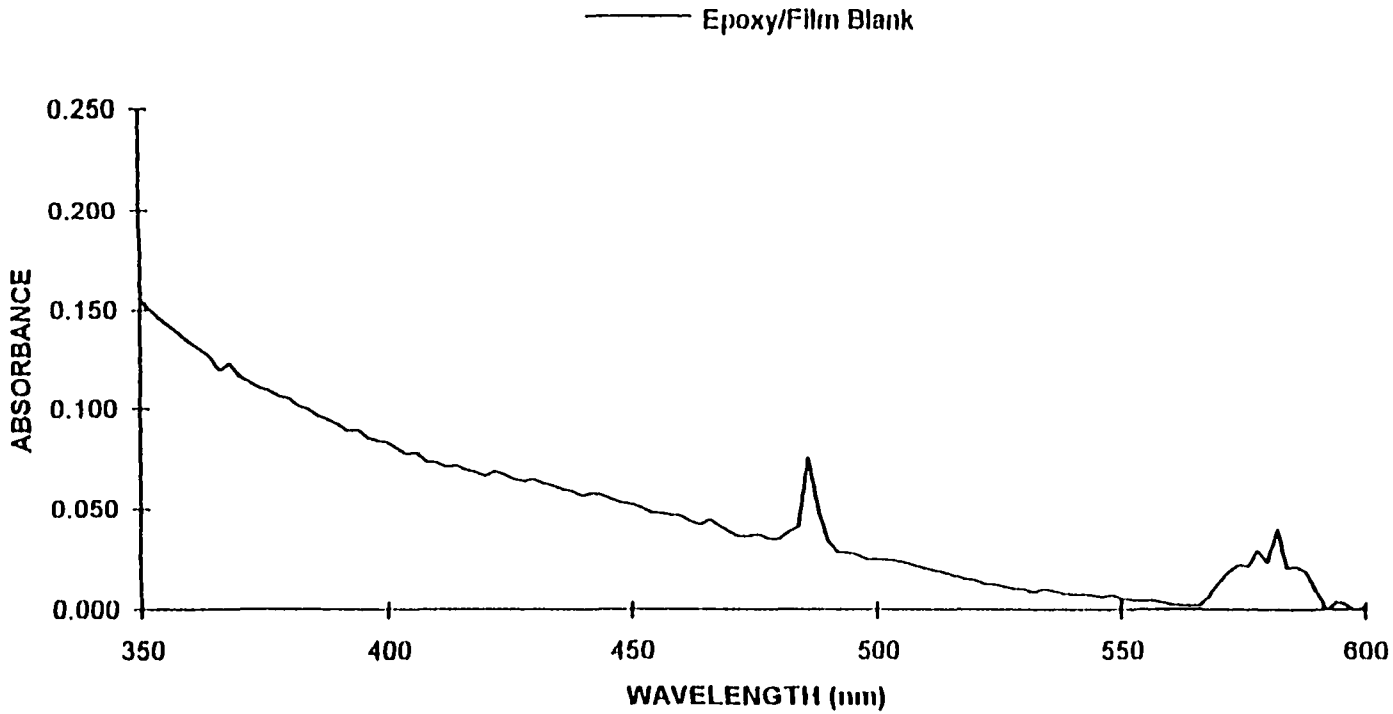

Figure 4. Background Spectra of Cellulosic Film and Crushed Epoxy Beads.

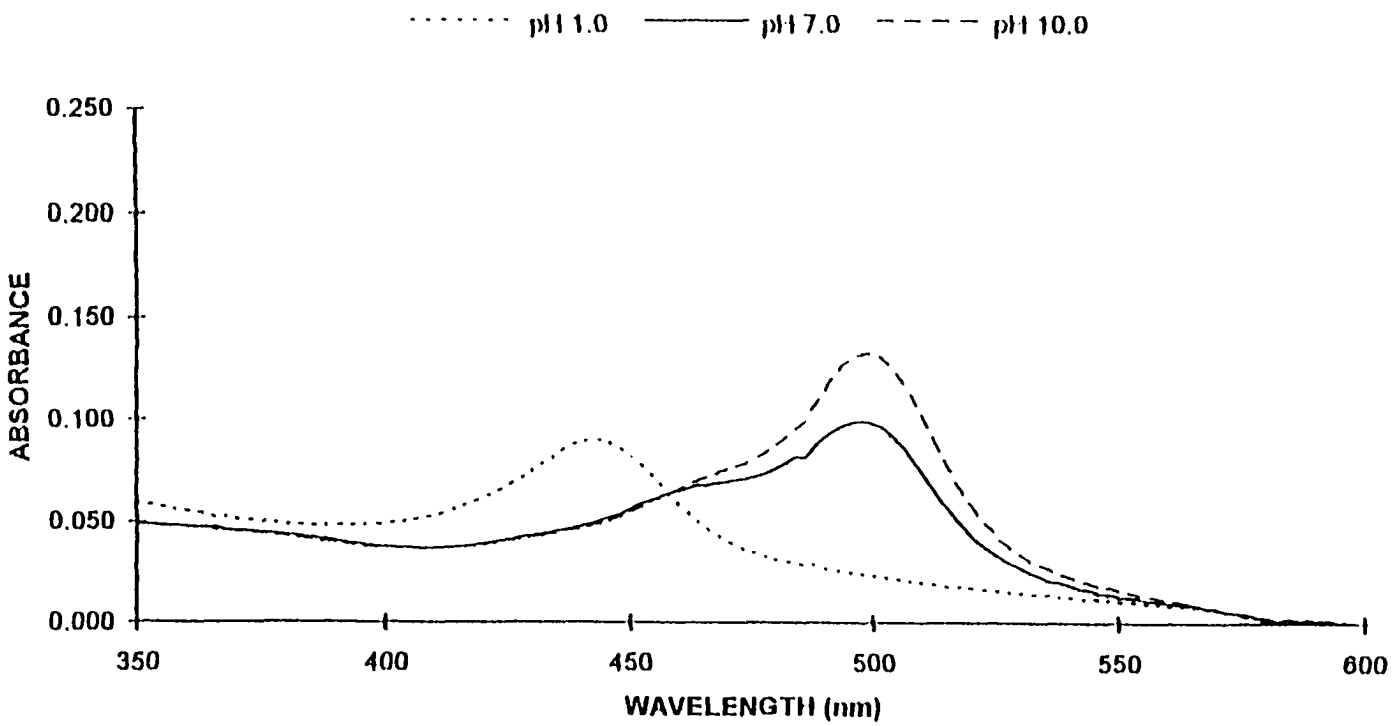

Figure 5. Background Subtracted Spectra of immobilized Fluoresceinamine.

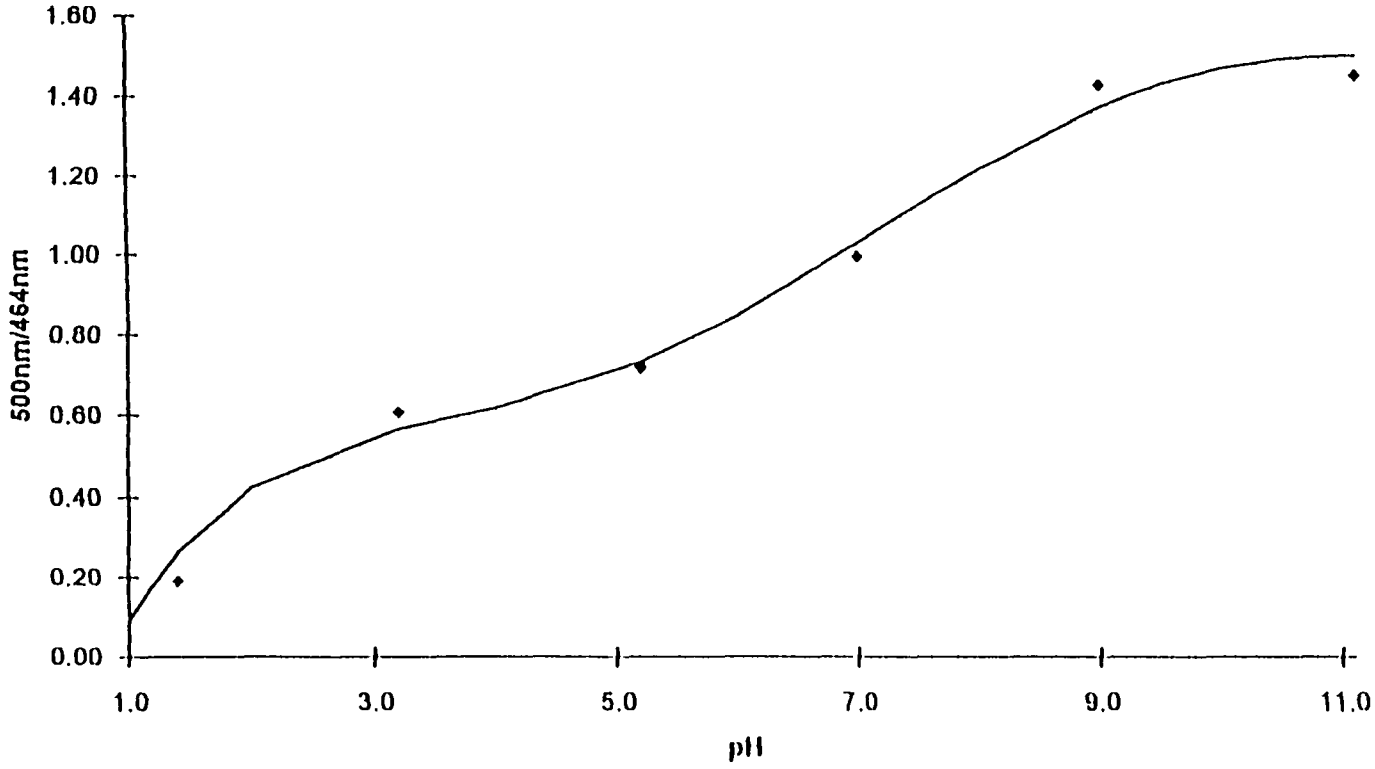

Figure 6. Calibration Curve of Immobilized Fluoresceinamine.

The normal pH range of human blood is 7.35 - 7.45.[29] Any compromise of the buffering capacity of the blood can lead to physiological problems and eventually death. Therefore, a resolution of at least 0.05 pH is imperative in monitoring blood pH. To assess the resolution of the thin -film sensor for this application, the spectral profile of the film was obtained for buffers from 6.6 to 8.0; this encompasses the extreme values for human blood.[30] The buffers were measured at 0.2 intervals. Statistical evaluation of the data yields a pH resolution of ± 0.03 units.

The long-term stability of the immobilized indicator was investigated. Two films were prepared similarly, one dyed and the other undyed (for background correction), and secured in separate flow through cells. Over a four month period, the films were subjected to deionized water, a variety of buffers, and various states of hydration. A calibration of the most sensitive, linear range of the film was constructed at the start and end of the trial period. From Figure 7, it can be seen that the largest variation in calculated values corresponded to ~ 0.1 pH. Therefore, it can be inferred that the films maintain calibration to within 0.1 pH over a 4 month period. Extended stability studies are being conducted.

The epoxy beads lend strength and durability to the films. Previous films prepared by adsorption of Congo Red at cellulose acetate produced very fragile films that were difficult to handle. However, the epoxy beads limit the minimum thickness of the films. The films prepared by using the beads as an immobilization intermediary are typically 40-90 μm in thickness, whereas the single component cellulose acetate films were, ~ 2 μm thick.[22] The

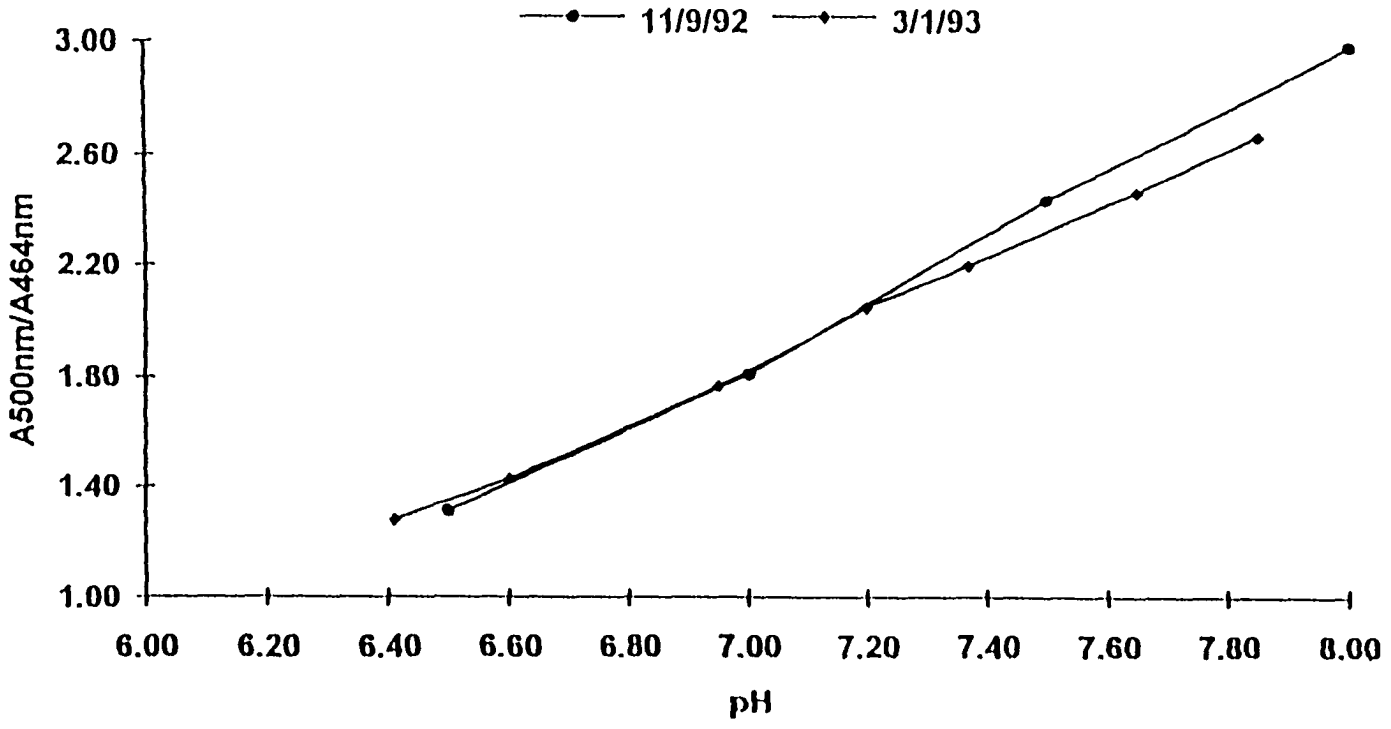

Figure 7. Four Month Film Stability Calibration.

thicker films respond slower, 40-60 sec, to changes in pH than the thinner Congo Red films, < 2 sec.

We are continuing experiments to modify the hydrolyzed cellulose acetate films for direct covalent immobilization of fluoresceinamine. For commercialization, the structural durability of the bead inclusion is desirable for ease of manufacture and handling of the films. We anticipate that with the development of a direct immobilization procedure, we will integrate opaque microscopic, polymeric beads in the film to maintain mechanical durability with improved response times.

The large dynamic range and ease of fabrication make this pH sensor film attractive in producing prototype instruments for commercialized sensor.[31] The immobilization technique described in this paper could be applied to the development of other sensor films. We are currently examining the extension of this research to the fabrication of sensors for quantifying other ions.

ACKNOWLEDGMENTS

The authors would like to expresses appreciation for the support of a NASA / Iowa Space Grant Fellowship given to Shelley Coldiron through the College Consortium under the NASA Space Grant Program. Also, this work was supported in part by the Center for Advanced Technology Development at Iowa State University under USDOC Grant ITA 87-02, by the Office of Basic Energy Research-Chemical Sciences Division of USDOE, and by the Advanced Life Support Division of the NASA-JPL (Contract No. 959452). Ames

Laboratory is operated for the U. S. Department of Energy by Iowa State University under Contract No. W-7405-Eng-82.

REFERENCES

1. J. I. Peterson and G. G. Vurek, *Science* **224**, 123 (1984).

2. W. R. Seitz, *Anal. Chem.* **56,** 16a (1984).

3. H. Wohltjen, *Anal. Chem.* **56**, 87a (1984).

4. T. Hirschfeld, J. B. Callis, and B. R. Kowalski, *Science* **226**, 312 (1984).

5. R. Narayanaswamy, *Anal. Proc. (London)* **22**, 204 (1985).

6. O. S. Wolfbeis, *Fresenius' Z. Anal. Chem.* **325**, 387 (1986).

7. J. F. Alder, *Fresenius' Z. Anal. Chem.* **324** 372 (1986).

8. D. M. Jordan, D. R. Walt, and F. P. Milanovich, *Anal. Chem.* **59**, 437 (1987).

9. J. B. Callis, D. L. Illman, and B. R. Kowalski, *Anal. Chem.* **59**, 624A (1987).

10. S. M. Angel, *Spectroscopy* (Springfield, Oregon) **2**, 38 (1987).

11. O. S. Wolfbeis, *Anal. Proc. (London)* **24**, 14 (1987).

12. J. Janata and A. Bezegh, *Anal. Chem.* **60**, 62R (1988).

13. S. Luo and D. R. Walt, *Anal. Chem.* **61**, 174 (1989).

14. S. M. Stole, T. P. Jones, L. K. Chau, and M. D. Porter, in *Chemical Sensors and Microinstrumentation*, R. W. Murray, R. E. Dessy, W. R. Heineman, J. Janata, W. R. Seitz, Eds., ACS Symposium Series 403 (American Chemical Society, Washington, D.C., 1989), Chap. 19.

15. J. P. Dakin, in *Optical Fiber Sensors*, H. J. Arditty, J. P. Dakin, and R. Th. Kersten, Eds., Springer Proceeding in Physics **44**, 186 (1989).

16. H. He, H. Li, G Mohr, B. Kovacs, T. Werner, and O. S. Wolfbeis, *Anal. Chem.* **65**, 123 (1993).

17. R. B. Thompson and E. R. Jones, *Anal. Chem.* **65**, 730 (1993).

18. T. L. Blair, T. Cynkowski, and L. G. Bachas, *Anal. Chem.* **65**,945 (1993).

19. J. C. Wells, P. G. Blystone, M. D. Johnson, W. R. Haag, and B. W. Colston, Jr., *3rd Int. Symposium on Field Screening Methods for Hazardous & Toxic Chemicals* (Las Vegas, Nevada), 1 (1993).

20. R. B. Thompson and J. R. Lakowicz, *Anal. Chem.* **65**, 853 (1993).

21. M. E. Collison and M. E. Meyerhoff, *Anal. Chem.* **62**, 425A (1990).

22. T. P. Jones and M. D. Porter, *Anal. Chem.* **60**, 404 (1988).

23. L. A. Saari, *Anal. Chem.*, **1982**, 54, 823-824.

24. Z. Zhujun, Y. Zhang, M. Wangbai, R. Russell, Z. M. Shaksher, C. L. Grant, and W. R. Seitz, *Anal. Chem.* **61**, 202 (1989).

25. R. Sternberg, D. S. Bindra, G. S. Wilson, and D. R. Thevenot, *Anal. Chem.* **60**, 24, 2782 (1988).

26. Y. Chang, A. Gee, A. Smith, and W. Lake, *Bioconjugate Chem.* **3**, 200 (1992).

27. K. Burg, O. Mauz, S. Noetzel and K. Sauber, *Die Angewandte Makromolekulare Chemie* **157**, 105 (1988).

28. D. D. Perrin, *Buffers for pH and Metal Ion Control*, Chapman and Hall, New York (1974).

29. C. Lentner, Geigy Scientific Tables: *Physical Chemistry Composition of Blood, Hematology, Somatometric Data*, Vol. 3, Medical Education Division, Ciba-Geigy Corporation, West Caldwell, New Jersey (1984).

30. E, Goldberger, *A Primer of Water, Electrolyte and Acid-Base Syndromes*, Lea & Febiger, Philadelphia, PA, 7th Edition (1986).

31. T. P. Jones, S. J. Coldiron, W. J. Deninger, and M. D. Porter, *Anal. Chem.* **45** 1271 (1991).